Doctoral Thesis

Robust Non-Rigid Registration of Medical Images

March, 2015

Doctoral Program in Integrated Science and Engineering
Graduate School of Science and Engineering
Ritsumeikan University

LIN CHEN-LUN

Doctoral Thesis Robust Non-Rigid Registration of Medical Images LIN CHEN-LUN

Doctoral Thesis reviewed

by Ritsumeikan University

Robust Non-Rigid Registration of Medical Images

医用画像に対するロバストな非剛体位置あわせ手法に関する研究

March, 2015

2015 年 3 月

Doctoral Program in Integrated Science and Engineering
Graduate School of Science and Engineering
Ritsumeikan University

立命館大学大学院理工学研究科

総合理工学専攻博士課程後期課程

LIN CHEN-LUN

リン　チェンルン

Supervisor: Professor Chen Yen-Wei

研究指導教員：陳 延偉 教授

Abstract

Recently, image registration process plays an important role in the analysis of medical image at medical treatment. Image registration has been widely applied at various fields such as surgical navigation, serial-image analysis, medical image fusion, etc... Image registration can be classified into two categories such as rigid and non-rigid image registration which depend on the objective of application classify.. Rigid registration is usually performed to match two rigid objects. Relatively, non-rigid registration is generally applied at to align two deformable organs for medical image analysis. The main difference between rigid and non-rigid method is transformation which is used by separately. In practice, method of global transformation such as rigid transformation is used for rigid image registration. In additions, some deformable local transformation methods such as affine transformation, B-spline transformation are applied for non-rigid registration also. This research of thesis is focused on research findings to explore for robust and achieve accurate non-rigid medical image registration and also as my contribution of this research.

Non-rigid registration is a process for maximizing a spatial image correspondence of two images within constrains of a transformation model. The process of registration can be divided into four phases, which are: transformation, interpolation, criterion, and optimization. In this thesis, the author proposed three novel approaches for robust and accurate medical image registration. Two of them are focused to improve similarity metric for the phase of criterion; another is to concentrate on an advance optimization method for the purpose of to enhance optimization. In addition, a well-developed system of non-rigid image registration for assessing quality of loco regional therapy of hepatocellular carcinoma. It is also described in this research. The major contributions of this thesis are summarized as follows:

1. In the past, optimization methods of registration were almost based on gradient. However, gradient based methods are failed very easily because the rationale is falling into local resolution. In recent years, some non-linear and multi-point searching based methods such as Genetic Algorithms (GA) and particle swarm optimization (PSO) were proposed to achieve as advanced optimization. In this research, I proposed a novel optimization method called hybrid particle swarm optimization (HPSO) as a new optimization approach for medical image registration to improve accuracy and achieve efficiency. The main idea of proposed method Combine the idea of PSO with concepts from GA, which are subpopulation and crossover. The proposed methods were also compared with conventional methods such as GA and PSO. From the experimental results showed that the proposed HPSO performs better for registration results than conventional GA and PSO as one of my research contribution.

2. Mutual information method (MI) is a widely used metric for criterion of multi-modality image registration. Although, MI was performed well in many cases of multi-modality image registration, however, there are some drawbacks of MI were found. The major disadvantage of MI is that it sensitive to noise because of lacking spatial information. In the 2004, regional mutual information (RMI) is proposed as a new similarity metric also including some spatial information. Unfortunately, RMI require a huge computing time to obtain the estimation of registration from a huge matrix of joint distribution. For reaching a robust and accurate registration, from my research, proposed a PCA based regional mutual information method (PRMI) as a robust similarity criterion to overcome these

disadvantages from traditional MI and performance problem of RMI. The contribution from my research method successfully contains spatial information into traditional MI, and also prevents the computing cost issue of RMI by combining the concepts of principle component analysis (PCA), MI, and RMI.

3. Locoregional therapy (LT) is a novel and popular method to cure hepatocellular carcinoma (HCC) of liver in the last few years. This method digs several probes into patient's abdominal cavity to burn tumor tissues of liver with frequency alternating current. However, estimating quality of treated margin of LT from two medical images (before and after operation comparison) becomes a difficult task because liver is a deformable organ. In the previous study, the classical method of non-rigid registration was applied to find overlap of tumor and treat region for evaluating the treat margin. Unfortunately, sometimes, classical method was failed to register intra tissues of liver by property of sensitive to distribute of intensity. To overcome this problem, the research proposed a new non-rigid registration method to evaluate treated margin of locoregional therapy of hepatocellular carcinoma from medical images of livers. This method overcomes the weakness of classical intensity based non-rigid registration by containing the anatomical structures as a constrained term. From the experimental results finding the research method not only can aligns the shape structure of livers very well, but also it can reasonably maintain the correspondence of internal structures.

4. From the research developed a non-rigid registration system to assess quality of loco regional therapy. The hepatocellular carcinoma applies this research proposed anatomical structures constrain based method. The result shows the utility and achieves accuracy from my research method by 3D visualization.

Contents

List of Figures

6.16 List of Table

Chapter 1

Introduction

The first chapter presents the concept of medical image, such as the modalities of medical image, the categories of medical image analysis, and contribution of our research findings. The main propose of this chapter is illustrating the motivation and rationale of this research.

1.1 Medical Image Techniques

The function of medical imaging can provide clinicians of the capability to view inside of the human body in order to diagnose the human's illness symptom. The major research is focused on developing an emerging technology and algorithm to improve the quality of the images for physician to evaluate patient's illness more accuracy and efficiently. Recently, computer technology becomes a sufficiently sophisticated technology to aid physician in the process of diagnosis patient disease. Therefore, a brief introduction in light of how the medical imaging techniques are applying by physician in the clinical diagnosis currently.

The accidental discovery of "X-rays" by Roentgen in 1895 began the history of clinical use of medical images for human beings. Also radiograph (X-ray image) is the first kind of medical imaging technique applied at medical care. The rationale is that radiograph can be produced by using a broad beam of X-rays to pass through a patient to generate the x-ray image. X-rays are high frequency beams of the electromagnetic spectrum which can pass more easily through materials such as bones, kidney stones, etc. solids tissues in the body with low density (lower atomic numbers) than through those with higher density (higher atomic numbers), to generate a radiographs which can be seen easily.

The human bones can be seen by given high intensities in the radiographs; while soft-tissues or organs can be viewed by given low intensities. Radiographs are 2-dimensional (2D) images. Each point contains the information integrated along the path of a beam of X-ray passed though, so radiographs can show the characteristics of radiated tissue of its transparency image. For example, each point of the chest radiograph shown by Fig. 1.1 (datasets are obtained from BrainWeb [15]) contains the information of both bones and soft-tissues. The transparent characteristics of x-ray are able to distinguished radiographs from other kinds of

medical images style.

Computed tomography (CT) [14] is another kind of medical imaging techniques which are generated by X-rays also. In CT, a thin beam of X-rays is passed through the patient's tissue which absorbed by a detector. Then, it collected signals which are generated by computers in order to produce the tomographic images or slices of the human tissue. Gathering all the CT slices by orders, therefore, we can get a 3-dimensional (3D) volume to view the tissue by 3D image. More detail illustrating, from the Fig. 1.1 provides an examples of CT images. CT, it can reflect an anatomical information to view human tissue. It likes a radiograph imaging such as bones may display various densities of its structure. The hard bone tissue generates high intensities and soft-tissues create low intensities displaying on the CT images for physician to diagnosis of patient's illness.

Magnetic resonance imaging (MRI) is one another primary diagnostic tool for generating structural images of the human tissue.. The fundamental structure of MRI imagining is a nuclear magnetic resonance (NMR) [1]; it is a physical phenomenon of atom's nucleus. The rationale of MRI is when first step, it placed in a constant magnetic field and then perturbed by an orthogonal alternating electric field. Because of human tissue is primarily composed of H_2O, therefore, NMR of the hydrogen nuclei (i.e. protons) provides strong signals which are collected by computers to generate tomographic slices imaging. CT, MRI images are 3D data, it be capable of reflecting anatomical imaging information of human tissue. The MRI has a higher contrast on the organic boundaries imaging compared with CT. There are three kinds of MR images, such as MR T1-weighted, MR T2-weighted and MR proton density weighted (PD-weighted) images. The Fig.1.1 provides examples of to illustrate its differences. MR T1-weighted images are well known as "anatomy scans". Because it can show the most clearly the boundaries among different tissues, this method is considered by physician as the first choice applies at clinical as one of the best diagnosis tool. MR T2-weighted images are popular applying at "pathology scans". It can be capable of collections of abnormal fluid which are brighter against the darker normal tissues for more clearly diagnosis. MR PD-weighted images are a byproducts composed of T2-weighted images. From this perspective view point , PD-weighted images are "free" when it produce T2-weighted images; however the drawbacks is that their contrasts are less than MR T1-weighted and T2-weighted images. Therefore, due to their weakness of imaging quality, PD-weighted images are seldom applied at clinical applications for diagnosis. The advantage of PD-weighted images unlike CT, MRI, it does not use ionizing radiation to generate the cross-section images (slices). X ray, CT have the radiation exposure of over dose which it may endanger patient's health. MRI is not associated with health hazards like CT. From the evidence based medicine perspective view, MRI is lack

of insignificant of evidences to effect of patient with long term exposure of strong magnetic fields to cause hazard of their health.

Positron emission tomography (PET) employs the main features of tracer techniques, it provided to develop the research to study the underlying mechanisms of physiological and biochemical processes in a living organism [8]. The radioactively labeled substances are injected intravenously and can be traced through the body by using external detectors device. In the case of PET, the rationale is that the tracer is labeled with an isotope that emits a positron. Such isotopes are available for a number of biologically relevant atoms, namely such as oxygen, carbon, nitrogen and fluorine etc... Labeling with a radioactive nuclide, it allows the synthesis of specific tracers, which are used to determine, such as tracing cerebral blood flow or glucose consumption in human brains. Hence, PET is representative of a functional image modality, and as the primary in the development of PET. The function of the PET is to quantify three-dimensional distribution of the radioactive tracer with subsequent interpretation in a framework by physiological models.

1.2 Medical Image Analysis

The rapid development and proliferation of medical imaging technologies are an emerging revolutionizing medicine as a high end physician aid diagnosis technology. Medical imaging allows scientists and physicians to glean potentially life-saving information by peering noninvasively into the human tissue. The role of medical imaging has expanded so confound more than previously as a simple visualization and inspection of anatomic structures. It has become a critical tool and important contributions for surgical planning, simulation, intra-operative navigation, radiotherapy planning, and for other tracking the progressive of disease evaluation. Therefore, the advanced medical imaging technologies are playing important roles and becoming more prominent role in the diagnosis and treatment of disease. The researcher community of medical image analysis team needs to solve confronting challenging problems of extracting high quality images by the assistance of computers of clinically useful information about anatomic structures imaged through CT, MR, PET, and other modalities. Although modern imaging devices can provide exceptional views of internal anatomy, however applying computers to achieve high image quantify and analyze the embedded structures with accuracy and efficiency is limited. In short, accurate, repeatable, quantitative data must be efficiently extracted in order to support the spectrum of biomedical investigations and clinical activities from diagnosis, to radiotherapy for surgery.

Techniques of medical image analysis can be divided into four categories (see Fig 1.1) which

are medical image registration ([2], [9], and [10]), medical image segmentation [11], medical image enhancement, and medical image modeling [12]. The purpose and function of medical image registration is to find a spatial transformation which can align two medical images. Medical image segmentation is to detect the boundary of a certain object, such as liver or heart, and separate it from the original medical images. Medical image enhancement is to remove the noise or artifacts and enhance the quality of the medical images. Medical image modeling is to find a modeling method which can represent the medical data efficiently. In the past, these techniques were developed separately; however, recently many researchers integrated with these techniques to pursue high quality medical image to aid the diagnosis more efficiently and effectiveness. This research explored an emerging method of medical image registration, and to apply the proposed innovative techniques to assist the evaluation of Locoregional therapy of liver tumors ([6], and [7]).

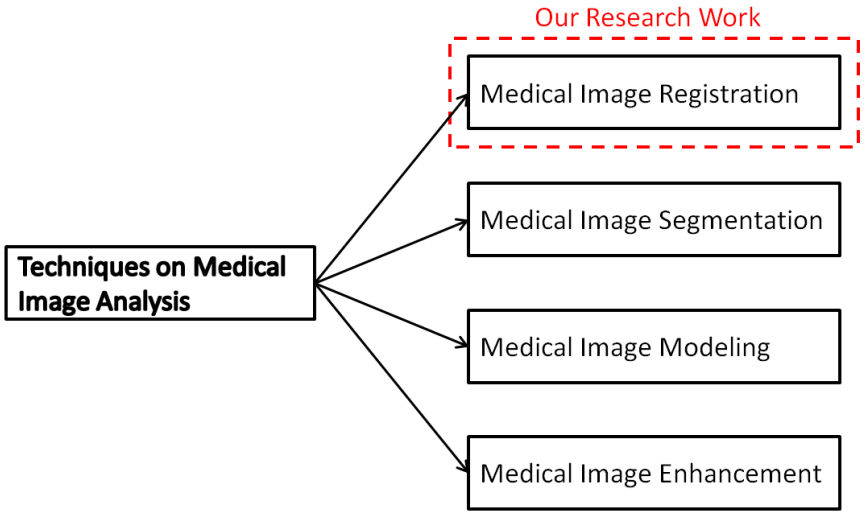

Fig 1.1: Category of our research works

1.3 Thesis Contribution and Overview

Non-rigid medical image registration plays an important role in the analysis of medical images to enhance image quality. Recently, a non-rigid image registration method applied to surgical navigation, serial-image analysis, medical image fusion etc..., it diffused to critical masses of medical care. Although classical non-rigid registration method has been widely used and proved to good results for most of all cases of registration applications. However, in this research found that the classical method was still failed when it encountered some special situations or requirements. Therefore, at this research started to apply theory of registration and to create some new methods to improve the classical method weaknesses.

This thesis is in light of new method to achieve better image quality compared with the traditional method. Moreover, it can work fine and illustrates the proposed method, and showing how they work in medical practice.

Non-rigid registration is a process for maximizing a spatial image correspondence of two images within constrains of a transformation model. The process of registration can be divided into four phases, which are: transformation, interpolation, criterion, and optimization. In this research, the author proposed three novel approaches to enhance medical image registration more robustly and accurately. Two of them are focused on improvements in the phase of criterions; another is concentrated on an advance method for optimization phase.

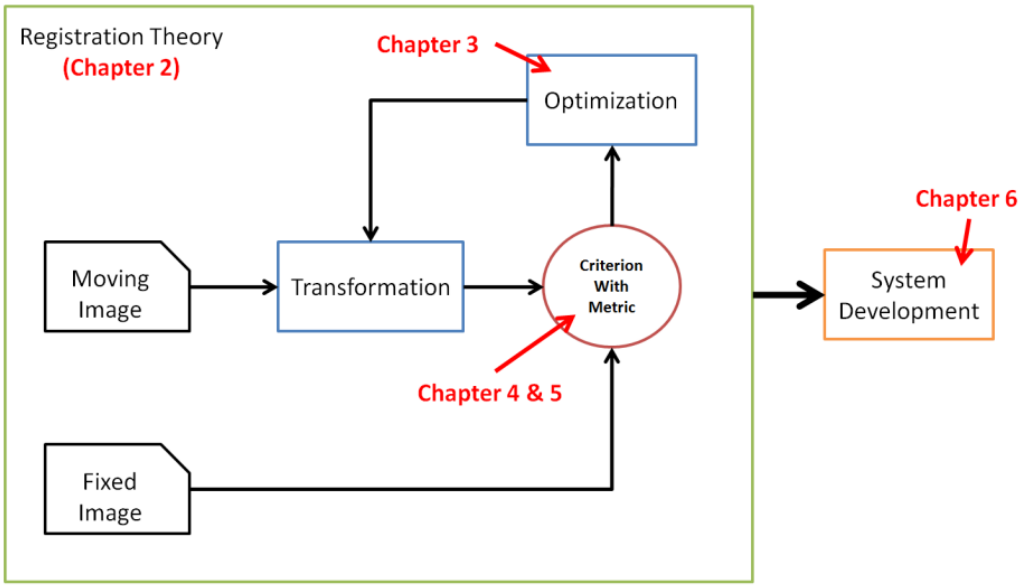

Fig 1.2: The contributions and overview of my thesis

The contributions of this research depend on six sections. First, the general concepts and details of registration are briefly summarized in Chapter 2. In Chapter 3, the author proposed a novel optimization method called hybrid particle swarm optimization (HPSO) as a new optimization approach of medical image registration to improve accuracy and efficiency of registration, especially for medical image registration with large geometric difference. This method is an advance emerging method compared with other methods such as general particle swarm optimization (PSO) and genetic algorithm (GA). In Chapter 4, the author proposed a PCA based regional mutual information method (PRMI) as a robust similarity criterion to overcome disadvantage of traditional mutual information method (MI) and performance problem of regional mutual information (RMI). The proposed PRMI is applied the idea of RMI to integrate spatial information into MI, and applies Principal component

analysis (PCA) statistics method to reduce the computing cost. In Chapter 5, the author proposed a new non-rigid registration method to evaluate treated margin of loco regional therapy of hepatocellular carcinoma from medical images of livers. This method overcomes the weakness of classical intensity based on non-rigid registration by containing the anatomical structures as a constrained term. In Chapter 6, the author developed a non-rigid registration system for assessing quality of loco regional therapy of hepatocellular carcinoma case which applies my proposed anatomical structures constrains based method. The result showed more efficiently, effectiveness and accuracy of applying this research method. Finally, in Chapter 7, the author presents conclusions and addresses future avenues of research. The contributions and overview of this thesis are illustrated at Fig 1.2.

Reference of Chapter 1

[1] D.W. McRobbie, E.A. Moore, M.J. Graves and M.R. Prince, *MRI From Picture to Proton, Cambridge University Press*, 2003.

[2] P.J. Besl and N.D. Mckay, A method for registration of 3D shapes. *IEEE Transaction on Pattern Analysis and Machine Intelligence*. Vol. 14, 1992, pp: 239-256.

[3] R. Xu, Y.W. Chen, Wavelete-based multiresolution medical image registration strategy combining mutual information with spatial information, *International Journal of Innovative Computing, Informatioin & Control*, Vol. 3, No. 2, 2007, pp: 285-296.

[4] R. Xu, Y.W. Chen, S.Y. Tang, S. Morikawa and Y. Kurumi, Di®erentiable normalized mutual information based on parzen-window method, *Proc. on Meeting on Image Recognition and Understanding*, 2007.

[5] R. Xu, Y.W. Chen, S.Y. Tang, S. Morikawa and Y. Kurumi, Parzen-window based normalized mutual information for medical image registration, *IEICE Transaction on Information and Systems*, 2008, (to be published).

[6] C.L. Lin, T. Tateyama, R. Inokuchi, T. Seki, and Y.W. Chen: "3D Non-rigid Medical Image Registration using Landmark Based Initialization for Locoregional Therapy of Liver," *IEICE Technical Report* , Vol.112, No. 411, pp.311-315, 2014.

[7] C.L. Lin, C.H. Dong, R. Inokuchi, T. Seki, T. Tateyama and Y.W. Chen: "Surgical Treated Margin Evaluation Assistant System for Locoregional Therapy of Liver using Semi-automatic Segmentation and Landmarks Constraint Based Registration," *International Journal of Emerging Technology and Advanced Engineering*, Vol. 4, pp.737-744, 2014.

[8] D.N. Levin, C.A. Pelizzari, G.T.Y. Chen, et. al., Retrospective geometric correlatioin of MR, CT and PET images, *Radiology*, Vol. 169, 1988, pp: 817-823.

[9] J.V. hainal, L.G. Hill and D.J. Hawkes, *Medical Image Registration*, CRC Press, 2001.

[10] D.L.G. Hill, P.G. Batchelor, M. Holden and D.J. Hawkes, Topical review: medical image registration, *Physics in Medicine and Biology*, Vol. 46, 2001, pp: 1-45.

[11] P. Campadelli and E. Casiraghi, "Liver segmentation from CT scans: A survey," Lect. Notes Comput. Sci., 4578, pp. 520-528, 2007.

[12] I. Drydden and K. Mardia, *Statistical Shape Analysis*, John Wiley and Sons, NY, 1998.

[13] G. Borgefors, Distance transformations in arbitrary dimensions. *Comput. Vision Graph. Image Process*, Vol. 27, 1984, pp: 321-345.

[14] M. van Herk and H.M. Kooy, Automated three-dimensional correaltion of CT-CT ,CT-MRI and CT-SPECT, *Med. Phys*, Vol. 21, 1994, pp: 1163-1178.

[15] BrainWeb: http://brainweb.bic.mni.mcgill.ca/brainweb/

Chapter 2

Image Registration

Medical image registration is the process to find a spatial transformation which is able to align the corresponding features in two medical images [1], [2]. Consider a scenario in which we might have a patient who is imaged with MR and CT over the course of a few hours as workup for neurosurgery. The process of registration will establish which point on one image corresponds to a particular point on the other. The “correspond” means that these points represent a measurement localized to the same small element of tissues within the patient. During the computational process of registration an appropriate transformation will be yielded between the coordinate systems of the two medical images.

2.1 Category of Registration

Registration algorithms compute image transformations that establish correspondence between points or regions within images, or between physical space and images. There are many several of classify methods of medical image registrations; therefore, we briefly describe them as follows.

2.1.1 Mono-modal and Multi-modal Registration

According to modalities of medical images, we can divide medical image registration into mono-modal (singular-modal) and multi-model registration. In mono-modal medical image registration, the two medical images have the same modality, e.g. registration of two MR images. These two images are usually taken in two different times and the time intervals. The time consuming may from the range as a few seconds to several days, months or even years. Mono-modal registration can eliminate the position difference on the two images in order to compare with the changes in size, shape or image intensity.

M Multi-modal registration is to align two medical images with different modalities. Different kinds of imaging modalities give different information of the human bodies. For example, some imaging modalities like CT or MRI give the anatomic information; while some nuclear imaging modalities like PET give the functional information. CT and MRI also provide

different anatomic information. For example, CT applying on the bones is very clearly but the organic boundaries are not so clearly to be seen; however by MRI, organs usually have high contrast, however bones are not so clearly. Therefore, it is necessary to apply different imaging modalities to generate the required information for assisting of clinical diagnose. Medical images are collected by different machines; however, several of machines have their different roles and functions among them. Multi-modal registration can be performed to solve these problems in order to eliminate such differences before combining the information by different machines.

2.1.2 Intra-subject and Inter-subject Registration

Considering subjects on medical images, we can divide medical image registration into intra-subject and inter-subject registration. Registration of two images collected from the same patient is called intra-subject registration; otherwise, registration is called inter-subject registration. For intra-subject registration, the modalities of the images can be either the same or different. The example of intra-subject registration for the same modal images can be found [28], where the breast MR images collected in different time are registered. Inter-subject registration is usually applied to register images of the same modality in order to build models. It can reflect the variation in anatomy from different people. A study of fetal liver shape is done [29], and reported that only five parameters are required to capture 89% of variation in shape.

2.1.3 Rigid and Non-rigid Registration

We can also divide medical image registration into rigid and non-rigid registration based on the underlying obtained transformation. The types of transformation determine whether a registration belongs to a rigid or non-rigid one. If a rigid transformation is used, it is called rigid registration; otherwise it is called non-rigid registration. Rigid transformation has less degree of freedom (parameters). In 2D case, a rigid transformation has only three parameters, one rotation angle and two translation vectors; a 3D rigid transformation has six parameters, three rotation angles and three translation vectors on each axis. Rigid registration is used when the subject in the medical images can be seen as a rigid object, i.e. Such as the human brain of the same patient on CT or MR images. Non-rigid transformation has more degrees of freedom. Affine transformation is a simple non-rigid transformation. In a 3D case, it has twelve parameters to describe translation, rotation, scaling and shearing on each axis. Non-rigid registration is used when the subjects on the medical images have deformation, i.e. abdominal organs or anatomic change due to long time duration.

2.2 Registration Methodology

Medical image registration can be formalized as an optimization problem to find the parameters of a spatial transformation on two medical images. It can maximize or minimize at a certain cost function. According to different ways to calculate the cost function, medical image registration can be divided into three categories which are point-based, surface-based and intensity-similarity based registration [3], [4].

2.2.1 Point-Based Registration Methods

We denote a spatial transformation as $T(\mathbf{x}|\mathbf{u})$, where x is the coordinate of a point and u is the parameter of the transformation. A point-based method is to determine the parameter of the transformation from two sets of points, $X = \{\mathbf{x}_1, \mathbf{x}_2, \ldots, \mathbf{x}_N\}$ and $Y = \{\mathbf{y}_1, \mathbf{y}_2, \ldots, \mathbf{y}_N\}$, which are the corresponding points determined manually or automatically before registration on two images. These corresponding points are sometimes called homologous landmarks to emphasize that they should represent the same feature in the different images. They can either be anatomical features or marks attached to the patients. The parameter $\mathbf{u}$ can be calculated by resolving the Procrustes problem which is an optimal fitting problem of least square: to minimize the cost function of $G(\mathbf{u}) = \sum_{i=1}^{N} \left\| \mathbf{T}(\mathbf{x}_i|\mathbf{u}) - \mathbf{y}_i \right\|^2$. It is a known solution when the transformation is for a rigid-body. A matrix representation of the rotational part can be computed using singular value decomposition (SVD) [5]. This approach is used not only for the medical image registration [6], [7] but also for construction of statistical shape models.

2.2.2 Surface-Based Registration Methods

Boundaries or surfaces of tissues or organs are usually more distinct than landmarks in medical images, since two kinds of tissues usually have contrast intensities in some imaging modalities, i.e. MR. Additionally, various segmentation methods can accurately locate the high contrast surfaces. These two reasons provide the research for the surface-based registration methods. A method called head and hat algorithm which is proposed in the works [13], [14]. In this method, the transformation is determined by iteratively transforming a list of unconnected 3D points of a surface referred as hat with respect to the head surface from the higher resolution modality. This method is successfully used in the registration of head [14] and heart [15]. The performance of head and hat algorithm can be improved by using a distance transform to preprocess the head images. A widely-used distance transform is the

chamfer filter proposed in [16] and this kind of approach is used for rigid-body registration in the works [17], [18]. Additionally, Euclidean distances transforms can also be used in place of the chamfer transform [19]. Another surface-based registration method is called iterative closest point (ICP). It is proposed in [2] and firstly not designed for medical imaging application. ICP is an iterated method to determine the transformation for two set of points. In the each iteration, the first step is to determine the corresponding point by finding the closest points according to the transformation calculated in the last iteration and then the transformation can be calculated by resolving the Procrustes problem. The iteration is terminated when the change of the mean square error of the two points set in two consecutive steps which are below to a certain threshold. It is probably that ICP is the most widely used surface-based registration method for medical imaging application [20], [21], [22].

2.2.3 Intensity-Similarity Based Registration Methods

In recent years a number of robust and accurate algorithms have been devised that use the intensities in two images alone without any requirement to segment or delineate corresponding structures. These are often collectively referred to as an intensity-similarity based registration. As these algorithms have been so successful, we abbreviately illustrate these algorithms as followings.

Intensity-similarity based registration can determine the transformation by considering the relationships of the intensities (voxels or pixels) on the medical images directly, so it does not need the preprocessing to obtain landmarks or surfaces. It is different from the point-based and surface-based methods. This kind method doesn't need any complicate preprocessing and can make the registration easily to be performed automatically.

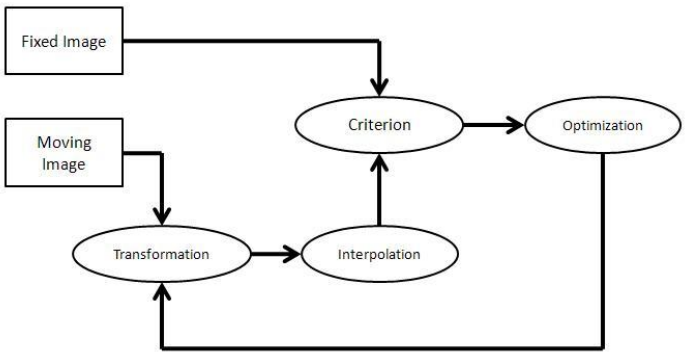

Fig 2.1: Framework of medical image registration

Fig 2.1 shows the framework of the image-to-image registration process and the

interconnection between each phase. The image which is not changed during registration is called fixed image; and the other image is called moving image. In the each iteration, the moving image is firstly transformed by transformation according to the parameter of the current time. After interpolation, the fixed image and the transformed moving image are then used to calculate the intensity-similarity based cost function which can evaluate whether the two images are registered or not under the current parameter of transformation. If the images are not registered, an optimization method will adjust the parameter and a new iteration will start.

It can be seen that there are four main aspects for intensity-similarity based registration, which are transformation, interpolation, criterion and optimization. We will give the brief reviews for all the four aspects in the following sections. Before the review, we will first describe the mathematical notation.

A transformation is denoted as $\mathbf{T}$ and its parameters are denoted as $\mathbf{u}$. Using the language of geometry, this transformation is a spatial mapping. We can consider the mapping $\mathbf{T}$ that transforms a point or position $\mathbf{x}$ on one image to get a new point or position $\mathbf{x}'$ on the other image according to parameters $\mathbf{u}$.

$$\mathbf{T}:\mathbf{x}\overset{\mathbf{u}}{\mapsto}\mathbf{x}' \quad \Leftrightarrow \quad \mathbf{T}\left(\mathbf{x}\middle|\mathbf{u}\right)=\mathbf{x}' \tag{2.1}$$

Let the fixed and moving images to be f_F and f_M respectively. $f_F(\mathbf{x})$ And $f_M(\mathbf{x})$ mean the intensity value of the position $\mathbf{x}$ on the two images. We use $I\left(f_F, f_M\middle|\mathbf{u}\right)$ the notation to represent the intensity-similarity based cost function which is calculated from the fixed and moving images when the parameter of transformation is $\mathbf{u}$. The optimization framework can be expressed by equation (1.2) which means to seek the optimal parameter $\mathbf{u}_{opt}$ that is able to maximize (or minimize) the cost function.

$$\mathbf{u}_{opt}=\arg\max_{\mathbf{u}} I\left(f_F, f_M\middle|\mathbf{u}\right) \;\; or \;\; \mathbf{u}_{opt}=\arg\min_{\mathbf{u}} I\left(f_F, f_M\middle|\mathbf{u}\right) \tag{2.2}$$

2.3 Relative Algorithms

Our works rely on intensity-similarity based method which was illustrated in Fig 2.1. This method contains several different relative algorithms to achieve an iterative mechanism for

obtaining a good result of registration. In this section, we abbreviate summarize the relative algorithms which are usually used for intensity-similarity based method.

2.3.1 Transformation

The final goal of registration is to obtain a mapping from the coordinate system of one image into the coordinate system of another image. This mapping is termed as a transformation. Transformation can be divided into two categories which are rigid and non-rigid transformation. We given a briefly review on them in this section.

2.3.1.1 Rigid Transformation (Global Transformation)

Rigid transformation is usually based on mathematical forms. There are two popular rigid transformations, one is rigid transformation method, and the other is affine transformation.

A. Rigid Transformation

In the case of 3D rigid transformation, a transform $\mathbf{T}_{Rigid}(\mathbf{x})$ is typically defined by a set of transform parameters, $\mathbf{u}$, which has three parameters. The parameters t_x, t_y, and t_z define a translation, while the parameter θ defines a rotation angle. Given a point, $\mathbf{x}=[x,y,z]^T$, and an rotation center, $\mathbf{x}_c=[x_c,y_c,z_c]^T$, in the coordinate system of image, the 2D rigid transformation, $\mathbf{T}_{Rigid}:\mathbf{x}=[x,y,z]^T \mapsto \mathbf{x}'=[x',y',z']^T$, can be expressed by equation (2.3).

$$\mathbf{x}'=\begin{pmatrix} x' \\ y' \\ z' \end{pmatrix}=\mathbf{T}_{Rigid}(\mathbf{x})=\mathbf{R}(\mathbf{x}-\mathbf{x}_c)+\mathbf{t}+\mathbf{x}_c$$
$$=\begin{pmatrix} \cos\theta_y\cos\theta_z & \cos\theta_x\sin\theta_z+\sin\theta_x\sin\theta_y\cos\theta_z & \sin\theta_x\sin\theta_z-\cos\theta_x\sin\theta_y\cos\theta_z \\ -\cos\theta_y\sin\theta_z & \cos\theta_x\cos\theta_z-\sin\theta_x\sin\theta_y\sin\theta_z & \sin\theta_x\cos\theta_z+\cos\theta_x\sin\theta_y\sin\theta_z \\ \sin\theta_y & -\sin\theta_x\cos\theta_y & \cos\theta_x\cos\theta_y \end{pmatrix}\begin{pmatrix} x-x_c \\ y-y_c \\ z-z_c \end{pmatrix}+\begin{pmatrix} t_x+x_c \\ t_y+y_c \\ t_z+z_c \end{pmatrix} \quad (2.3)$$

Where $\mathbf{R}$ is a rotation matrix which is calculated from the rotation angle $\theta=[\theta_x,\theta_y,\theta_z]^T$

and the translation vector $\mathbf{t} = \left[t_x, t_y, t_z \right]^T$.

B. Affine Transformation

Though, affine transformation can be considered as a simple non-rigid transformation, we classify it as a family of rigid registration. In the 3D case, it has 12 degrees of freedom. Its definition can be expressed by equation (2.4).

$$\mathbf{T}_{Affine}\left(\mathbf{x}\right) = \mathbf{A}_{\mathbf{X}} + \mathbf{t} = \begin{pmatrix} a_{11} & a_{12} & a_{13} \\ a_{21} & a_{22} & a_{23} \\ a_{31} & a_{32} & a_{33} \end{pmatrix} \begin{pmatrix} x \\ y \\ z \end{pmatrix} + \begin{pmatrix} t_x \\ t_y \\ t_z \end{pmatrix} \tag{2.4}$$

2.3.1.2 Non-rigid Transformation (Local Transformation)

The non-rigid transformations can be divided into two types. One type is called as Free-form deformation (FFD), which is based on B-spline. Another type is called Thin-plate spline (TPS), which is based on radial-basis functions. Here, we review the FFD and the TPS.

A. Free form deformation

Free form deformation is also called cubic B-spline based free form deformation (FFD). FFD is widely used for animations in computer graphics. It is based on locally controlled functions such as B-splines and has been successfully applied for image registration [29], [30]. The basic idea of FFD is to deform an object by manipulating an underlying mesh of control points. B-spline transformation is defined on a regular mesh of control points with uniform spacing. Fig 2.2 shows a 2D example of B-spline transformation.

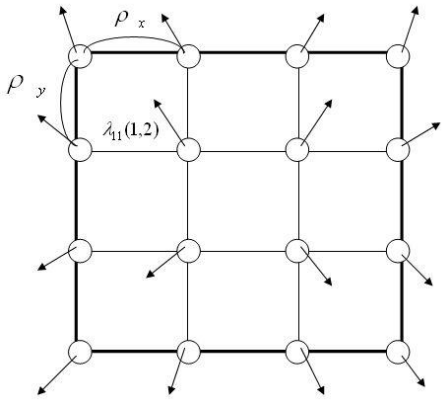

Fig 2.2: Example of 2D B-spline transformation

Let $\boldsymbol{\rho} = \left[\rho_x, \rho_y\right]^T$ to be the spacing of the control points along each axis, the coordinate of a control point can be expressed by $\boldsymbol{\varphi}_{ij} = \left[\varphi_{ij,x}, \varphi_{ij,y}\right]^T = \left[i\rho_x, j\rho_y\right]^T$, where i, j are the sequence number of the control points. Given the coefficients (translations) of the control points denoted as $\boldsymbol{\lambda}_{ij} = \left[\lambda_{ij,x}, \lambda_{ij,y}\right]^T$. The coefficients of the control points, $\boldsymbol{\lambda}_{ij}$, are the parameters of B-spline transformation. Since the cubic B-spline kernel has the width of four, the deformation of each point is only determined by the coefficients of its neighboring 64 control points. This means the B-spline transformation has the ability to control the localized deformation.

For more pragmatic, the 3D B-spline transformation of a point $\mathbf{x}$ can be expressed by equation (2.6).

$$\mathbf{T}_{B-spline}(\mathbf{x}) = \sum_{ijk} \begin{pmatrix} \lambda_{ijk,x} \\ \lambda_{ijk,y} \\ \lambda_{ijk,z} \end{pmatrix} \beta^{(3)}\left(\frac{x-\varphi_{ijk,x}}{\rho_x}\right) \beta^{(3)}\left(\frac{y-\varphi_{ijk,y}}{\rho_y}\right) \beta^{(3)}\left(\frac{z-\varphi_{ijk,z}}{\rho_z}\right) \qquad (2.5)$$

Where $\beta^{(3)}(s)$ is the cubic B-spline kernel defined by equation (2.7).

$$\beta^{(3)}(s) = \begin{cases} (1/2)|s|^{(3)} - |s|^{(2)} + 2/3 & , \; if \;\; 0 \le |s| < 1 \\ -(1/6)|s|^{(3)} + |s|^{(2)} - 2s + 4/3, & if \;\; 1 \le |s| \le 2 \\ 0 & otherwise \end{cases} \qquad (2.6)$$

B. Thin-plate spline transformation

The use of thin-plate spline (TPS) interpolation as point-based elastic registration method of medical images was proposed [32]. This method based on an analogy to the approximate shape of thin metal plates deflected by normal forces at discrete points. The transformation based on thin-plate splines is determined which maps the source and target landmarks

exactly to each other.

We briefly introduce point based registration with TPS transformation in the general context of 3D image in this section. For N pairs of landmarks $(x, y, z) \rightarrow (x', y', z')$, 12+3$N$ coefficients (12 affine and 3N coefficients of radial-basis functions) have to be found to satisfy equation (2.7).

$$\begin{aligned} x' &= a_0 + a_1 x + a_2 y + a_3 z + \sum_{i=1}^{N} F_i r_i^2 \ln r_i^2 \\ y' &= b_0 + b_1 x + b_2 y + b_3 z + \sum_{i=1}^{N} G_i r_i^2 \ln r_i^2 \\ z' &= c_0 + c_1 x + c_2 y + c_3 z + \sum_{i=1}^{N} L_i r_i^2 \ln r_i^2 \end{aligned} \tag{2.7}$$

Where $r_i^2 = (x - x_i)^2 + (y - y_i)^2 + (z - z_i)^2$ and x_i, y_i are the coordinates of the landmark *i*. If we have N pairs landmarks, we will have 3N equations of Eq.2.7 with different landmarks. Then, (x', y', z') can be computed for every point in the image by adding following 12 equations (see equation 2.8).

$$\begin{aligned} &\sum_{i=1}^{N} F_i = 0 \quad \sum_{i=1}^{N} F_i = 0 \quad \sum_{i=1}^{N} L_i = 0 \\ &\sum_{i=1}^{N} x_i F_i = 0 \quad \sum_{i=1}^{N} x_i F_i = 0 \quad \sum_{i=1}^{N} x_i L_i = 0 \\ &\sum_{i=1}^{N} y_i F_i = 0 \quad \sum_{i=1}^{N} y_i F_i = 0 \quad \sum_{i=1}^{N} y_i L_i = 0 \\ &\sum_{i=1}^{N} z_i F_i = 0 \quad \sum_{i=1}^{N} z_i F_i = 0 \quad \sum_{i=1}^{N} z_i L_i = 0 \end{aligned} \tag{2.8}$$

The (12+3N) parameters of TPS are computed by solving the above (12+3N) linear equations. In other words, TPS also has close-form solution for parameter estimation. TPS behaves well for point based registration, but it requires corresponding landmarks for solving the linear equation for obtaining the parameters of transformation. Since it is difficult to find corresponding landmarks in medical images, TPS is not very suitable for medical image registration. On the other hand, FFD do not need any corresponding landmarks and can be solved as an optimization problem by using intensity-based similarity (which will be

described in Sec.2.3.3). So FFD is widely used for non-rigid registration of medical images. In this thesis, we only use FFD for non-rigid registration.

2.3.2 Interpolation

Interpolation is used to generate the transformed moving image during registration. When we transform a point by the spatial transformation, the coordinates of the transformed point usually will fall on a non-grid position in the target image. Since an image is defined on the grids whose coordinates are integral numbers; we can't directly retrieve the intensity value on a point with floating coordinates (See Fig 2.3). In this situation, we can use interpolation to estimate the intensity value of that point from its neighboring points with integral coordinates.

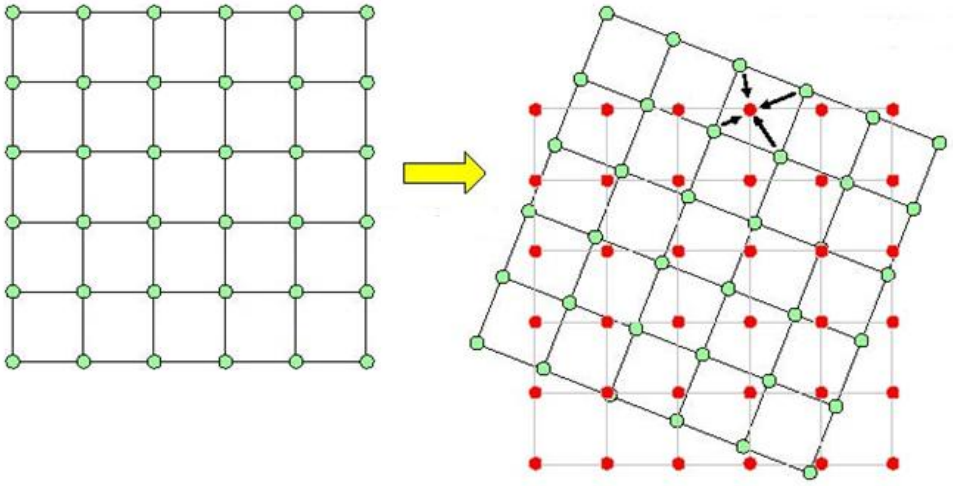

Fig 2.3: The grid coordinate system and the non-gird positions which are caused by transformation

A. Nearest neighbor interpolation

The simplest way is called nearest neighbor (NN) interpolation where the intensity value of a point is assigned as the value of the nearest point with the integral coordinate. The NN method can be performed by Fig 2.4.

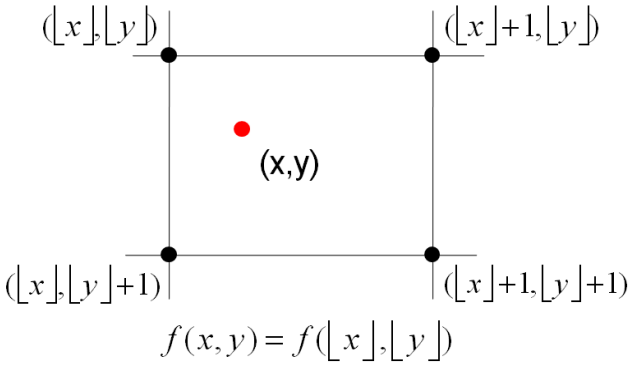

Fig 2.4: The 2D nearest interpolation method

B. Linear interpolation

Linear interpolation is a widely used method in image registration. In 2D case, it is called bilinear interpolation. In bilinear interpolation, the intensity value of a point is calculated by the linear summation from its four neighbors (See Fig 2.5).

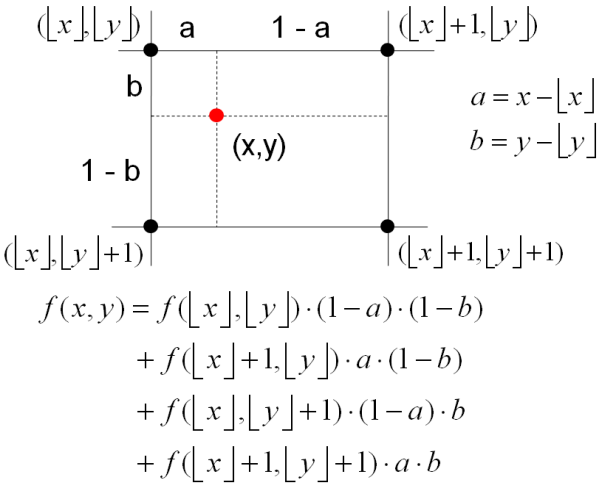

Fig 2.5: The 2D bilinear interpolation method

Linear interpolation is more accurate than NN method and its calculation is efficient.

A survey on interpolation methods is applied at medical image processing [31]. It suggested that cubic B-spline interpolation was the best one considering the accuracy and computing cost. We also tried cubic B-spline interpolation in registration but we found its result was similar to linear interpolation and it needed more time for calculation. Therefore, linear interpolation is applying at this research.

2.3.3 Similarity Criterion

There are many functions of criteria that have been used as the basis for aligning of two images. These criteria functions can be divided into landmark-based, segmentation-based, and intensity-based method. Our works focus on intensity-based methods, because they are more flexible than the others. These kind methods operate directly on the image intensity, so they are also called as a pixel-based or voxel-based method. From another perspective view point, intensity-based method involves minimizing or maximizing a cost function that measures the similarity between the image intensity of corresponding points of two images.

A. Sum of squared intensity difference

One of the simplest intensity similarity based on cost function is the sum of squared intensity difference (SSD) between two medical images which should be minimized during registration. It can be defined by equation (2.9).

$$I_{SSD}\left(f_F, f_M \middle| \mathbf{u}\right) = \frac{1}{N}\sum_{x\in V}\left(f_F\left(\mathbf{x}\right) - f_M\left(T\left(\mathbf{x}\middle|\mathbf{u}\right)\right)\right)^2 \qquad (2.9)$$

Where $\mathbf{x}$ is a set of points in the overlapping region V of the fixed and moving image? SSD is based on the strict assumption that the two images only differ from the Gaussian noise; however this is not the truth for medical images, especially for the multi-modality images. Therefore, this method can be only used for the mono-modal registration, such as the registration of serial MR images [23] [24].

B. Mutual Information

Majority of researches, recently, focus on biomedical image registration utilizes information theoretic of intensity-similarity measures. Mutual information (MI) has been shown to be robust for multi-modality registration, and does not depend on the specific dynamic rang or intensity scaling of images [25], [26], [27]. This research method is based on Shannon definition entropy to use to measure the amount of information contained of signals. Given the probability density function of a signal $p(a)$, the contained information can be calculated by the Shannon's entropy H, shown by equation (2.10).

$$H = -\sum_{a} p(a)\log_2 p(a) \qquad (2.10)$$

Mutual information can measure the information which contained on both two images. It is assumed that when two images are registered that their mutual information can achieve to the maximum volume. Mutual information of two images can be calculated by three entropies of equation (2.11).

$$\begin{aligned} I_{MI}\left(f_F, f_M|\mathbf{u}\right) &= H\left(f_F\right) + H\left(f_M|\mathbf{u}\right) - H\left(f_F, f_M|\mathbf{u}\right) \\ &= -\sum_m p_F\left(m\right)\log_2 p_F\left(m\right) - \sum_n p_M\left(n|\mathbf{u}\right)\log_2 p_M\left(n|\mathbf{u}\right) + \sum_m\sum_n p\left(m,n|\mathbf{u}\right)\log_2 p\left(m,n|\mathbf{u}\right) \end{aligned} \tag{2.11}$$

Where $H(f_F)$ and $H\left(f_M|\mathbf{u}\right)$ are marginal entropies of the fixed and transformed moving images respectively; and $H\left(f_F, f_M|\mathbf{u}\right)$ is the joint entropy of the two images under the transformation parameter $\mathbf{u}$. It can be seen that the three entropies are calculated respectively from two marginal histograms (probability density functions), $p_F\left(m\right)$ and $p_M\left(n|\mathbf{u}\right)$, and the joint histogram $p\left(m,n|\mathbf{u}\right)$. Actually, both of the two marginal histograms can be determined from the joint histogram by equation (2.12). It can be seen that the fixed marginal histogram is not related to the transformation parameter u. This is because that the fixed image is not changed during the registration.

$$\begin{aligned} p_F\left(m\right) &= \sum_n p\left(m,n|\mathbf{u}\right) \\ p_F\left(n|\mathbf{u}\right) &= \sum_m p\left(m,n|\mathbf{u}\right) \end{aligned} \tag{2.12}$$

From equation (2.11) to (2.12) formula processing, it can be concluded that mutual information is actually determined only from the joint histogram $p\left(m,n|\mathbf{u}\right)$. In order to know how mutual information works, we need to understand what is the joint histogram. The joint histogram is determined by the transformation parameter u. During the registration, if the parameter is changed, the joint histogram is also changed. The two variables m,n of $p\left(m,n|\mathbf{u}\right)$ are the intensity bins of the fixed and moving images. The calculation of joint

histogram can be illustrated by Fig 2.6. The $\mathbf{x}$ is a point on the fixed image and the intensity value on this position of m, where $m = f_F(\mathbf{x})$. When the transformation parameter is $\mathbf{u}$, the point $\mathbf{x}$ will be transformed into the coordinate system of moving image and this transformed position is $\mathbf{x}'$, where $\mathbf{x}' = \mathbf{T}(\mathbf{x}|\mathbf{u})$. The intensity value on $\mathbf{x}'$ in the moving image is n, where $n = f_M(\mathbf{x}')$. Then the value on the position (m,n) in the joint histogram will be increased by 1, where $p(m,n|\mathbf{u})++$. This process is terminated until all the samples are used and then the joint histogram of the fixed and moving images under the parameter u can be calculated. It should be noted that only corresponding point pairs inside the overlapping region ($\mathbf{x}$ should be inside the region of the fixed image and meanwhile $\mathbf{x}'$ also should be inside the region of the moving image) can be used for the calculation of joint histogram.

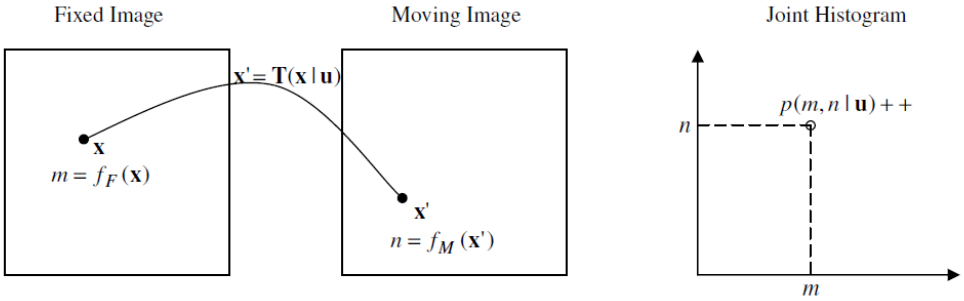

Fig 2.6: Illustrations on calculation of joint histogram

2.3.4 Optimization

Optimization methods of registration are usually adopted to approach the maxima or minima of the cost function by gradually adjusting the parameters of transformation. Generally, there are two kinds of optimization methods which are the gradient and non-gradient based methods. For gradient-based methods, we need to calculate the gradient of the cost function. This gradient-based information is used for adjusting the parameters. Usually, gradient-based method can perform fast, especially when the cost function is smooth and has a large number of parameters. Non-gradient based methods can approach the maxima or minima of the cost function without calculating the gradient. When the gradient is difficult to be calculated, this method is more desirable. But non-gradient based method usually will cost more time for convergence. We will briefly review some of the most widely used optimization methods in the following section.

2.3.4.1 Non-Gradient Based Optimization Methods

A. Powell's Method

Powell's method is a widely used non-gradient based optimization method. It can be represented as the iterated framework shown by equation (2.13).

$$\mathbf{u}_{i+1} = \mathbf{u}_i + \lambda_i \mathbf{d}_i \qquad (2.13)$$

Where $\mathbf{d}_i$ *a set of is* conjugate searching directions; and λ_i is the searching step length which can be determined by searching the minimum from the last iteration position $\mathbf{u}_i$ along the direction $\mathbf{d}_i$.

In Powell's method, the searching directions are constructed by a basic iterative procedure which requires $N+1$ times iterations of linear minimization. The linear minimization can be seen as a 1-dimension problem and it can be resolved by Brent's method [35]. It can be shown that if the cost function is a quadratic function, the minimum can be achieved by $N(N+1)$ times of linear iterations.

B. Genetic Algorithm

A genetic algorithm (GA) [32][33] is a global search technique used in computing to find true or approximate solutions to optimization and search problems. This method maintains a population of candidate solutions (chromosomes) for the problem, and makes it evolve by iteratively applying a set of stochastic operators such as inheritance, mutation, selection, and crossover. Each stochastic operations has special particular function: Inheritance is the ability of modeled objects to mate, mutate (similar to biological mutation), and propagate their problem solving genes to the next generation. Mutation randomly perturbs a candidate solution. Selection replicates the most successful solutions found in a population at a rate proportional to their relative quality. Crossover decomposes two distinct solutions and then randomly mixes their parts to form novel solutions. The general algorithm of GA is described as follow:

produce an initial population of individuals
evaluate the fitness of all individuals
while termination condition not met **do**
select fitter individuals for reproduction
recombine between individuals
mutate individuals

evaluate the fitness of the modified individuals
generate a new population
End while

The advantage of GA is that it can solve every optimization problem which can be described with the chromosome encoding, and weekly depend on initial state. Although GA is an advanced method for global optimization, it requires huge computation cost because of slow astringency, and still falls into local resolution since lacking the fine tuning capabilities or precocity.

2.3.4.2 Gradient Based Optimization Methods

A. Gradient Descent

In this research exploration, it prefers to use gradient-based optimization method in registration. The simplest one is gradient descent (GD) which can be expressed by equation (2.14).

$$\mathbf{u}_{i+1} = \mathbf{u}_i + \lambda \nabla I_i \qquad (2.14)$$

Where ∇I_i is the gradient of the cost function I when the parameter is $\mathbf{u}_i$, λ is the step length.

The main idea of gradient descent is that we can minimize the cost function value if we adjust the parameters along the direction which is opposite to the current gradient. The rationale is that the gradient cost function always points to the direction while the value of cost function increases.

The step length is important for gradient descent. It is a fixed value during the optimization. If it is too small, it will take a long time before cost function approaches to a local minimum; however, if it is too large, there will be an oscillation. There is not a fixed method to choose the step length and usually it can be determined only according to some experiences or several times attempts to try and test. So it is more desirable to find a more smart method which can adjust the step length by itself. Regular step gradient decent is a more clever method which overcomes the oscillating problem of gradient descent. It is also searching the minima along the opposite direction of gradient; however it has a scheme to adjust the step length by itself which can be described by equation (2.15).

$$\begin{cases} if \quad \nabla I_{i-1}^{T} \cdot \nabla I_i \le 0 \quad \rightarrow \quad \lambda_i = \dfrac{\lambda_i - 1}{2} \\ if \quad \nabla I_{i-1}^{T} \cdot \nabla I_i > 0 \quad \rightarrow \quad \lambda_i = \lambda_{i-1} \end{cases} \tag{2.15}$$

Where ∇I_{i-1} and ∇I_i are the gradients of cost function in the two consecutive iteration times.

The inner product of the gradients in the two consecutive iterations is used to judge whether a minimum is passed over. If the minimum is not encountered, the step length will stay as the same. When the inner product is less than zero, the gradient direction in the current time is opposite to one another in the last time which means a minimum is just passed over. The step length will be shortened in this situation in order to avoid the oscillation and ensure this local minimum can be captured. This is the main idea of the regular step gradient descent.

B. Broyden-Fletcher-Goldfarb-Shanno Method

Broyden-Fletcher-Goldfarb-Shanno Method (BFGS) is one of Quasi-Newton method. In numerical optimization, BFGS is an iterative method for solving unconstrained nonlinear optimization problems. As all Newton method, this method uses a matrix of second order derivatives and gradient to determine search direction to find minimum/maxima of objective function.

The algorithm of BFGS method is explained by following step. First, set an initial parameters $\mathbf{u}_0$ and an approximate Hessian matrix $\mathbf{B}_0 = \mathbf{I}$, and a direction $\Delta\mathbf{u}_k$ can be obtained by equation (2.18).

$$\mathbf{B}_k \Delta\mathbf{u}_k = -\nabla E(\mathbf{u}) \tag{2.16}$$

Then, the new parameters $\mathbf{u}_{k+1}$ can be updated by following equation with step-size α_k.

$$\mathbf{u}_{k+1} = \mathbf{u}_k + \alpha_k \Delta\mathbf{u}_k \tag{2.17}$$

In Quasi–Newton methods, the idea is to use matrices which approximate the Hessian matrix

$\mathbf{B}_k$ and/or its inverse $\mathbf{B}_k^{-1}$, instead of exact computing of the Hessian matrix. $\mathbf{B}_k$ can be updated by:

$$\mathbf{B}_{k+1} = \mathbf{B}_k + \frac{\mathbf{y}_k \mathbf{y}_k^T}{\mathbf{y}_k^T \mathbf{s}_k} - \frac{\mathbf{B}_k \mathbf{s}_k \mathbf{s}_k^T \mathbf{B}_k}{\mathbf{s}_k^T \mathbf{B}_k \mathbf{s}_k} \tag{2.18}$$

Where $\mathbf{S}_k = \alpha_k \Delta \mathbf{u}_k$, and $\mathbf{y}_k = \nabla E(\mathbf{u}_{k+1}) - \nabla E(\mathbf{u}_k)$.

BFGS is a very fast and efficient optimization algorithm, but not very robust.

2.4 Issues of Implementation of Registration

Medical image registration is based on the profound mathematical knowledge and algorithm. Moreover, there are some tricks to implement registration method.. It is necessary to in light of some to implement the registration process. The details are illustrated at the following section.

2.4.1 Rotation Center

How to choose rotation center is a very important method in image registration process. Facing different ways of choosing the rotation centers can make the results quite different. In Fig. 2.7 illustrates the effect on rotation angles when different rotation centers are selected. It can be clearly view that even though it is the same rotation the result of rotation angles is different when we choose different rotation centers. The angle, θ is smaller than the angle, θ'. If the rotation center is chosen too far away, however, there are some dangers arising when we do registration. This is due to a small change on the rotation angles which will result in large rotation in this situation. Remember that it needs to gradually adjust the parameters of transformation during registration. If such an adjustment is too large, it will get unreasonable result and registration will be failed. We also can not choose the rotation centers which are too near. This is because the rotation is slowly if we adjust the rotation angles in this situation. Optimization can be easy to be trapped into local minima (maxima).

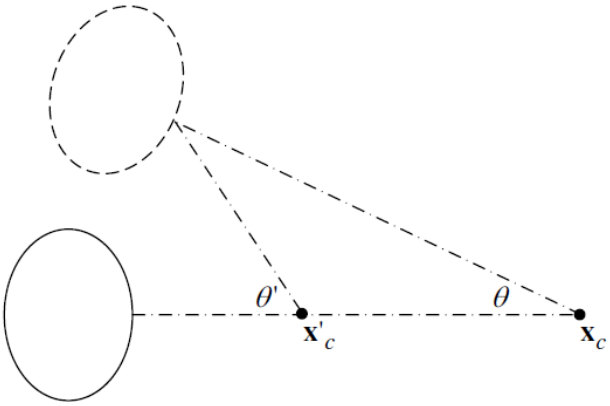

Fig 2.7: Effect on rotation angle

Usually there are two kinds of methods to set the rotation centers. One is to choose center of the fixed image as the rotation centers. The other is to choose the gravity center of the fixed image. In 2D case, the gravity center $\mathbf{x}_c = [x_c, y_c]^T$ can be calculated by equation (2.15).

$$\begin{cases} x_c = \dfrac{\sum_{x,y} x \cdot f_F(x,y)}{\sum_{x,y} f_F(x,y)} \\ y_c = \dfrac{\sum_{x,y} y \cdot f_F(x,y)}{\sum_{x,y} f_F(x,y)} \end{cases} \tag{2.18}$$

2.4.2 Initial Values

The optimization of registration is an iterated way to adjust the parameters to make the cost function approach to reach the minima or maxima level. We need to set initial values for the parameters to let iterated methods at the beginning process. If good initial values are chosen, the optimization can converge very fast; however if bad values are given, the convergence is very slowly and even the registration can be failed.

Usually we use the following method to choose the initial values for parameters of rigid transformation. The initial translations are set as the difference between two gravity centers on the fixed image and moving image. The initial rotation angles are all set to be zero degree under the assumption that usually the rotation difference on the two medical images is not too large. For non-rigid registration, usually we first process rigid registration first. Then, the

results of rigid registration will be used as the initial values for the parameters of non-rigid registration. This can usually ensure the non-rigid registration will reach the reasonable results.

Another method is to determine the initial values according to some corresponding points. We need to determine some corresponding points before registration. By using the point-based method, a rough registration can be done and the results can be used as the initial values for following fine registration. But usually, it is difficult to find the reliable corresponding points in advance.

2.4.3 Partial Derivatives

If gradient-based optimization methods are adopted in registration, we need to calculate the gradient of the cost function. In this calculation, we usually need the partial derivatives of images with respect to each coordinate. Based on our experience, the best way to calculate image derivatives is to convolve image with the partial derivatives of a Gaussian kernel. For the 2D case, this can be expressed by equation (2.16).

$$\begin{cases} \dfrac{\partial f(x,y)}{\partial x} = f(x,y) \otimes \dfrac{\partial G(x,y)}{\partial x} \\ \dfrac{\partial f(x,y)}{\partial y} = f(x,y) \otimes \dfrac{\partial G(x,y)}{\partial y} \end{cases} \tag{2.19}$$

Where $G(x,y)$ is denoted as the 2D Gaussian kernel and the notation of $\otimes$ means the operation of convolution.

Reference of Chapter 2

[1] P.J. Besl and N.D. Mckay, A method for registration of 3D shapes. *IEEE Transaction on Pattern Analysis and Machine Intelligence*. Vol. 14, 1992, pp: 239-256.

[2] D.L.G. Hill, P.G. Batchelor, M. Holden and D.J. Hawkes, Topical review: medical image registration, *Physics in Medicine and Biology*, Vol. 46, 2001, pp: 1-45.

[3] J.V. hainal, L.G. Hill and D.J. Hawkes, *Medical Image Registration*, CRC Press, 2001.

[4] I. Drydden and K. Mardia, *Statistical Shape Analysis*, John Wiley and Sons, NY, 1998.

[5] A.C. Evans, C. Beil, S. Marret, C.J. Thompson and A. Hakin, Anotomical-functional correlation using an adjustable MRI-based region of interest atlas with positron emission tomography, *J. Cereb. Blood Flow Metab*, Vol. 8, 1988, pp: 513-530.

[6] D.L.G. Hill, D.J. Hawkes, J.E. Crossman, et. al., Registration of MR and CT images for skull base surgery using point-like anatomical features, *Br. J. Radiol.*, Vol. 64, 1991, pp: 1030-1035.

[7] C.A. Pelizzari, G.T.Y. Chen, D.R. Spelbring, et. al., Accurate three-dimensional registration of CT, PET and MR images of brain. *J. Comput. Assist. Tomogr.*, Vol. 13, 1989, pp: 20-26.

[8] D.N. Levin, C.A. Pelizzari, G.T.Y. Chen, et. al., Retrospective geometric correlatioin of MR, CT and PET images, *Radiology*, Vol. 169, 1988, pp: 817-823.

[9] T.L. Faber, R.W. McColl, et. al., Spatial and temporal registration of cardiac SPECT and MR images: methods and evaluatioin, *Radiology*, Vol. 179, 1991, pp: 857-861.

[10] G. Borgefors, Distance transformations in arbitrary dimensions. *Comput. Vision Graph. Image Process*, Vol. 27, 1984, pp: 321-345.

[11] H. Jiang, R.A. Robb and K.S. Holton, A new approach to 3-D registration of multomodality medical images by surfaces matching, *Visualization in Brimed. Computing 1992*, Vol. Proc. SPIE 1808, 1992, pp: 196-213.

[12] M. van Herk and H.M. Kooy, Automated three-dimensional correaltion of CT-CT ,CT-MRI and CT-SPECT, *Med. Phys*, Vol. 21, 1994, pp: 1163-1178.

[13] C.T. Huang and O.R. Mitchell, A Euclidean distance trasform using graysalce morphology decomposition, *IEEE Trans. Pattern Anal. Mach. Intell.*, Vol. 16, 1994, pp: 443-448.

[14] E. Cuchet, J. Knoplioch, D. Dormont and C. Marsault, Registration in neurosurgery and neuroradiotherapy appliction, *J. Image Guided Surg.*, Vol. 1, pp: 198-207, 1995.

[15] J. Declerck, J. Feldmar, M.L. Goris and F. Betting, Automatic registration and alignment on a template of cardia stress and rest reoriented SPECT images, *IEEE Trans. Med. Img.*, Vol. 16, 1997, pp: 727-737.

[16] C.R. Maurer, Jr., R.J. Maciunas, and J.M. Fitzpatrick, Registration of head CT images to physical space using multiple geometrical features, *Med. Imaging 1998: Image Process.*, Vol. Proc. SPIE 3338, 1998, pp: 72-80.

[17] H. Jiang, R.A. Robb and K.S. Holton, A new approach to 3-D registration of multomodality medical images by surfaces matching, *Visualization in Brimed. Computing 1992*, Vol. Proc. SPIE 1808, 1992, pp: 196-213.

[18] M. van Herk and H.M. Kooy, Automated three-dimensional correaltion of CT-CT ,CT-MRI and CT-SPECT, *Med. Phys*, Vol. 21, 1994, pp: 1163-1178.

[19] C.T. Huang and O.R. Mitchell, A Euclidean distance trasform using graysalce morphology decomposition, *IEEE Trans. Pattern Anal. Mach. Intell.*, Vol. 16, 1994, pp: 443-448.

[20] E. Cuchet, J. Knoplioch, D. Dormont and C. Marsault, Registration in neurosurgery and neuroradiotherapy appliction, *J. Image Guided Surg.*, Vol. 1, pp: 198-207, 1995.

[21] [21] J. Declerck, J. Feldmar, M.L. Goris and F. Betting, Automatic registration and alignment on a template of cardia stress and rest reoriented SPECT images, *IEEE Trans. Med. Img.*, Vol. 16, 1997, pp: 727-737.

[22] [22] C.R. Maurer, Jr., R.J. Maciunas, and J.M. Fitzpatrick, Registration of head CT images to physical space using multiple geometrical features, *Med. Imaging 1998: Image Process.*, Vol. Proc. SPIE 3338, 1998, pp: 72-80.

[23] J.V. Hajnal, N. Saeed, E.J. Soar, et.al., A registration and interpolation procedure for subvoxel matching of serially aquired MR image, J. Comput. Assist. Tomogr., Vol. 19, 1995, pp: 289-296.

[24] J.V. Hajnal, N. Saeed, A. Oatridge, et.al., Detection of subtle brain changes using subvoexl registration and subtraction of serial MR images, J. Comput. Assist. Tomogr., Vol. 19, 1995, pp: 677-691.

[25] J.P.W. Pluim, J.B.A. Maintz and M.A. Viergever, Mutual information based registration of medical images: a survey, *IEEE Transactions On Medical Imaging*, vol. 22, no. 8, 2003, pp. 986-1004.

[26] A. Collignon, F. Maces, et.al., Automated multi-modality image registration based on information theory. *Proc. of Information Processing in Medical Imaging*, 1995, pp: 263-274.

[27] F. Maces, A. Collignon, et.al., Multimodality image registration by maximization of mutual information, *IEEE Trans. on Medical Imaging*, Vol. 16, 1997, 187-198.

[28] D. Rueckert, L.I. Sonoda, C. Hayes, et.al., Non-rigid registration using free-form deformations: application to breast MR images. *IEEE Trans. on Med. Imgaging*, Vol. 18, No. 8, 1999, pp: 712-721.

[29] C.F. Ruff, S.W. Hughes and D.J. Hawkes, Volume estimation from sparse planar images

using deformable models. *Image Vision Computing*, Vol. 17, 1999, pp: 559-565.

[30] G.E. Christensen, R.D. rabbitt and M.I. Miller, Deformable templates using large deformation kinematics, *IEEE Trans. on Image Process.*, Vol. 5, No. 10, 1996, pp: 1435-1447.

[31] T.M. Lehmann, C. GÄonner and K. Spitzer, Survey: interpolation methods in medical image processing, *IEEE Trans on Med. Imaging*, Vol. 18, No. 11, 1999, pp: 1049-1075.

[32] J. M. Rouet, J. J. Jacq, and C. Roux, "Genetic algorithms for a robust 3-D MR-CT registration," *IEEE Transactions on information Technology in Biomedicine*, vol. 4, no. 2, pp. 126–136, 2000.

[33] C. K. Chow, H. T. Tsui, and T. Lee, "Surface registration using a dynamic genetic algorithm," Pattern Recogn., vol. 37, pp. 105–117, 2004.

Chapter 3

Hybrid Particle Swarm Optimization and Its Application to Multimodal 3D Medical Image Registration

3.1 Introduction

In the area of medical image analysis, multi-modality 3D image registration is an important issue [1]. The propose of image registration is to register a target image (moving image) to a reference image (fixed image) so that we can combine the information of two images to obtain more detailed information or some specific features. For example, the PET image usually shows metabolic activity of organs and abnormal tissues clearly but leaks the texture of organ tissues. On the other hand, the MR image is described by more complex intensities to represent the texture of organ tissues more clearly.. If we implement the MR-PET image registration to combine the information of two images which are different modality, then we can get the accurate shape, volume, and location of abnormal tissues form the registered image. This application is very ponderable contribution and very helpful for medical diagnosis or for surgeon to perform surgical operation.

The processing of registration can be seen as an iterated optimization framework and it can be divided into 3 parts: transformation, cost function, and optimization. In the each iteration, the target image is firstly transformed by transformation according to the parameter of the current time. Then, the reference image and the transformed target image are used to calculate the cost function which can evaluate whether the two images are registered or not under the current parameter of transformation. If the images are not registered, an optimization method will be used to adjust the parameters and a new iteration will start. We have performed non-rigid registration with a very good result by modifying the cost function in our previous achievement [2]. Now, we try to find an advance optimization method to improve the accuracy of registration problem.

The application of registration can be classified by dimensionality of image, modality of image, and model of transformation. There are 2D to 2D, 3D to 2D, and 3D to 3D image registration

for many different applications. The 3D to 3D image registration usually needs to estimate more parameters than the 2D to 2D image registration, so it does require a more advance optimization. Then, if two images which have different scope of intensity have to be registered, such as CT-MR registration, it is called multi-modality registration. On the other hand, if register two image which have same range of intensity, it is called mono-modal registration. Depend on the modal of registration, the different cost function have been used, such as the sum of squared intensity difference (SSD) for mono-modal registration or mutual information (MI) for multi-modality registration. Moreover, the model of transformation determines whether a registration belongs to rigid or non-rigid one. If target objects which we want to register them with different shapes or deformable image such as liver, the non-rigid transformation is used, it is called non-rigid registration; otherwise it is named a rigid registration. Our research work which is described in this paper is focus on rigid multi-modality 3D medical image registration and it is a marvelous challenge to complete difficult task.

As our previous explaining, we estimate the parameter of transformation by optimizing a cost function (similarity metric) in the processing of registrations. Some local optimization techniques, such as the gradient decent method, are frequently used for medical image registrations [3] [9]. However, since the transformation parameters are generally non-convex and irregular, this kind of methods require very good initial values in order to avoid the local minimum.

To overcome the local resolution problem, the genetic algorithm (GA), which is one of the global optimization techniques, has been proposed for medical image registrations [4]. Although GA is an advanced method for global optimization, it requires consuming a huge computation time and lacks of fine tuning capabilities. It needs a more powerful approach to solve this problem. Particle swarm optimization (PSO) is a new global optimization technique. This method is a stochastic, population-based evolutionary computer algorithm [5] [6]. PSO is an extremely simple algorithm and it seems to be more effective for optimizing a wide range of functions, and has been shown very effective for 2D rigid image registration [7], but it is less diversity compare with GA [14].

In our experiments, we found that conventional GA and PSO can't find the global optimum resolution well, when it faces to estimate a huge number of parameters and large geometric difference between two images. Thus, we propose a new approach named hybrid particle swarm optimization (HPSO) by combining both idea of PSO and GA. This research shows the experimental results with both mathematical test functions and medical volume data, and it

is demonstrated that the proposed HPSO performs much better results than conventional gradient decent, GA and PSO methods, especially for the 3D image registration with large geometric difference between two images. Furthermore, we also applied our research method to 2D non-rigid registration and show the experimental results in this article.

The chapter is composed as follows: the particle swarm optimization (PSO) and the proposed hybrid particle swarm optimization (HPSO) are presented in Sec 3.2, the experimental results with both mathematical test functions and medical volume data are presented in Sec 3.3, finally, the conclusion and future works are given in Sec 3.4.

3.2 Hybrid Particle Swarm Optimization

In this section, we propose a new approach named hybrid particle swarm optimization (HPSO) for 3D rigid medical volume registration. For describing more detailed, we show the traditional PSO first.

3.2.1 Particle Swarm Optimization

Swarm Intelligence (SI) is an innovative distributed intelligent paradigm for solving optimization problems. Particle Swarm Optimization (PSO) incorporates swarming behaviors observed in flocks of birds, schools of fish, or swarms of bees, and even human social behavior. This method is also a stochastic, population-based evolutionary computer algorithm which can be implemented and applied easily to solve various function optimization problems. The main strength of PSO is its fast convergence, which compares favorably with many global optimization algorithms such as GA. For applying PSO, one of the key issues is finding how to map the problem solution into the PSO particle, which directly affects its feasibility and performance.

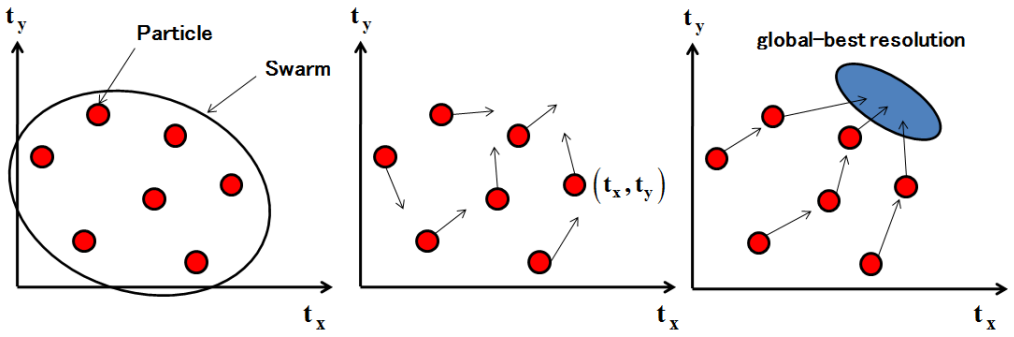

Fig 3.1: The illustrations of PSO simulation

The Fig 3.1 shows the basic idea of PSO. Assume an extent diffuse population existing which is called a swarm and an individual member of the swarm, now is termed as a particle. A particle can be imaged as a point which is searching optima position in a D-dimensional search space. A group of particle tent to cluster at a position where optimized results are identified. Therefore, to achieve particle swarm optimization, each particle adjusts its moving speed dynamically corresponding to the previous experiences of itself and its colleagues for finding the optimized position. The movement of each particle is shown in Fig 3.2.

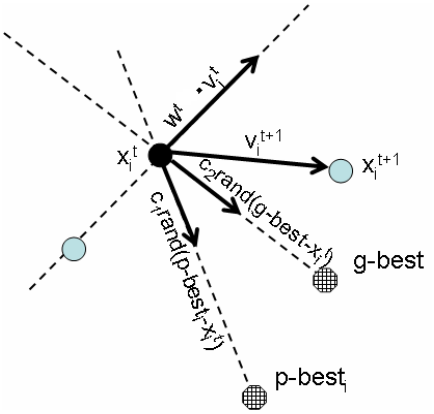

Fig 3.2 : The movement of each particle

Each particle remembers its best value so far (**p_best**) and its position. Moreover, each particle knows the best value so far in the group (**g_best**) among all **p_best**. This information is analogy of knowledge of how the other particles around them have performed. Each particle tries to modify its position using the distance between the current position and **p_best,** and also tend to gather at optimized position with the distance between the current position and **p_best**.

In each iteration *t*, the position of particle *i* is represented as $\mathbf{x}_i^t = [x_{i1}, x_{i2}, \cdots, x_{iD}]^t$, each particle also maintains a memory of its previous best position is represented as $\mathbf{p\_best}_i^t$, and the best position of whole group is indicated as $\mathbf{g\_best}^t$. Since a particle in a swarm is moving with a velocity, which can be represented as $\mathbf{v}_i^t = [v_{i1}, v_{i2}, \cdots, v_{iD}]^t$. The formula of particle swarm optimization can be represented as follows:

$$\mathbf{v}_i^{t+1} = w^t \mathbf{v}_i^t + c_1 \cdot rand_1 \cdot \left[\mathbf{p\_best}_i^t - \mathbf{x}_i^t\right] + c_2 \cdot rand_2 \cdot \left[\mathbf{g\_best}^t - \mathbf{x}_i^t\right] \qquad (3.1)$$

Where c_1 and c_2 determine the relative influence of the cognitive component and the relative influence of the social component separately. The *rand1* and *rand2* are the random numbers distributed in the interval [0,1], and are used to maintain the diversity of the population. The *w* is called as the inertia factor which controls the influence of previous velocity on the new velocity.

$$w(t+1) = w(t) + dw,\ dw = \frac{(w_{\min} - w_{\max})}{T} \tag{3.2}$$

Finally, current position of each particle can be modified by equation (3.3).

$$\mathbf{x}_i^{t+1} = \mathbf{x}_i^t + \mathbf{v}_i^{t+1} \tag{3.3}$$

All particles tend to move towards better positions, because the best position (optimum solution) can eventually be obtained through the combined effort of the whole population.

The flowchart of PSO for image registration is shown in Fig 3.3.

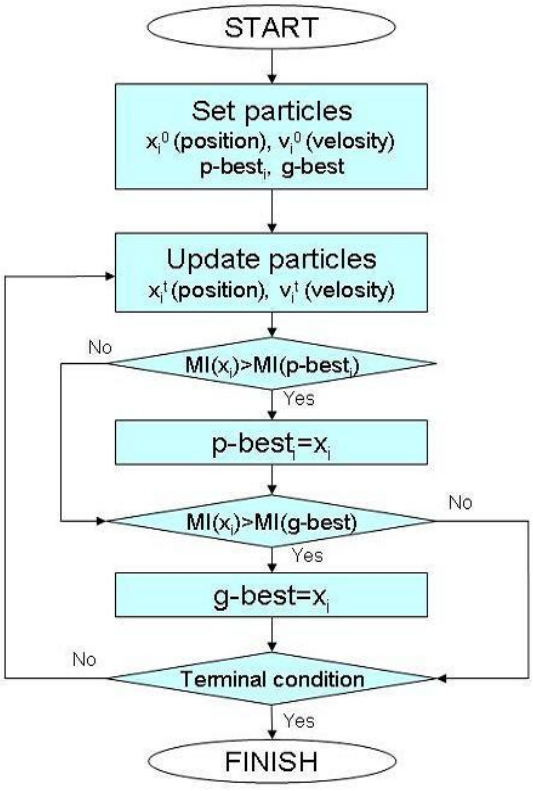

Fig 3.3: Flowchart of PSO

3.2.2 Hybrid Particle Swarm Optimization

In this section, we propose a new approach named hybrid particle swarm optimization (HPSO) for 3D rigid medical volume registration. Our method incorporates two concepts of genetic algorithms, which are subpopulation and crossover, into the traditional PSO. We expect that our proposed method will improve the accuracy of registration by taking advantage of subpopulation and crossover. The flowchart of HPSO is shown in Fig 3.4.

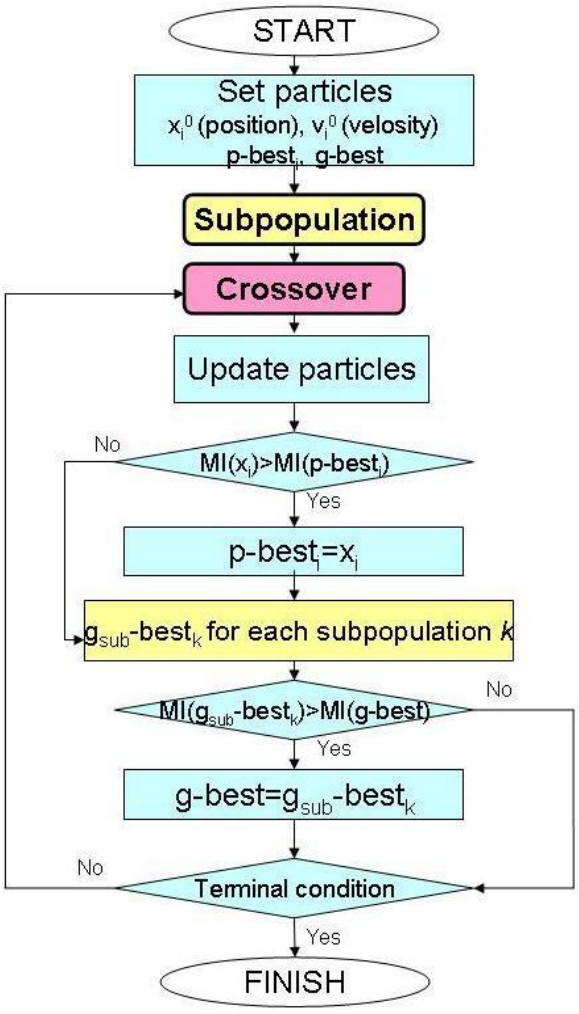

Fig 3.4: Flowchart of HPSO

Subpopulation: The particles are divided into a number of subpopulations. Each subpopulation have own best optimum, g_{sub}-$best_k$.. The process of PSO is done for each subpopulation group. If g_{sub}-$best_k$ is better than *g-best, then g-best* is replaced by the g_{sub}-$best_k$, where k is the subpopulation number.

Crossover: The g_{sub}-$best_i$ is sorted in order with large mutual information. The top two g_{sub}-$best$ are selected as parents ($\mathbf{x}_i$ and $\mathbf{x}_j$) for crossover, where i and j are their subpopulation number. The offspring are generated for each by arithmetic crossover, which are shown as follows:

$$\begin{aligned} \mathbf{x}_i' &= rand \cdot \mathbf{x}_i + (1 - rand) \cdot \mathbf{x}_j \\ \mathbf{x}_j' &= rand \cdot \mathbf{x}_j + (1 - rand) \cdot \mathbf{x}_i \end{aligned} \tag{3.4}$$

And the velocities are given by:

$$\begin{aligned} \mathbf{v}_i' &= \mathbf{v}_i V \\ \mathbf{v}_j' &= \mathbf{v}_j V \qquad V = \frac{(\mathbf{v}_i + \mathbf{v}_j)}{\left\| \mathbf{v}_i + \mathbf{v}_j \right\|} \end{aligned} \tag{3.5}$$

Where *rand* is a uniformly distributed random number which among 0 to 1. The worst particle in the same subpopulation is replaced by the offspring.

3.3 Experiments and Results

In this section, we perform several registration experiments with both test functions and medical volume data to evaluate the performance of the proposed HPSO technique. Meanwhile, it also performs conventional GA and PSO for comparison. Finally, it implements the parallel technique to reduce computation cost and show the efficiency of our implementation.

3.3.1 Benchmark Function Evaluation

In this part, we apply 4 of Benchmark functions which have different number of parameters to estimate the accuracy of our proposed method. The functions which were used are shown as below:

The functions are commonly used for evaluation experiments and cover a variety of characteristics that affect algorithmic performance [10]. F1 is unimodal with global minimum at center and has 3 parameters to be estimated. F2 is strong epitasis with global minimum at center and has 2 parameters to be estimated. F3 is highly multi-modal with global minimum

at center and has 20 parameters to be estimated. F4 is multi-modal with global minimum at corner and has 10 parameters to be estimated. F3 and F4 are more difficult than F1 and F2, and F3 is the most difficult problem.

$$F1: \quad f(x_i|_{i=1,\ldots,3}) = \sum_{i=1}^{3} x_i^2 \qquad x_i \in [-5.12, 5.11] \tag{3.6}$$

$$F2: \quad f(x_i|_{i=1,2}) = 100(x_1^2 - x_2) + (1 - x_1^2)^2$$

$$x_i \in [-2.048, 2.047] \tag{3.7}$$

$$F3: \quad f(x_i|_{i=1,\ldots,20}) = (20 \times 10) + \left[\sum_{i=1}^{20} (x_i^2 - 10\cos(2\pi x_i)) \right]$$

$$x_i \in [-5.12, 5.11] \tag{3.8}$$

$$F4: \quad f(x_i|_{i=1,\ldots,10}) = 1 + \sum_{i=1}^{10} \frac{x_i^2}{4000} - \prod_{i=1}^{10} \cos\left(\frac{x_i}{\sqrt{i}}\right)$$

$$x_i \in [-5.12, 5.12] \tag{3.9}$$

A total of 40 runs of 100 generations each for each function and each method were performed. The population size is 56 for GA, PSO and HPSO, respectively and the number of subpopulation is 4 for HPSO. The relative mean square error between the estimated solutions and real solutions is calculated for each trial. Table 3.1 shows the averaged relative mean square error over 40 trials for each method.

Table 3.1: Averaged relative mean square error over 40 trials for each method

	Number of parameters	GA(%)	PSO(%)	HPSO(%)
F1	3	0.09	0	0
F2	2	0.89	0	0
F3	20	70.13	67.65	11.49
F4	10	15.62	11.38	1.64

As shown in Table 3.1, both PSO and HPSO can get perfect solutions and GA can also get a reasonable result for F1 and F2 in which the number of parameters are only 3 and 2,

respectively. On the other hand, as increasing the number of parameter (F3 and F4), both conventional GA and PSO fail to get a reasonable results especially for F3, while the proposed HPSO can get perfect solutions even for F3 and performs much better results than conventional GA and PSO.

According to our experiments, we also found that our method is strongly affected by the number of subpopulations. The Fig. 3.5 shows the average square error of experiments which evaluate the F3 for 40 runs in different number of subpopulations; all of experiments which use 5600 particles have been set. We can see that the curve of average square error is getting down when the number of subpopulations is increased. This result indicates that our HPSO method can provide higher accuracy while using more subpopulation. Judging by our experimental results, the best number of subpopulation for our method is 8.

Fig 3.5: The curve of average square error shows more subpopulations will increase the accuracy of our method

3.3.2 Medical Volume Registration

In this section, we perform several registration experiments with medical volume phantom data to evaluate the performance of the proposed HPSO technique.

(A) Simulation Data

Firstly, it uses some simulate data to test our proposed. Fig.3.6 shows some slices of our test

data for 2 experiments which have different transformation parameters. The size of each volume is resized by $128\times128\times15$, and the spacing of each volume is $2.59\times2.59\times8.0$ (mm).

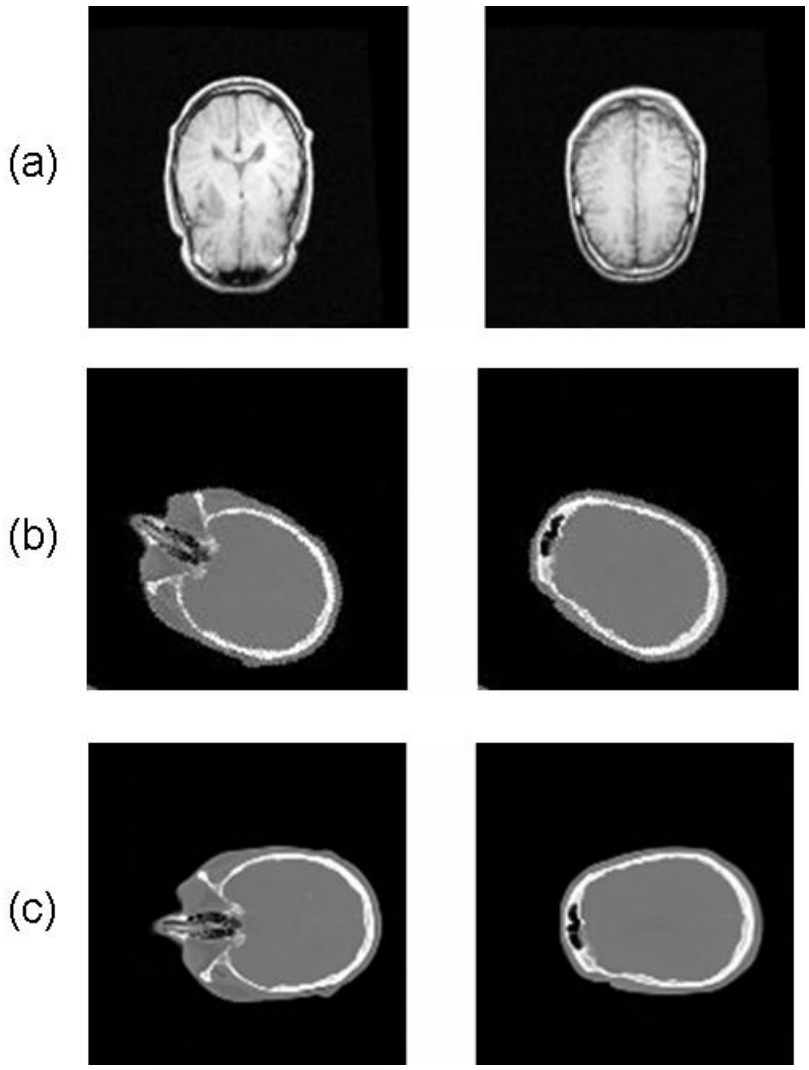

Fig 3.6: (a) MR volume (fixed image data); (b) CT volume (moving image data) of experiment 1 ((b) to (a)); (c) CT volume (moving image data) of experiment 2 ((c) to (a))

These simulate data is made by specific parameters which we give it, so that we can easily estimate the result of registration parameters by using these answers (ground troth). Table 3.2 and Table 3.3 show the comparative results of our HPSO and the previous method (GA and PSO), that the diff is defined as difference between experimental results and ground troth. According to the experimental results which are shown above, we realize our proposed method can provide more exact result of registration parameters than conventional method. This is the first evidence to prove that our HPSO is a better optimization approach.

Table 3.2: Comparison result of registration parameters ((b) to (a))

	Translation				Rotation (Degree)			
	T_x	T_y	T_z	diff	θ_x	θ_y	θ_z	diff
Answer	20.0	10.0	2.0	-	0.0	0.0	120.0	-
GA	-2.6	-13.3	-0.01	10.84	44.93	45.25	149.49	23.42
PSO	-4.84	-9.95	0.09	10.64	53.41	60.39	120.27	26.87
HPSO	20.04	11.16	1.75	0.40	-0.25	-0.48	117.57	0.83

Table 3.3: Comparison result of registration parameters ((c) to (a))

	Translation				Rotation (Degree)			
	T_x	T_y	T_z	diff	θ_x	θ_y	θ_z	diff
Answer	10.0	5.0	2.0	-	0.0	0.0	90.0	-
GA	5.33	0.21	0.50	2.29	31.58	40.42	61.94	19.49
PSO	-4.84	2.25	-0.03	2.05	29.21	35.67	92.30	15.39
HPSO	9.98	5.11	1.83	0.07	-0.20	-0.52	87.95	0.71

(B) Clinical Data

The Vanderbilt database [11] is also used to evaluate the performance of our proposed HPSO (see Fig 3.7). This database gives both multi-modality brain volumes and their marker-based golden standard transforms. These rigid transforms are determined by marker-based prospective registration techniques and represented by eight couples of 3-D points on both of two medical volumes. Such a golden standard transform can be considered as a ground truth (correct one). The size of each volume is resized to, $256\times256\times29$ and the spacing of each volume is $1.25\times1.25\times4.0$ (mm).

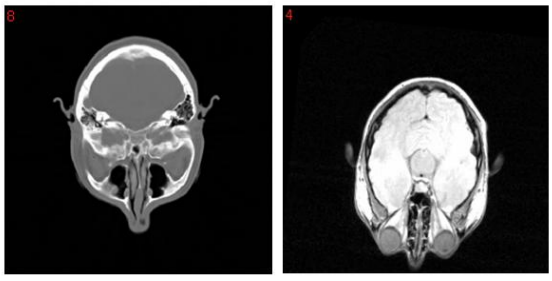

(a) (b)

Fig.3.7: (a) A slice of CT image of Vanderbilt database; (b) A slice of MR image of Vanderbilt database

At this point, we try gradient decent method, GA, PSO and HPSO on CT to solve MR registration problem. A total of 3 runs with different random initial values for each method were performed. Eq 3.13 is used to compare the registration accuracy between transformed landmarks in moving image $\left(T\left(\mathbf{x}_{Mi}|\mathbf{u}\right)-\mathbf{x}_{Fi}\right)$ and landmarks in fixed image $\left(\mathbf{x}_{Fi}\right)$.

$$e=\frac{1}{8}\sum_{i=1}^{8}\left\|T(\mathbf{x}_{Mi}|\mathbf{u})-\mathbf{x}_{Fi}\right\| \tag{3.10}$$

The averaged accuracy of registration results for each method is shown in Table 3.4. It can be prove that this research proposed HPSO performs have much better results than conventional gradient decent method, GA and PSO.

Table 3.4: Comparison of registration accuracy (mm)

gradient decent	GA	PSO	HPSO
5.62	9.75	8.89	2.36

3.3.3 2D Non-rigid Registration

The problem for application of HPSO to 3D non-rigid registration is its large computational cost. Suppose the size of a volume image is 512 x 512 x 512, a 15 x 15 x 15 mesh should be used for FFD, and the number of control points will be 16 x 16 x 16 = 4096. Therefore, the number of parameters for FFD is 4096 x 3 = 12288. For estimated such a huge number of parameters, we have to use at least 10 times amount of particles, so the number of particles will be 12288 x 10 = 122880. Each particle should save 12288 parameters for FFD, 12288 parameters for velocity, and 12288 parameters for personal best results. Hence, amount of all particles is 12288 x 3 x 122880 x 2 = 9059696640 bytes with 16 bit double, about 8.44 Giga byte. Moreover, we have to give at least one volume for each subpopulation. According to our experiments, we used 8 subpopulations. The total amount of memory for 8 volumes is 512 x 512 x 512 x 8 = 1073741824 bytes with 8 bit volume, about 1 Giga bytes. Therefore, to consider the remain memory requirements such as parameters of 8 best results for each subpopulations, parameters of global best result, and operation system, we need about 10 Giga bytes memory to implement 3D non-rigid registration, and our current device can't satisfy this memory requirement.

Instead of 3D non-rigid registration, we performed a 2D non-rigid registration to evaluate our

proposed method. In situation of 2D non-rigid registration, we first execute a magnifying process to Fig 3.8 (a) with the 2D FFD method which is represented by Eq (3.11).

$$\mathbf{T}_{B-spline}(\mathbf{x}) = \sum_{ijk} \begin{pmatrix} \lambda_{ij,x} \\ \lambda_{ij,y} \end{pmatrix} \beta^{(2)}\left(\frac{x-\varphi_{ij,x}}{\rho_x}\right) \beta^{(2)}\left(\frac{y-\varphi_{ij,y}}{\rho_y}\right) \tag{3.11}$$

Where $\beta^{(2)}(s)$ is the linear B-spline kernel defined by Eq (3.12).

$$\beta^{(2)}(s) = \begin{cases} -1.8|s|^2 + 0.1|s| + 1.0, & if\ 0 \le |s| < 0.5; \\ 1.8|s|^2 + 3.7|s| + 1.9, & if\ 0.5 \le |s| \le 1; \\ 0, & otherwise; \end{cases} \tag{3.12}$$

Then we obtain a new fixed image which is shown by Fig 3.8 (b).

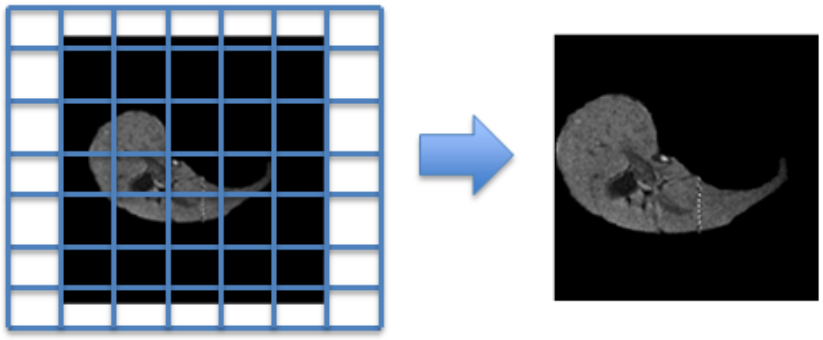

Fig 3.8: (a) Magnifying original image as a new fixed image with a 7x7 mesh using FFD. (b) Magnified fixed image.

A non-rigid registration processing can be divided into two parts: rigid registration and non-rigid registration. To depend on executing the rigid registration before non-rigid image registration, we can get a more reasonable initial position of a moving image for the non-rigid registration. In rigid registration, 2 parameters of translation and 2 parameters of rotation were estimated for rigid transformation. For non-rigid registration, a 2D FFD was applied

with a 7x7 mesh (8x8=64 control points). Therefore, there are totally 128 parameters have to be estimated.

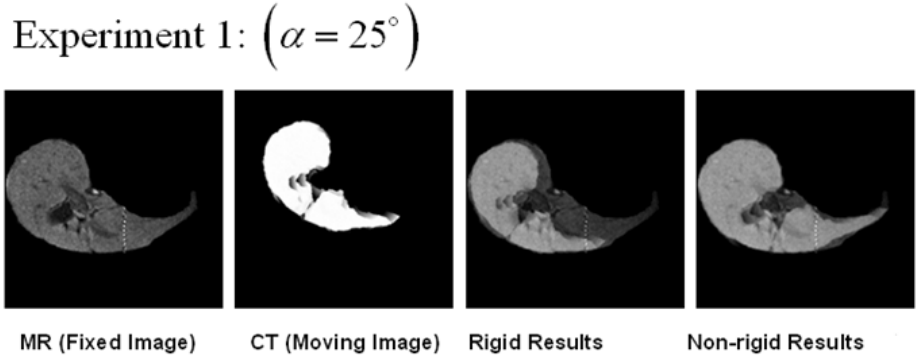

（a）

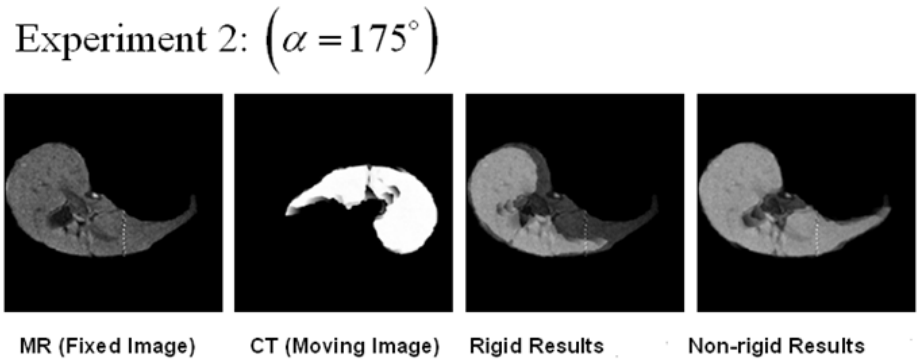

（b）

Fig 3.9: The results of non-rigid registration. (a) Result of EX1, the moving image was rotated with 25 degree. (b) Result of EX2, the moving image was rotated with 175 degree.

Two experiments have been performed to test the capability of our proposed method in case of non-rigid registration. In this experiment, two moving images which have different rotation angel are used. The experimental results of non-rigid registration have been displayed by Fig 3.9. This result indicates the research proposed method can provide a good registration result even if the moving image has a larger rotation angle in case of non-rigid registration.

3.3.4 Parallel implementation

The efficiency of registration is an important issue presently [12] [13]. Although, we have

shown the accuracy in the previous description but almost global optimization have a big drawback which is it will consume a huge computation cost. We applied our proposed HPSO to a computer which has multi-core CPU and implement it with parallel technique to overcome this problem. For register two images with size of $512 \times 512 \times 512$, the average computation cost of 10 times experiments is reduced to 1893.637 sec from 3661.747 sec by our implementation. This improving makes our proposed method more useful.

3.4 Conclusion and Future Works

This research article introduces a new global emerging optimization approach named hybrid particle swarm optimization (HPSO) which composed of two concepts, one is subpopulation and another is crossover of genetic algorithms into the conventional PSO. We performed both functional evaluation and 3-D rigid medical volume registration to estimate the proposed method. First, 4 functions have been applied to test the ability of our method for finding the global resolution and avoiding the local resolutions. Then, in case of 3-D rigid medical volume registration, we applied our HPSO to both simulate data and Vanderbilt data to discover the capability of this method for real medical volume registration. In order to comparison the result conventional methods such as GA and PSO are also used for each experiment. All experimental results prove that the proposed HPSO performs have much better image quality results than conventional GA and PSO. Therefore, at this research, we can summarize that this research finding and contribution of HPSO is an advance optimization method.

Furthermore, this work can be extended to 3D non-rigid registration in order to cover more computer assisted surgery application such as real time liver tumor resection. Moreover, extending this research, we are striving for to explore a more powerful non-rigid transformation and provide improvement of lesser parameters and empower 3D non-rigid registration capability by contains more parameters.

Reference of Chapter 3

[1] S. Morikawa, T. Inubushi, Y. Kurumi, S. Naka, K. Sato, T. Tani, I. Yamamoto, M. Fujimura. "MR-Guided microwave thermocoagulation therapy of liver tumors: initial clinical experiences using a 0.5 T open MR system". *J. Magn. Reson. Imaging*. Vol. 16, pp. 576-583, 2002.

[2] R. Xu, Y. W. Chen, Y.T. Song, S. Morikawa and Y. Kurumi, "Application of Non-rigid Medical Image Registration on Open-MR based Liver Cancer Surgery", *International Journal of Computer Assisted Radiology and Surgery*, Vol. 1, pp.286-288, 2006.

[3] L. Brown, "A survey of image registration technique", *ACM Comput. Surv.*, Vol. 24, pp: 325-376, 1992.

[4] J. M. Rouet, J. J. Jacq, and C. Roux, "Genetic algorithms for a robust 3-D MR-CT registration," *IEEE Trans. Inform. Techno .Biomed,* Vol. 4, pp.126–136, 2000.

[5] J. Kennedy and R.C. Eberhart, "Particle swarm optimization," in *Proc. IEEE Int. Conf. Neural Networks*, Vol. 4, pp. 1942-1948, 1995.

[6] Q. Bai, "Analysis of Particle Swarm Optimization Algorithm," Computer and Information Science, vol. volume 3 No 1, Pebruari 2010 2010.

[7] Mark P. Wachowiak, Renata Smolíková, Yufeng Zheng, Jacek M. Zurada, and Adel S. Elmaghraby, "An Approach to Multimodal Biomedical Image Registration Utilizing Particle Swarm Optimization", *IEEE Transactions on Evolutionary Computation*, Vol. 8, 2004.

[8] Y.-W.Chen, C.-L. Lin and A. Mimori, "Multimodal Medical Image Registration Using Particle Swarm Optimization", *Proc. of ISDA2008*, Vol.3, pp.127-131, 2008.

[9] J. Pluim, A. Maint, "Mutual information-based registration of medical image: a survey", *IEEE Transactions on Medical Imaging*, pp. 986-1004, 2003.

[10] D.Whitley, S.Rana, and K.Mathias, "Evaluating evolutionary algorithms", *Artificial Intelligence*, Vol.85, pp.245-276(1996).

[11] J.West et al., "Comparison and evaluation of retrospective intermodality brain image registration techniques", *J. Comput. Assist. Tomogra.*, Vol.21, pp.554-566, 1997.

[12] Ramtin Shams, Parastoo Sadeghi, Rodney A. Kennedy, and Richard I. Hartley, "A Survey of Medical Image Registration on Multicore and the GPU", IEEE SIGNAL PROCESSING MAGAZINE 27(2), Pages 50–60, March 2010.

[13] Ramtin Shams, Parastoo Sadeghi, Rodney Kennedy, Richard Hartley, "Parallel computation of mutual information on the GPU with application to real-time registration of 3D medical images", Computer Methods and Programs in Biomedicine Volume 99, Issue 2 , Pages 133-146, August 2010.

[14] K. Premalatha, "Hybrid PSO and GA for Global Maximization", Int. J. Open Problems Compt. Math., Vol. 2, No. 4, December 2009

Chapter 4

Principal Component Analysis Based Regional Mutual Information for Robust Medical Image Registration

4.1 Introduction

Medical image registration is becoming more and more important research topic in biomedical research [1-3]. The process of medical image registration can be represented by four phases, which are transformation, interpolation, criterion and optimization in Fig 4.1 illustration. In criterion phase, many images with similarity metrics have been used as the basis to align two images. Therefore, the metric is one of the most critical components of medical image registration processing.

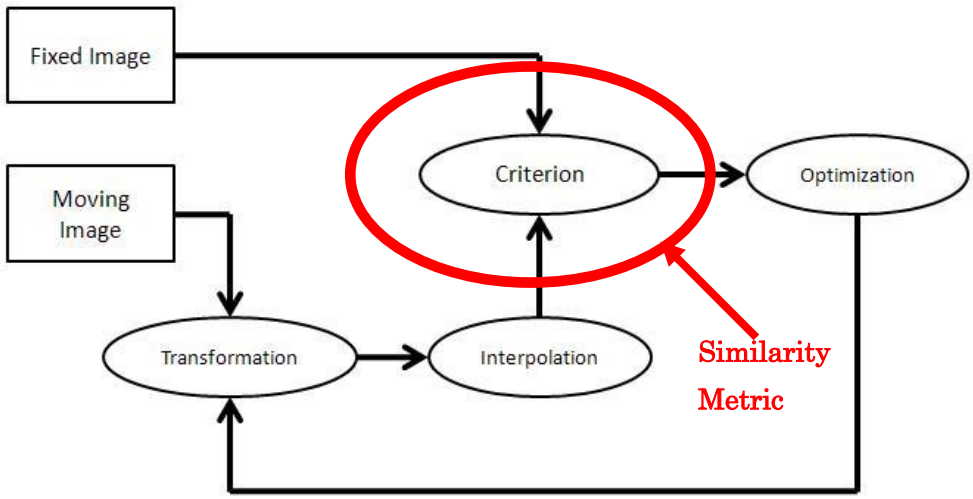

Fig 4.1: Framework of medical image registration

Mutual information (MI) was first invented by Shannon [12] as a measure method of the statistical independence between two signals and applied as a similarity metric of image alignment by Viola and Wells [6]. From MRI being created till now, MI has been widely used and has proven to be a particularly well suited and attractive option for medical image registration. However, MI has its drawbacks such as that MI based image registration does

fail when images have poor quality. Since MI is usually calculated by only using the corresponding intensities of two images, and it is never considers the spatial information perspective, it would be strongly influenced by noise of images and would easily cause misalignment happening.

Therefore, it is necessary to use of additional information to improve the robustness and precision of similarity criterion when registering difficult image pairs has been proposed as one of a possible solution method. Russakoff [11] has provided a high order MI that includes regional information of images within a specific radius, he call it as Regional mutual information (RMI). The main drawback of this approach is that it requires too much computing time to approximate the high-dimensional probability distributions by calculating the covariance matrix. This situation would make RMI useless to case of practical 3D volumes registration.

In the present research we propose a novel idea as a smart method to improve the efficiency of RMI and overcome the too much time consuming of computation time to process problem. We try to combine the approach of high dimensional feature extraction and method of dimension reduction to implement a new criteria mechanism that could make registration processing more robust and faster. Therefore, we have obtained a basic idea of high dimensional feature extraction from RMI. Striving to the optimization solution and overcome the weakness of MRI processing, we strive to find a way of smart solution to implement, the method is as dimension reduction. Thus, we apply principle components analysis (PCA) [13] to reduce the dimension of the joint distribution matrix. Then we can explore to find a new way to make a new criterion by the new joint distribution which from our research finding, we create by the previous step.

4.2 Background Knowledge

In this section, first, we apply the general approach of adapting multi-modality registration techniques to develop for robust registration. There are several similarity metrics we have used for measuring how well the two images are registered. Then, it briefly introduces the principal component analysis as we proposed a critical section of similarity metrics method.

4.2.1 Mutual Information

Mutual information of MI [7] is as a widely used entropy method based on similarity measurement for medical image registration. It has been shown to be robust and does not

depend on the specific range or intensity of images. Assume two images F and M is given, according to build a joint histogram of two images (See Fig 4.2 (a) and (b)) by the pixel of corresponding points. Finally, 2D joint distribution would be used to estimate the value of mutual information (See Fig 4.2 (c)).

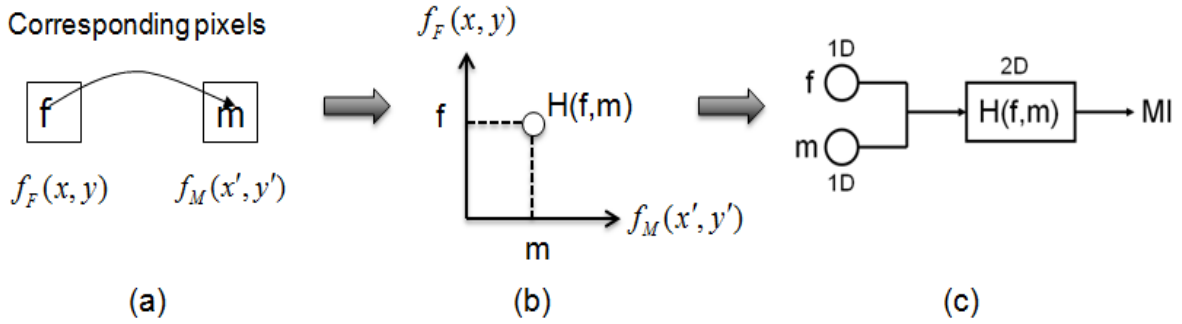

Fig 4.2: Joint histogram of mutual information. (a) MI only considers relationship between two corresponding pixels. (b) Joint histogram of MI is two dimensions. (c) Using the 2D Joint histogram to calculate value of MI.

Then the joint entropy can be calculated from joint histogram by equation (4.1).

$$H\left(f_F, f_M \middle| \mathbf{u}\right) = -\sum_{m\in F, n\in M} P\left(m,n\middle|\mathbf{u}\right)\log P\left(m,n\middle|\mathbf{u}\right) \tag{4.1}$$

And we can calculate the individual entropy of images by equation (4.2).

$$\begin{aligned} H\left(f_F\right) &= -\sum_{m\in F} P\left(m\right)\log P\left(m\right) \\ H\left(f_M \middle| u\right) &= -\sum_{b\in B} P\left(n\middle|\mathbf{u}\right)\log P\left(n\middle|\mathbf{u}\right) \end{aligned} \tag{4.2}$$

Then, MI can be defined in terms of entropy as equation (4.3).

$$MI\left(F, T\left(M\middle|\mathbf{u}\right)\right) = H\left(f_F\right) + H\left(f_M\middle|\mathbf{u}\right) - H\left(f_F, f_M\middle|\mathbf{u}\right) \tag{4.3}$$

The MI criterion of two images is defined as equation at (4.4) formula.

$$\mathbf{T}' = \underset{\mathbf{T}}{\arg\max}\, MI\left(\mathbf{F}, \mathbf{T}\left(\mathbf{M}|\mathbf{u}\right)\right) \tag{4.4}$$

Image registration is defined as the process to find the transformation T which relies on a set of parameters u that maximizes the value of similarity metric.

However, mutual information has some drawbacks, since it sensitive to noise because of lacking spatial information. Therefore, mutual information would fail if input images include noise.

4.2.2 Regional Mutual Information

There is a relatively new similarity metric which is termed as region mutual information (RMI) could contain some spatial information [11]. The concept of RMI is to extend the dimensionality of histograms (See Fig 4.3).

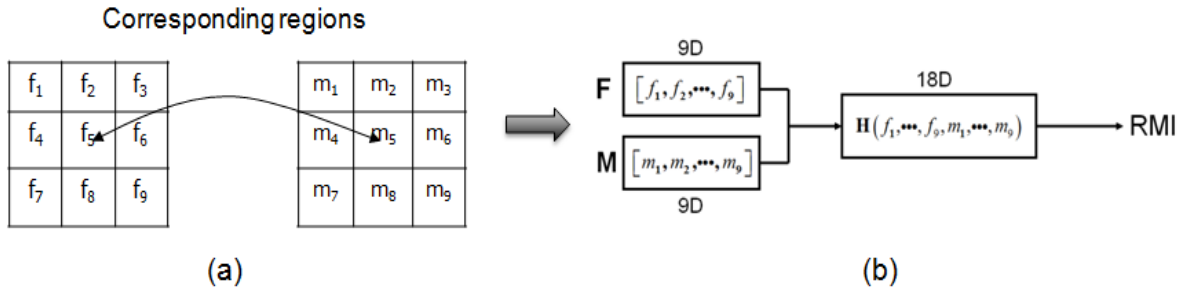

Fig 4.3: Joint histogram of regional mutual information. (a) RMI takes corresponding regions to build joint histogram. (b) Value of RMI would be calculated by a high dimensions joint distribution.

If we not only use the pixel of corresponding points to make histogram, but also consider their immediate 3×3 neighborhood. We could obtain a 9 dimension histogram for marginal probabilities and an 18 dimension histogram for joint distribution (See Fig 4.4).

According to Fig 4.4 (b), we can make a vector of the joint distribution and combine each vector as a $d\times N$ matrix of joint distribution. Given a specified square radius r, here $d=2\left(2r+1\right)^2$ and $N=\left(m-2r\right)\left(n-2r\right)$. Applying this method to extract feature information and create joint a distribution would allow users try to rotate and translate such

high-dimensional distribution into a space where each dimension is independent. Independence in each dimension allows us to decouple the entropy calculation

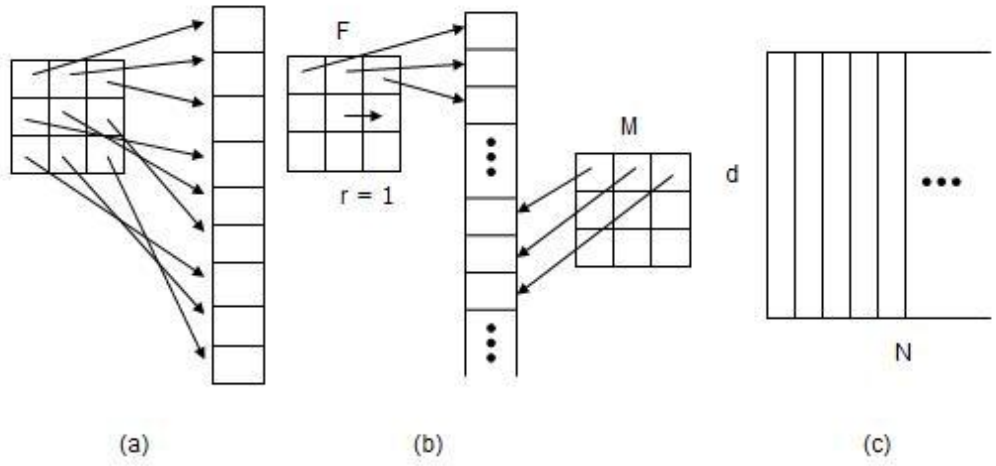

Fig 4.4: Feature extraction and joint distribution creation for RMI. (a) The relationship between an image region and its corresponding multi-dimensional point. (b) Corresponding image neighborhoods and the multi-dimensional point representing them in the joint distribution. (c) The joint distribution matrix of RMI.

We could then calculate the marginal and joint entropies in equation (4.5).

$$H_g(\Sigma_d) = \log((2\pi e)^{\frac{d}{2}} \det(\Sigma_d)^{\frac{1}{2}}) \qquad (4.5)$$

At last, we can obtain the value of RMI by equation (4.6).

$$RMI = H_g(C_A) + H_g(C_B) - H_g(C) \qquad (4.6)$$

Since Σ_d means a covariance matrix of the joint distribution matrix, so that it leads to a critical drawback that is it must spend a lot of computing time. To calculate the covariance matrix, we should make the matrix of sample multiplied it by its transpose but the multiply operation usually requires more computing time especially when two matrices should be multiplied by each other are large. For two 256×256 images, the N is going to be more than 30,000. That is the reason why this method always executes slowly and is not very useful. Therefore, we should find another method to improve it.

4.2.3 Principal Component Analysis

Principal component analysis (PCA) [15][16] is a major method of covariance structure analysis in multivariate statistics, and it is also an important method of feature extraction on originally swatch in multivariate information classification. The main idea of PCA is that mapping the input data from pattern space into a feature space. Feature space is a much lower dimensionality, until now, it preserves most of popular process to get the intrinsic information method.

The objective of the principal component analysis is to derive a linear transformation that will emphasize the difference between the pattern samples belonging to different categories. In other words, the principal component analysis is to define a new coordinate axes in direction of high information content (or principal component) useful for classification purposes. In PCA, a principal component will have more effect classification.

Suppose we have M samples. Each sample is expressed as a column vector $\mathbf{a}_i, i = 1, 2, \ldots, M$ by equation (4.7)

$$\mathbf{A} = \left[\mathbf{a}_1, \mathbf{a}_2, \ldots, \mathbf{a}_M\right] \tag{4.7}$$

Find the empirical mean $\mathbf{u}_x =$ along each dimension $D = 1, \ldots, d$ with equation (4.8)

$$\mathbf{u}_\mathbf{A} = \frac{1}{M}\sum_{m=1}^{M}\mathbf{a}_i \tag{4.8}$$

Subtract the empirical mean from $\mathbf{A}$ for without loss of generality by equation (4.9).

$$\mathbf{a}_i = \mathbf{a}_i - \mathbf{u}_\mathbf{A} \tag{4.9}$$

The problem is we want to find an $D \times D$ orthonormal transformation matrix $\mathbf{W}$ such that equation at (4.10) formula.

$$\mathbf{B} = \mathbf{W}^T \mathbf{A} \tag{4.10}$$

The D-dimensional vector will be transformed into a new vector $\mathbf{B}$ with a dimensionality P which is less than D by a $P \times D$ transformation matrix $\mathbf{W}$. PCA is based on eigenvalue decomposition of the covariance matrix $\mathbf{Cov}$, as equation (4.11).

$$\mathbf{Cov} = \mathbf{A}\mathbf{A}^T = \mathbf{W}\boldsymbol{\Sigma}\,\mathbf{W}^T \tag{4.11}$$

Where $\boldsymbol{\Sigma}$ is a diagonal matrix corresponding of eigen values and $\mathbf{W}$ is a $D \times D$ matrix, whose column vectors $\mathbf{w}_i, i = 1,2,\cdots,D$ are eigenvectors of $\mathbf{Cov}$. The leading J eigenvectors, where $J \le D$ construct the subspace and the vector $\mathbf{a} \in \mathbf{R}^D$ can be represented by its coefficient vector, $\mathbf{b} = [\mathbf{w}_1, \mathbf{w}_2, \cdots, \mathbf{w}_J]^T \cdot \mathbf{a} \in \mathbf{R}^J$.

On the other hand, a matrix $\mathbf{A} \in \mathbf{R}^{D \times M}$ can be decomposed by SVD as equation (4.12).

$$\mathbf{A} = \mathbf{U}\mathbf{S}\mathbf{V}^T \tag{4.12}$$

Where $\mathbf{U} \in \mathbf{R}^{D \times D}$ and $\mathbf{V} \in \mathbf{R}^{M \times M}$ are orthogonal matrices. $\mathbf{S} \in \mathbf{R}^{D \times M}$ is a diagonal matrix corresponding of singular values. From equation (4.13),

$$\mathbf{A}\mathbf{A}^T = \mathbf{U}\mathbf{S}\mathbf{V}^T\mathbf{V}\mathbf{S}^T\mathbf{U}^T = \mathbf{U}\mathbf{S}^2\mathbf{U}^T \tag{4.13}$$

It is clear that the squares of the non-zero singular values of $\mathbf{A}$ which are equal to the non-zero eigen-values of $\mathbf{A}\mathbf{A}^T = \mathbf{Cov}$ and the columns of $\mathbf{U}$ (left singular vectors) are eigenvectors of $\mathbf{Cov}$. Thus we just need to apply SVD to $\mathbf{A}$ in order to get the principal orthogonal vectors (bases).

Since PCA can achieve on both feature extraction and dimensionality reduction, it requires that the input data must be normally distributed. The high-dimensional distribution of RMI [11], which we created it by Fig 4.4 is approximately normally distributed, so that we choose PCA as an improved approach to modify the regional mutual information.

4.3 PCA Based Regional Mutual Information

Though RMI is an effective method to include spatial information, however, it requires a huge amount of computational cost as we mentioned in previous section. Therefore, we propose a novel PCA based regional mutual information. The basic concept of our method is to combine the ideas of RMI and dimension reduction technique to achieve improved registration robustness and speed. We combine RMI, MI, and the principal component analysis (PCA) into a new similarity metric, thus we name it as PCA based regional mutual information (PRMI).

The main concept of our method has shown by Fig 4.5. First, we create two regional feature vectors for two images separately. Then, we perform a principal components analysis (PCA) to reduce the both two high dimension vectors into two dimensions vectors with two components. Finally, two reduced feature vectors would be used to create a four dimensional joint histogram, and value of our proposed PRMI can be calculated from this four dimensional histogram.

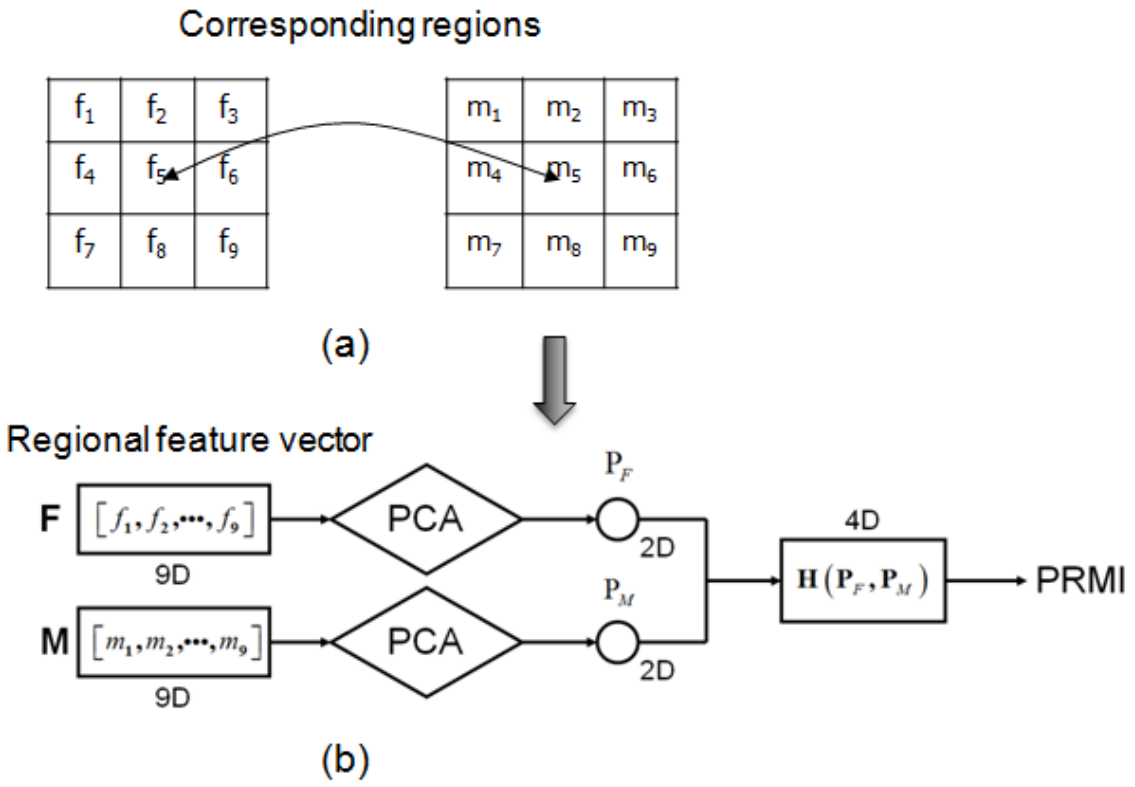

Fig 4.5: Joint histogram of PCA based regional mutual information. (a) Our proposed method also considers relationship between two corresponding regions. (b) Principal component analysis is used to reduce high dimension of regional feature vectors into two 2D feature vectors.

According to Fig 4.6, we obtained two $d \times N$ feature matrices which are created by combining all regional feature vectors of two images individually, where $d = (2r+1)^2$. Thereupon, we used theses vectors to make a four dimensions joint histogram.

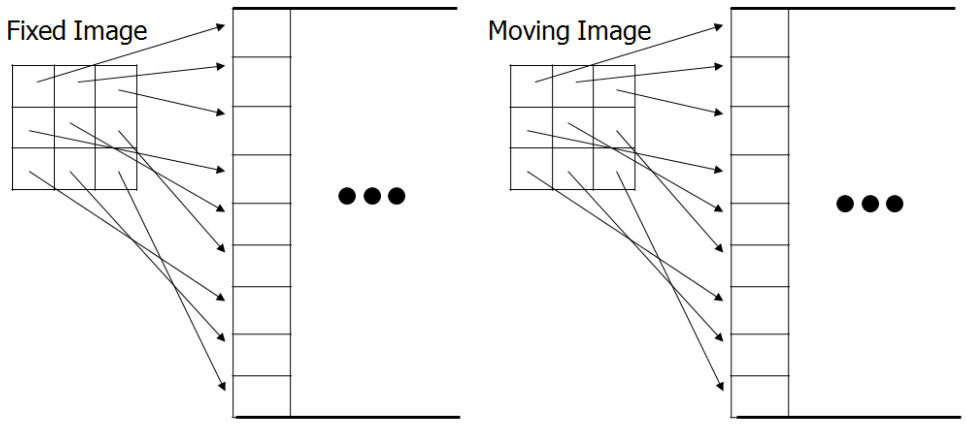

Fig 4.6: The approach of regional information extracting of PRMI

Therefore, it can calculate both joint and individual entropies from equation (4.1) and (4.2). Finally, we could obtain the value of PRMI according to equation (4.3), and find the best result by equation (4.4).

For more measures, we have to calculate the rate of data representing, since we interested in how many components which are obtained by PCA should be used to project the feature vectors. As with equation (4.14), were M is total number of components which are obtained by PCA, n are number of used components, and λ_j is the eigen-values of jth eigen-vector.

$$R_M = \frac{\sum_{j=1}^{n} \lambda_j}{\sum_{i=1}^{M} \lambda_i} \tag{4.14}$$

On the other hand, we draw out the result as the curves of accumulation on Fig 4.13. It clearly represents that two components can represent over 95% of original data. That means even we only choose the first and second components to project the feature vectors, these feature

vectors still have strong ability to represent all of original data.

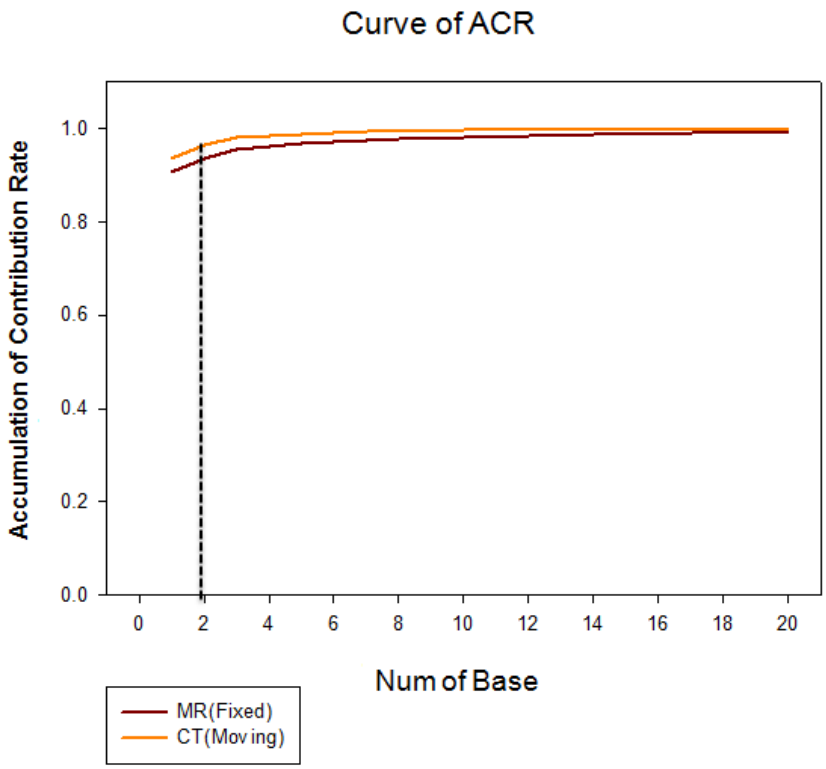

Fig 4.7: The curves of data representing rate of accumulation which are plotted by using different number of components.

4.4 Experiments and Results

In order to evaluate our proposed method, we applied the PRMI to several 2D datasets that include noise. A mean square error (ΔT and $\Delta\theta$) are used as quantitative measures, which are shown in Eq(4.15) and (4.16). T_x, T_y are true translation parameters. θ is true rotation angle. T_x', T_y', θ' are estimated translations and rotation angle. N is the number of samples. We used 10 MR images obtained from BrainWeb[17].

$$\Delta T = \frac{1}{N}\left(\sum_{n=1}^{N}\left\|Tx_n - Tx_n'\right\| + \sum_{n=1}^{N}\left\|Ty_n - Ty_n'\right\|\right) \tag{4.15}$$

$$\Delta\theta = \frac{1}{N}\left(\sum_{n=1}^{N}\left\|\theta_n - \theta_n'\right\|\right) \tag{4.16}$$

The examples of registration with our proposed PRMI are shown in Fig 4.8, and we also show the results of MI for making comparison with the difference findings. Moreover, it is displaying the results of both single-modality registration and multi-modality registration.

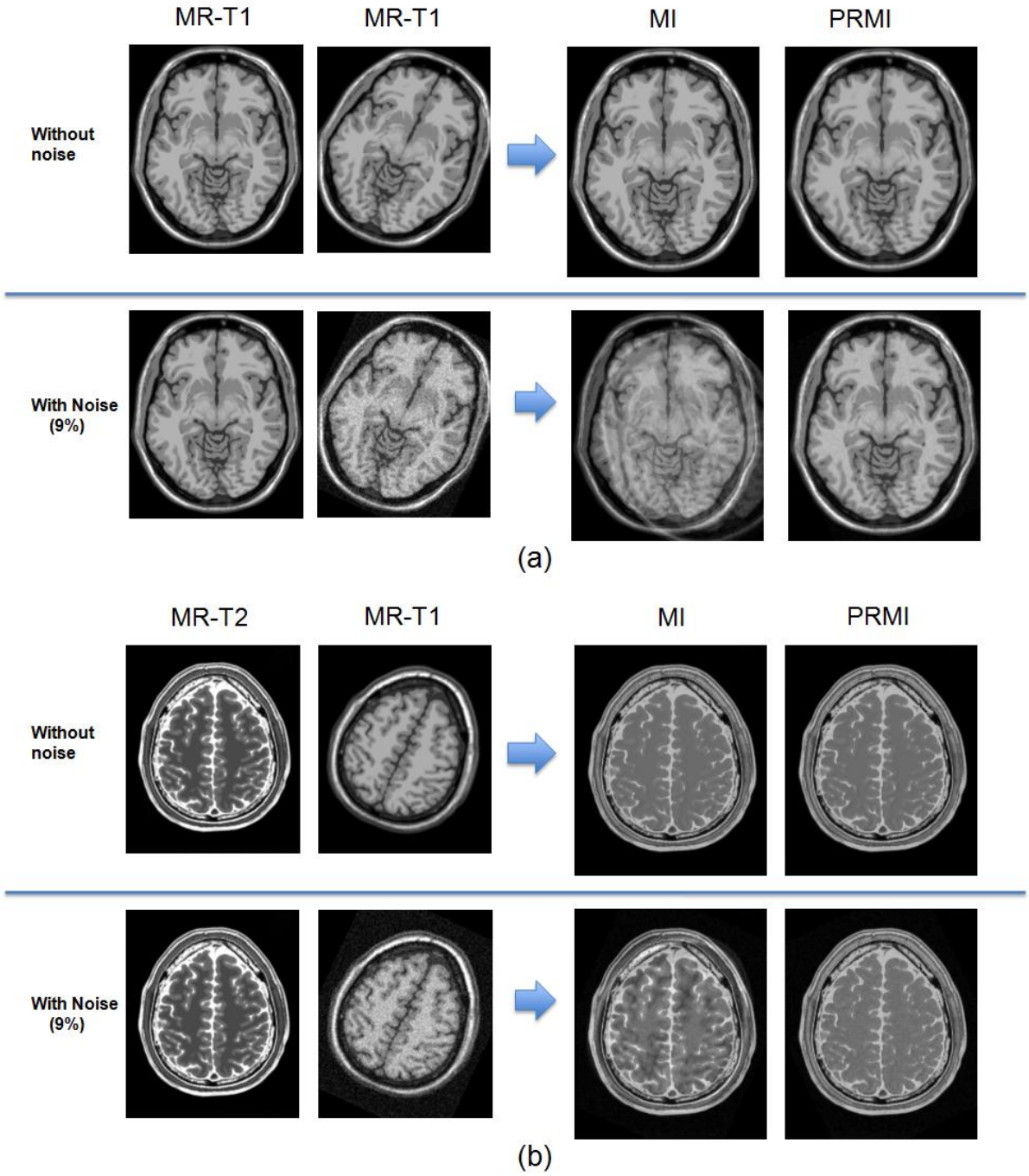

Fig 4.8: The comparison results of registration with both common MI and our proposed PRMI. (a) The comparison results in single-modality registration for both without and with noise. (b) The comparison results in single-modality registration for both without and with noise.

This result shows our proposed method has high margin for noise so that it will not be influenced by noise interference.

4.5 Discussion and Conclusion

In short, we show some relative experimental results. The most of them can be used for demonstrating our research proposed method which is really better than the previous methods. From the discussion and researching finding view point, we can then provide some researching findings and discussions depend on these results. Finally, we also provide for future research tasks which illustrates in this section.

4.5.1 Discussion

In the present research finding, we have proved our proposed PRMI possesses which have the capability to overcome the drawbacks of common MI method. Moreover, we would like to illustrate by comparative results to demonstrate our PRMI finding which is much robust than common MI and provide more effectively than RMI and continuously process results.

First, we display the joint distributions of RMI and MI by the Fig 4.9 for observing the difference by the two methods. From the Fig 4.9 illustration, we can find our joint distributions of PRMI which are more approximate to a diagonal line. According to basic theory of MI, we believe that it represents PRMI has potential ability for providing better result of registration with noised images.

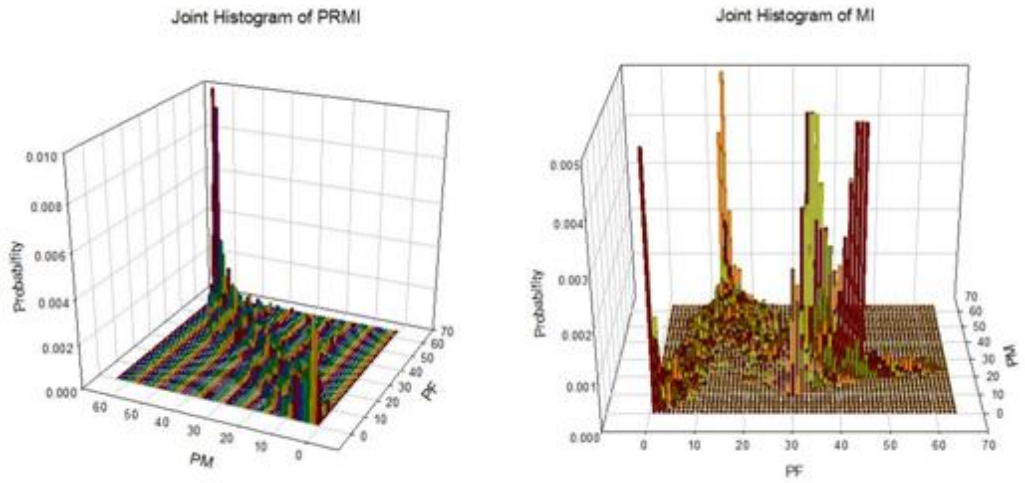

Fig 4.9: Joint distributions of both PRMI (left) and MI (right)

Second, we want to evaluate the accuracy of our designed algorithm. Hence we have drawn the curve of MSE for estimate error of transformation parameters. Therefore, we can easily discover that PRMI produced good results independent on noise of input data from Fig 4.10. The Fig 4.10 (a) and (b) illustration, demonstrate our PRMI is more robust than common MI for noised medical data.

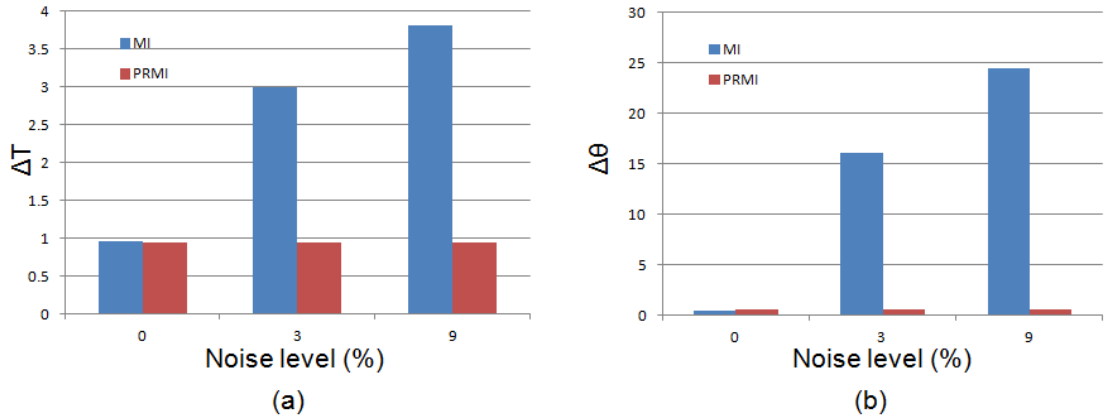

Fig 4.10: The histogram of MSE (for both translation (left) and rotation (right)): (a) shows the difference of translation parameters in each level of noise. (b) shows the difference of rotation parameters in each level of noise.

Finally, we show computational time per each iteration in Table 4.1. Though PRMI takes longer computational time than MI, it takes only 12 iterations for convergence. So the total computational time is about 1.8 sec which is acceptable for clinical application.

Table 4.1: Iteration cost for comparing the performance of PRMI, common MI.

Method	Region size	Dimension of joint distribution	Time (s/iteration)
MI	1x1	2	0.06
PRMI	3x3	4	0.158

4.5.2 Conclusions and Future Works

Although, MI is extensively used as a similarity metric for medical image registration but lacking special information is an existence drawback, so that MI is a very weak in datasets which have noise. RMI contain special information to perform a better registration but the

cost of computing is too high that it can't be accepted. For including advantage of previous methods and overcome their disadvantage, we proposed a novel PRMI. We have confirmed that our designed PRMI can perform well in 2D medical image registration by our experiments, however, we are strive to provide more profound and high quality imaging result from our further research contribution.

For future research, we plan to apply our proposed method to deal with real 3D medical dataset, so we are thinking about how to extract the regional information from a 3D volume. Then we try to explore an emerging method to improve execution performance by our proposed method. Finally, we would like to implement our method embedded in the Insight Toolkit (ITK) which is a most useful library of medical image research. We believe that, from our research finding and contribution would show our PRMI is a so powerful and useful method to put into in practice to generate one of the best qualities imaging result.

Reference of Chapter 4

[1] J. V. Hajnal, D. L. G. Hill, and D. J. Hawkes, "View of the future", in Medical Image Registration, J. V. Hajnal, D. L. G. Hill, and D. J. Hawkes, Eds. Boca Raton, FL: CRC, 2001.

[2] D. L. G. Hill, P. G. Batchelor, M. Holden, and D. J. Hawkes, "Medical image registration", Phys. Med Biol., vol. 46, pp. R1-R45, 2001.

[3] L. Brown, "A survey of image registration technique", ACM Comput. Surv., vol. 24, pp: 325-376, 1992.

[4] D. L. G. Hill and P. G. Batchelor, "Registration methodology: concepts and algorithms", in Medical Image Registration, J. V. Hajnal, D. L. G. Hill, and D. J. Hawkes, Eds. Boca Raton, FL: CRC, 2001.

[5] N. Dowson and R. Bowden, "Metric mixtures for mutual information(m3i) tracking", In *Proc.17thInt.Conf. on Pattern Recognition* ,pages 1051–4651, 2004.

[6] Viola, P., Wells III, W.M. "Alignment by maximization of mutual information", International Journal of Computer Vision 24, pp: 137–154, 1997.

[7] J. Pluim, A. Maint, "Mutual information-based registration of medical image: a survey", IEEE Transactions on Medical Imaging, pp: 986-1004, 2003.

[8] Maes, F., Collignon, A., Vandermeulen, D., Marchal, G., Suetens, P. "Multimodality image registration by maximization of mutual information", IEEE Transactions on Medical Imaging 16, pp: 187–198, 1997.

[9] D. L. G. Hill, C. Studholme, D. J. Hawkes, "Voxel similarity measure for automated image registration", Proc. Visualization in Biomedical Computing, Rochester Mn., U.S.A., vol. 2359, pp: 205-216, SPIE Press, 1994.

[10] H. K. Pong and T. J. Cham, "Alignment of 3d modelstoimages using region-based mutual information and neighborhood extended gaussian images", In *Proc. Asian Conf. for ComputerVision*,pages 60–69, 2006.

[11] D. Russakoff, C. Tomasi, T. Rohlfing, and C. Maurer, "Image similarity using mutual information of regions", In *Proc. Europ.Conf. onComp.Vision*,pages 596–607, 2004.

[12] Shannon, "A mathematical theory of communication ", *Bell System Tech.*, 27:370-423, 1948.

[13] R. O. Duda, P. E. Hart, D. G. Stork, "Pattern Classification", John Wiley and Sons Inc. (2001).

[14] A. Bell, T. Sejnowski, "An information-maximization approach to blind separation and blind deconvolution", *Neural Computation 7* (1995), pp: 1129-1159.

[15] I.T. Jolliffe, Principal Component Analysis. Springer, 2002.

[16] M. Turk, A. Pentland, "Eigenfaces for Recognition", Journal of Cognitive Neuroscience, Vol.3, No.1, pp. 71-86, 1991.
[17] BrainWeb: http://brainweb.bic.mni.mcgill.ca/brainweb/

Chapter 5

Robust Nonrigid Image Registration with Anatomical Structure Constraint for Assessing Treated Margin of Locoregional Therapy of Hepatocellular Carcinoma

5.1 Introduction

Locoregional therapy (LT) is a novel and popular method to cure hepatocellular carcinoma (HCC) of liver in the last few years. This method digs several probes into patient's abdominal cavity to burn tumor tissues of liver with frequency alternating current. The originally idea is that to stab a probe into belly and to burn the tumor with electric current by this probe. Through these few year improvements, this technique was developed and improved to more faultless, three probes are used to locate and burn the tumor instead.

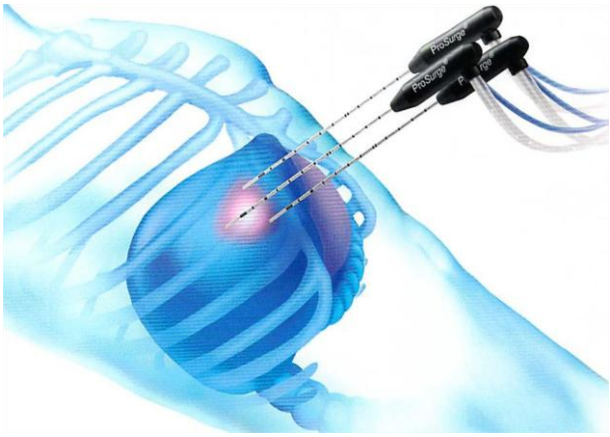

Fig 5.1: A diagram of LT using perfused-cooled electrode (Provided by Professor Seki)

The advantages of LT are that the infection probability occurring is reduced and recovery time for patient is becoming shorter. In the case of hepatocellular carcinoma treatment,

applying LT method for treatment is an excellent method. However, there are still some limitations about this method, such as accuracy of treatment. If the position where the probes hit is inaccurate or tumor tissues aren't burned clearly, patients will get a recurrence of HCC. Therefore, evaluating the treated margin is a critical factor for predicting local recurrence after locoregional treatment is done.

The standard method for evaluating the treated margin of LT is to compare 2D images of CT (or MR) which are taken before and after LT, but this method is very roughly and inaccurate since it is lack of 3D information. Currently, doctors and radiologists tend to apply some manual applications of 3D image fusion [1] to replace the standard method, but this method is also not very smart which has its drawbacks. That is because of livers are deformable objects so that it is impossible to match each other perfectly with simple rigid fusion application. On the other hand, segmenting a liver from sliced medical dataset manually, it will consume a lot of work, due to a volume of liver usually contains about six hundred slices. We receive some requirements and ideas from doctors due to several discussions, and start to build a useful system to support their works. We developed an innovative new surgical treated margin evaluation assistant system with several advance segmentation and registration methods.

To resolve problems by previous methods, we applied 3D non-rigid registration method, which has been widely applied to measure treated margin instead of 3D image fusion process. Applying 3D non-rigid registration process, two corresponding liver volumes which are taken both before and after surgery have been reasonably mapped by each other. For measuring treated margin of surgery, the ablative margin has to be aligned onto tumor. Moreover, geometric difference between the result of registration and the corresponding of liver volume is taken before LT which is calculated as an evaluating quantification of registration. Although traditional 3D non-rigid registration, it may appear well established in treated margin application. However, from the research exploration finding, traditional method is essential to keep stability of anatomical structure of shape, but it is failed to register the organ tissues within liver because of using intensity based similarity metric.

This chapter is illustrating as follows: the detail of registration technique and our proposed method are explained in Sec.5.2, some implemented issue such as pre-process are described in Sec.5.3, the experimental results are presented in Sec.5.4, and the conclusion and future works are finally given in Sec.5.5.

5.2 Materials and Methods

Medical volume registration has been widely proposed in view of the practical importance in the field of medical image processing [6][7]. With the increase of number of medical diagnosis and surgery assistance applications, people recognize the registration is one of critical mechanism for these applications. Though existing registration techniques can be used to evaluate the treated margin after surgical operation, those techniques usually perform a classical 3D non-rigid registration process to simply merge two volumes of object organ so that the treated margin can be accessed by overlapping of ablative margin and tumor. However, the internal structure cannot be guaranteed to coincide by using the classical 3D non-rigid registration technique, because it causes the treated margin miss-align to tumor position. So from this research proposed an improvement method to overcome these drawbacks. Thus, this section explains both traditional 3D non-rigid registration method and our proposed method.

5.2.1 3D Non-rigid Registration Framework

The objective of image registration is to find the optimal transformation matrix, which maps every points in the post-operation liver volume (called moving volume) $M(\mathbf{x})$ onto its corresponding point in the pre-operation liver volume (called fixed volume) $F(\mathbf{x})$. The input images are given as two 3D discrete signals: The moving image M and the fixed image F with intensities $f_M(\mathbf{x})$ and $f_F(\mathbf{x})$. A similarity metric which measures the difference between transformed $M(\mathbf{x})$ and $F(\mathbf{x})$ can be minimized, and the optimal transformation matrix can be found. The transformed moving image $M(\mathbf{x}|\mathbf{u})$ can be obtained by using the optimal transformation parameters $\boldsymbol{\mu}$, that can be defined as $f_M(\mathbf{x}|\mathbf{u})$.

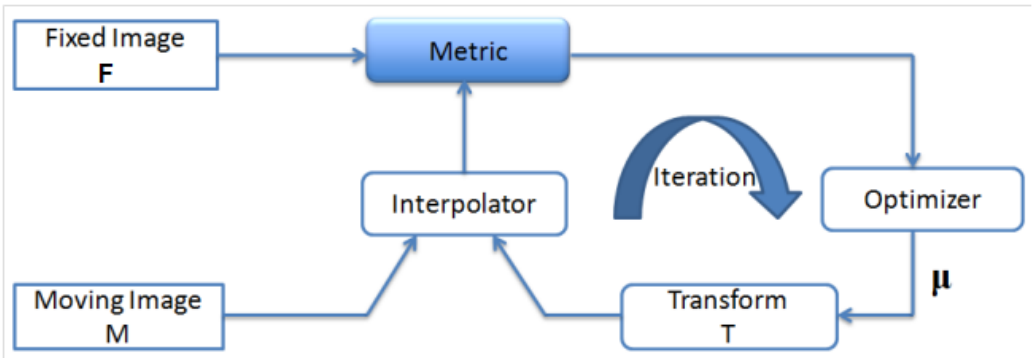

Fig 5.2: Flowchart of non-rigid registration

The majority of the image registration methods can be viewed as a combination by the four distinctive components such as: transformation, interpolation, similarity metric, and optimization. As shown in Fig 5.2, among the four components, the similarity metric is based on cost function which is the most important significant for the registration algorithm. This algorithm also defines the goal of optimization and measures how well the transformed moving image W matches the fixed image R.

5.2.2 Conventional Similarity Metric

Usually, we estimate the parameter of transformation by optimizing a similarity metric in the processing of registration. In general, the solution to the registration problem can be computed by optimizing as illustrating as the following function.

$$\mathrm{E}(\boldsymbol{\mu}) = \mathrm{E}(\mathrm{f}_F(\mathbf{x}), \mathrm{f}_M(\mathbf{x}|\boldsymbol{\mu})) \tag{5.1}$$

The aim of registration is to minimize/maximize the similarity E between the two images. Mutual information (MI) [1] is the most widely to be used for medical image similarity measures. It also can apply at for both mono-modality and multi-modality. MI can also measure the statistical dependence or information redundancy between the image intensities of corresponding voxels in both images. The definition of the MI can be presented as follow:

$$E(\mathbf{u}) = MI(f_F(\mathbf{x}), f_M(\mathbf{x}|\mathbf{u})) = H(f_F) + H(f_M|\mathbf{u}) - H(f_F, f_M|\mathbf{u}) \tag{5.2}$$

where $H(W)$ and $H(R)$ are the marginal entropy, $H(W,R)$ is the joint entropy.

Although traditional MI may appear at well established in treated margin application, but it also exists a drawback. The traditional method tends to maintain the similarity of anatomical structure of shape, but also miss-align to internal structures of volume, due to only based on distribution of intensity. This drawback causes tumors can't be accurately overlap to their corresponding treated regions in extreme cases.

5.2.3 Our proposed method

The classical non-rigid registration based on intensity exhibits on an inherent weakness, it failed to register internal structures of two volumes because intensity distribution of post-operation volume is changed by LT. To resolve the problem of traditional intensity based non-rigid registration, from this research, it applies a novel anatomical structure term to constrain deformation of non-rigid registration by some additional landmarks. For constraining the anatomical structure, we add a landmark on penalty of terms on the basis of minimizing the energy function. The illustrating is as follows:

$$E(\mathbf{u}) = -I_{MI}(f_F(\mathbf{x}), f_M(\mathbf{x}|\mathbf{u})) + \frac{\lambda}{L}\sum_{i=1}^{L}\left[(\mathbf{p}_F)_i - (\mathbf{p}_M|\mathbf{u})_i\right]^2 \quad (5.3)$$

The first term of the new cost function defines the amount of information that fixed image $F(\mathbf{x})$ which contains transformed moving image $M(\mathbf{x})$. The second term is the landmark constraint which maintains the inner anatomical structure stability. The constant λ define the relative importance of our additional term in the energy function. This cost function is minimized when two volumes are registered well and the corresponding landmarks are aligned. Since specific landmarks are used as constraint to improve the accuracy of registration, our proposed method can be called as landmark constraint based mutual information (MI-LC).

5.3 Issues of Implementation

5.3.1 Pre-processing

As all image processing applications, data pre-process is an important part to our system. Pre-processing usually edits the input data, and provides applicable data and parameter for the main function of system. In case of this research system, pre-process can be divided as three parts: liver segmentation, tumor extraction, and landmark selection. In short, from this research exploration, it explains the pre-processing of our method in this section.

A. Liver Segmentation

Liver segmentation ([2],[3], and [4]) usually is a fundamental step for all hepatic CAD (Computer Aided Diagnostics) and CAS (Computer Aided Surgery) systems, but it also is considered as a challenging task due to large shape variations, non-homogenous texture, and low-contrast. In our method, a random walks [5] method is applied to segment livers form medical datasets of both pre-operation and post-operation. This method is based on a small set of pre-labeled pixels as seed points. The algorithm function by assigning each unseeded pixel to the label of the seed point that a random walker starting from that pixel would be

most likely to reach first. The relative work have demonstrated this approach which can provide a good imaging result and is robust to weak its boundary.

B. *Tumor Extraction*

Segmenting tumor from liver is also one of the most challenging tasks in medical image analysis because of their unpredictable appearance and shape. In case of our system, the tumor and treat margin must be segmented from the pre-operation liver volume and the post-operation liver volume, respectively, for comparing their location and overlapping. Therefore, the tumor segmentation approach is playing important roles as to this research method. The random walks method is also applied to tumors and treated margins from each pair of dataset (pre-operation and post-operation). An example result of tumor segmenting is illustrating as Fig 5.3.

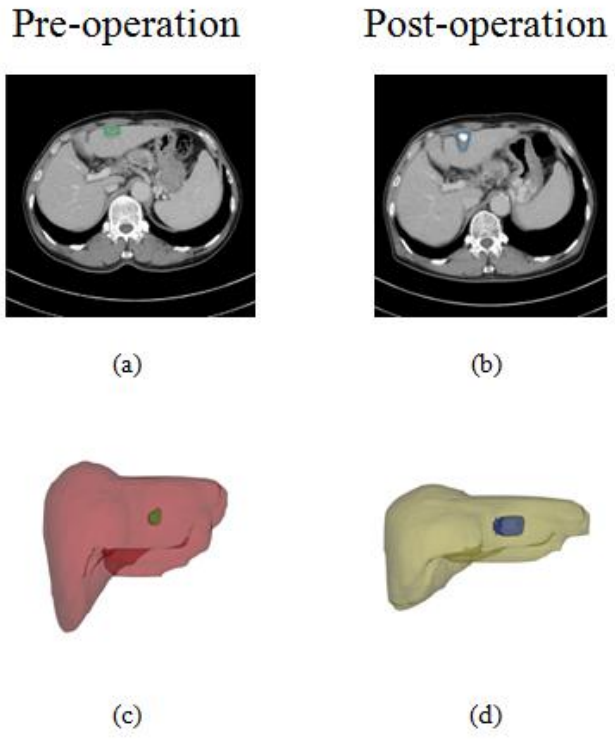

Fig.5.3: The results of tumor segmentation. (a) Segmented tumor from the pre-operation liver volume. (b) Segmented threat margin from the post-operation liver volume. (c) 3D visualization of (a). (d) 3D visualization of (b).

C. *Landmark Selection*

The main exploration concept of this research system for treated margin evaluation is that

add a term of constrain to cost function in order to control deformation of non-rigid registration by applying several landmarks, so the location of landmarks are a critical key point of this process. To be reliable, landmarks are chosen by Doctors (co-authors of this paper) of Kansai Medical University. We have manually defined four landmarks as shown in Fig 5.4 which are processed by the assistance of a medical expert such as: (a) the branch of the right hepatic veins (Landmark 1), (b) the first branch of the portal vein (Landmark 2), and (c) the second branch of the portal vein (Landmark 3). From this research observation, these landmarks have discernible geometrical features in medical volume so that these Landmarks are reasonable to be selected.

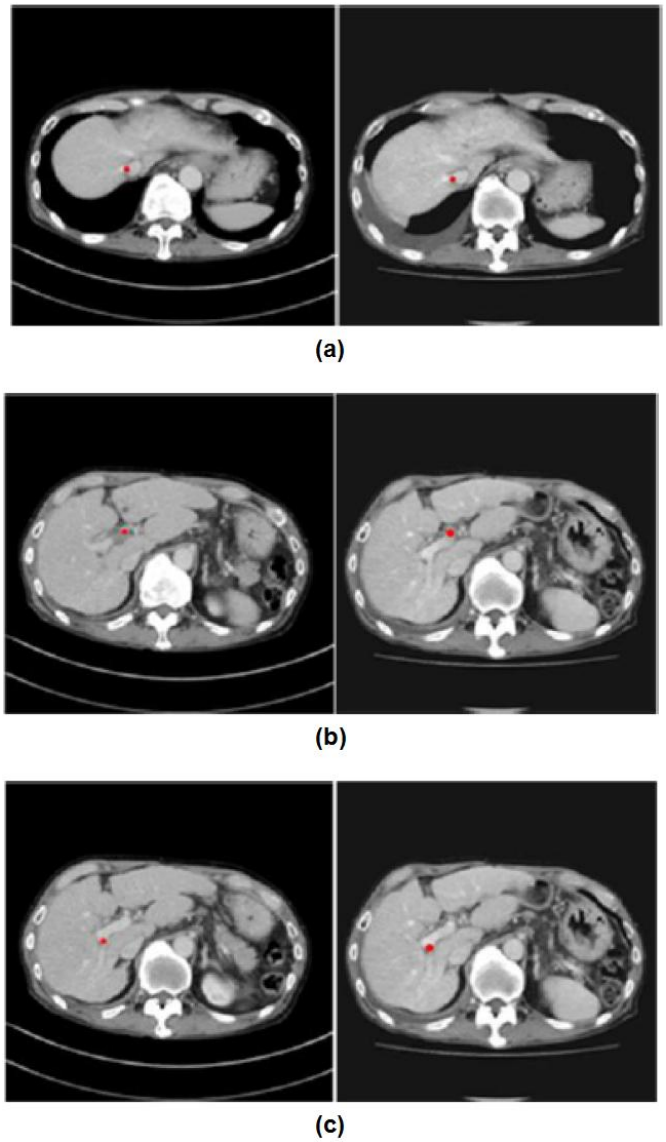

Fig. 5.4: The position of chosen landmarks. (a) Landmark 1: the branch of the right hepatic veins, (b) Landmark 3: the first branch of the portal vein, and (c) Landmark 4: the second branch of the portal vein.

5.3.2 Transformation

In general, only depending on the global deformation, it is not sufficient for image registration. Therefore, a method that can capture the local deformation was needed. To achieve better accuracy result, the transformation in our algorithm comprised of a global and a local transformation. The research task goal aimed to attain a local warp that is not affected the stability of the structure. The global transformation describes the global or large motions on these two volumes, such as rotation, translation and scaling; while the local transformation describes the local or detailed motions, such as deformation of the tissues. The parameters of global transformation are determined by rigid registration first and the results are the initial values to estimate the parameters of local transformation for non-rigid registration.

Affine transformation is applied as a global transformation for a rigid registration. The transformation of rigid registration is shown as following Eq 5.4.

$$\mathbf{T}_{Affine}(\mathbf{x}) = \begin{bmatrix} a_{11} & a_{12} & a_{13} \\ a_{21} & a_{22} & a_{23} \\ a_{31} & a_{32} & a_{33} \end{bmatrix} \begin{bmatrix} x \\ y \\ z \end{bmatrix} + \begin{bmatrix} t_x \\ t_y \\ t_z \end{bmatrix} \tag{5.4}$$

The non-rigid registration finds the optimal local transformation as a deformation inference in the second step. Usually, B-spline [11] transformation is applied for local transformation of non-rigid registration. B-spline can be expressed by following.

$$\mathbf{T}_{B-spline}(\mathbf{x}) = \sum_{ijk} \begin{pmatrix} \lambda_{ijk,x} \\ \lambda_{ijk,y} \\ \lambda_{ijk,z} \end{pmatrix} \beta^{(3)}\left(\frac{x-\varphi_{ijk,x}}{\rho_x}\right) \beta^{(3)}\left(\frac{y-\varphi_{ijk,y}}{\rho_y}\right) \beta^{(3)}\left(\frac{z-\varphi_{ijk,z}}{\rho_z}\right) \tag{5.5}$$

Where $\beta^{(3)}(s)$ is the cubic B-spline kernel which is defined by the following illustration

$$\beta^{(3)}(s) = \begin{cases} (1/2)|s|^{(3)} - |s|^{(2)} + 2/3 & , \; if \;\; 0 \le |s| < 1 \\ -(1/6)|s|^{(3)} + |s|^{(2)} - 2s + 4/3, & if \;\; 1 \le |s| \le 2 \\ 0 & otherwise \end{cases} \tag{5.6}$$

5.3.3 Optimization

In order to intra-livers registration, the L-BFGS-B optimization [6] is applied to find the optimal transformation parameters because of small geometric difference between two livers. Since a non-rigid registration processing can be divided into two parts: rigid registration and non-rigid registration, so the parameters of global and local transformation are optimized separately for initial rigid registration and final non-rigid registration. For rigid registration, the parameters of affine transformation are adjusted by L-BFGS-B optimization. Result of global transformation is set to be an initialization for non-rigid registration when optima rigid registration is achieved. Then, the L-BFGS-B optimization method is applied to find the optimal parameters of local transformation in non-rigid registration.

5.4 Experimental Results

5.4.1 Database

A dataset consisting of 6 clinical subjects with the HCC of pathological scenarios was used from a Kansai Medical University clinical dataset. Each sets of the clinical subject were imaged CT image from the same patients at pre-operation and post-operation (Before LT and After LT). Meanwhile, each CT volume had one contrast-enhanced portal-phase CT, one is arterial-phase CT and another one is venous-phase CT. The contrast-enhanced portal phase CTs were performed in all registration process. For these CT volumes, the data had 49-55 slices with 5-7mm section thickness and their in-plane dimensions were 0.65mm×0.65mm with a 512×512 mm2 in field of view (FOV). To achieve a better observation the hepatocellular carcinoma (HCC), the portal-phase scanning was imaged after injection of a nonionic iodinated contrast agent.

From the research, it proposed an algorithm was implemented in ITK [14] process, and the experimental result of 3D visualization were provided by VTK [15]. All experiments were run

with a MS-Windows-based personal computer (Intel^R CoreTM-i7 3770QM 3.40GHz and 16GB-DRAM).

5.4.2 Accuracy Measure

To verify the effectiveness of our proposed algorithm, we performed several experiments with different registration methods by two criteria functions.

(i) Evaluation of the local warp

To assess the quality of the local warp of the entire medical images to achieve more detail, we have calculated the intensity differences by using the warping index (WI).

$$WI(f_F, f_M|\mathbf{u}) = \frac{1}{|I|}\sum_{x\in 1}\left[f_F(\mathbf{x}) - f_M(\mathbf{x}|\mathbf{u})\right]^2 \qquad (5.7)$$

Where I is a three-dimensional discrete interval which represents the set of all voxel indexes in the two volumes.

(ii) Evaluation of the anatomical structure

The distance of the correspondence landmarks provides a direct measure of anatomical structure stability as the positions of the landmarks change.

$$LDE(f_F, f_M|\mathbf{u}) = \frac{1}{L}\sum_{i=1}^{L}\left[(\mathbf{p}_f)_i - (\mathbf{p}_m|\mathbf{u})_i\right]^2 \qquad (5.8)$$

Where L represents the number of landmarks.

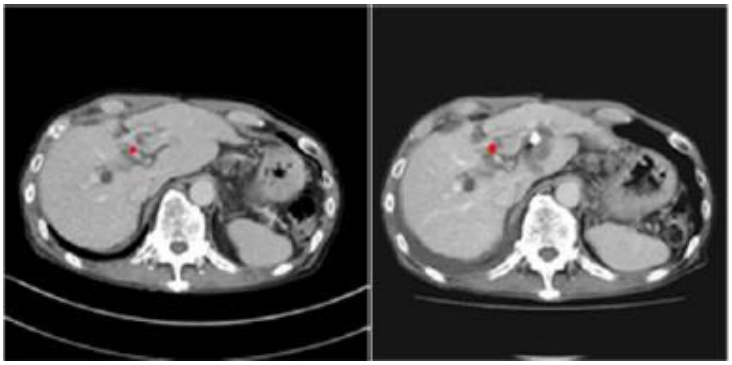

Fig 5.5: The umbilical portion as landmarks of criterion for LDE

For this measure, we usually select a specific landmark: the umbilical portion between two livers to be the correspondence landmarks (see Fig 5.5). This landmark has been seen as an invariable feature of liver, because of less amount of geometric changing. Therefore, we constantly use it as a criterion to calculate LDE.

5.4.3 Registration Results

Fig 5.6 shows the results based on the classical (MI) non-rigid registration and the proposed (MI-LC) non-rigid registration. The tumor (orange) in preoperative volume (red) and the treated region (blue) in the post-operative volume (yellow) were shown in the same coordinate system. The liver transformed by our proposed method looked similar to the registered liver applying the classical MI-based non-rigid registration. However, the distance between the fixed landmark and the transformed moving landmark was different. It could be found regardless of how many landmarks applied in our proposed research method, a significant result of reduction in LDE values using registrations based on MI-LC compared with those based on MI was confirmed.

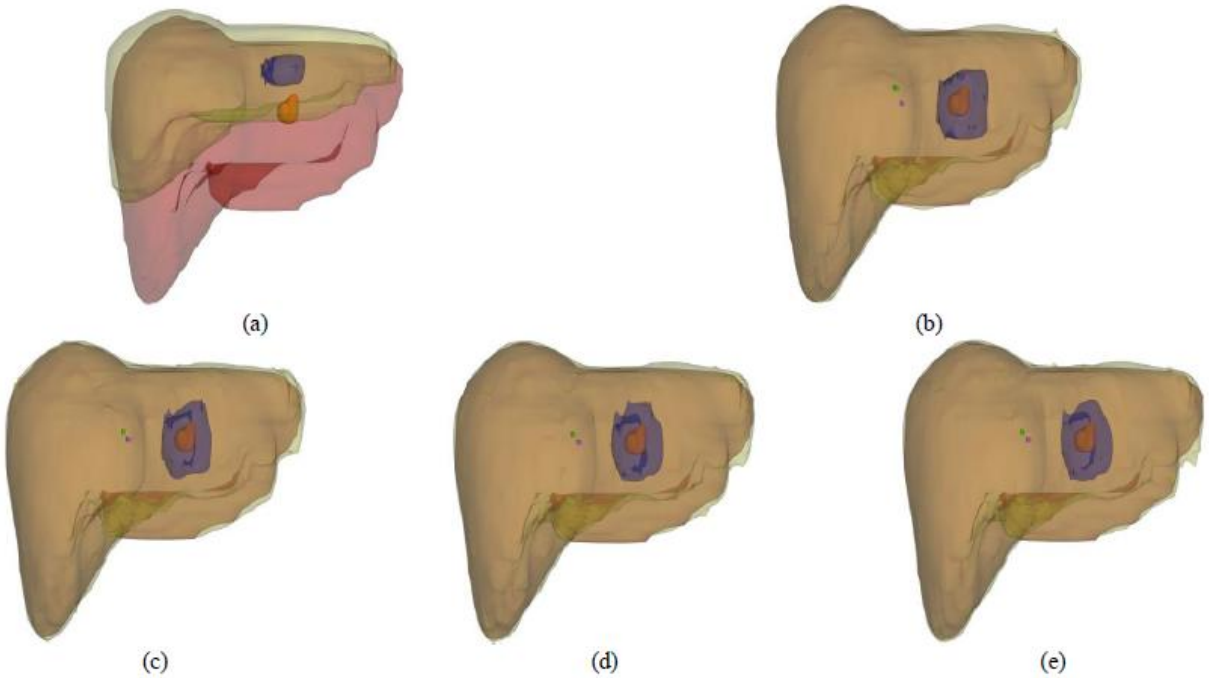

Fig 5.6: 3D view of registration results with the same constrained weights using different landmarks (from 1 to 3 landmarks). (a) The original data; (b) The MI non-rigid registration result (Purple represent the fixed landmark, Green represent the moving landmark); (c) The MI-LC non-rigid registration result with one landmark; (d) The MI-LC non-rigid registration result with two landmarks; (e) The MI-LC non-rigid registration result with three landmarks.

As seen in Fig 5.6, all the moving livers were transformed back to the coordinate system of fixed livers by using different registrations. Following the corresponding transformation parameters, the treated region of the moving liver can also be aligned onto the tumor of the fixed liver. Apart from a visual inspection, a quantitative evaluation was also conducted between the structure volume of fixed liver and the transformed structure volume of moving liver. Hence, for Fig 5.6(c)-(e), Table 5.1 provides a more detailed insight view of the corresponding accurate results for our proposed method with λ = 0.0001. The results clearly showed that our proposed non-rigid registration method had better performance for maintaining the anatomical structure stability.

Table 5.1: Registration accuracy for different methods

	One Landmark (λ=0.0001)	Two Landmark (λ=0.0001)	Three Landmark (λ=0.0001)	Non-rigid MI
WI	34.740	34.665	34.398	49.825
LDE	8.501	8.605	8.750	9.891

5.4.4 Evaluation

A. Effect of constrained weight λ

To investigate the function of constrained weight, we tested the performance of the algorithm by different weights. We randomly chose one real clinical subject in our database to perform our proposed method with different weights λ. We defined three pairs of landmarks between image before LT and image after LT in this article. One pair was randomly selected for the purpose of effect evaluating. The remaining landmarks were regarded as the constrained landmarks. Fig 5.6(a) shows one landmark applied to constrain the anatomical structure. First, we can observe an important improvement for the LDE values compared with the MI-based non-rigid registration. A significant reduction in LDE values using in non-rigid registrations based on MI-LC compared with those MI was confirmed. It can be seen the WI value to increase accordantly with the reduction of the weight values. Then, it was observed that with smaller weight values, the LDE value will be closer to that of the unconstrained model (MI-based non-rigid registration). Due to the difference unit of quantity between LDE and WI, the square root of WI was calculated, as shown in the Fig 5.6.

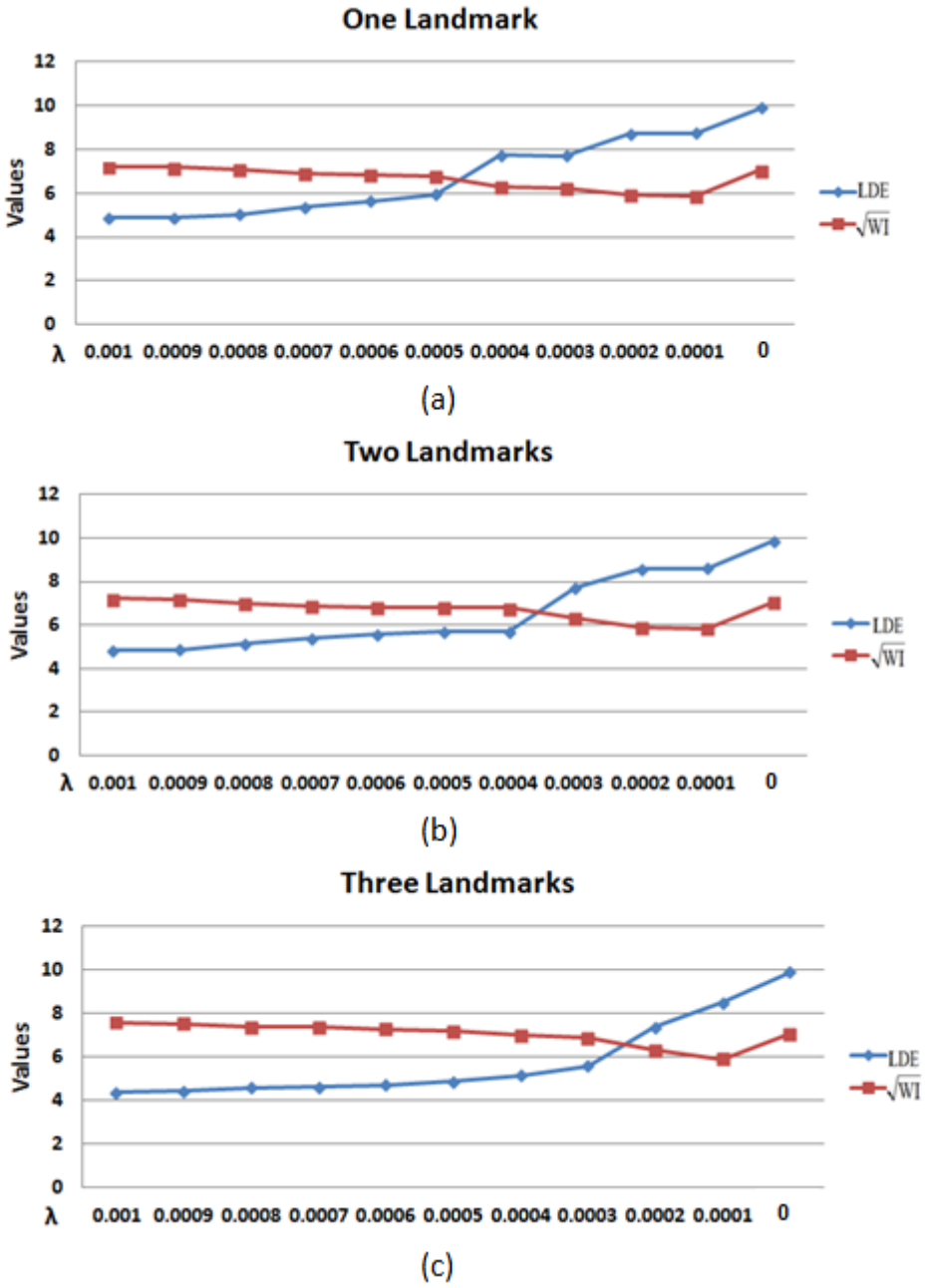

Fig 5.7 illustration: Registration with different constrained weights. (a) One landmark applied to constrain the anatomical structure; (b) Two landmarks applied to constrain the anatomical structure; (c) Three landmarks applied to constrain the anatomical structure. Accuracy comparison of the registration results by using the same one landmark method.

The additional experiments were performed by the different weight parameters to assess the capability of this research algorithm. Various numbers of landmarks, from 1 to 3 were applied as structuring constrains term, and the effect on the registration results were studied by using the same one landmark. Fig 5.7 (a)-(c) shows the effect on the registration results of the

number of landmarks in one real subject for the MI-LC criteria. The overall WI value was a slow but steady downward curve. All of the LDE curve were approximated a stretched upward shape, and can be considered to be a classical (MI) non-rigid registration when $\lambda = 0$. In general, events along an upward LDE (downward WI) curve can be compatible with an uninterrupted decreasing of the constrained weights among these curves. The curve was included points of to represent the WI/LDE assets.

B. Effect of number of landmarks

In order to explore the effect on the registration results accuracy by using different number of landmarks for the MI-LC criteria, we have performed independent registration experiments on all six data sets with the same constrained weight $\lambda = 0.0001$ to check the effect within the real context. In this section, we only applied the number of landmarks from 1 to 3 as the structure constrained term for each subject.

Numerical registration results were summarized in Table 5.2. Improved results were obtained of all criteria with the respect to MI-LC to compare with MI. It can be shown that LDE/WI improvements with MI-LC with respect to the use of MI in the non-rigid registration. It can be found regardless of how many landmarks were applied in our proposed experimental method, a significant reduction in LDE values using registrations based on MI-LC compared with those based on MI was confirmed. Wherein, MI-LDE and MI-WI presented the LDE and WI value using the MI-based non-rigid registration method. These showed that our method slightly outperforms MI-based registration. Meanwhile, comparison of Fig 5.5(a), (b), and (c), indicates that as the number of landmarks increased, the value of constrained weight λ for obtaining an equilibrium state decreased.

Table 5.2: Registration accuracy with different landmarks _=0.0001 (from Case 1 to Case 6)

	Case 1				Case 2				Case 3			
Landmark	Our MI-LC		MI		Our MI-LC		MI		Our MI-LC		MI	
s	LDE	WI	MI-LDE	WI	LDE	WI	MI-LDE	WI	LDE	WI	MI-LDE	WI
1	5.72	80.4	6.86		3.63	67.54	6		6.84	94.37	8	
2	6.39	82.45	7.85	86.71	4.25	66.61	7	73.1	8.77	93.71	9.5	73.1
3	10.3	82.34	11.61		6.85	66.25	9.9		11	93.47	13.78	
	Case 4				Case 5				Case 6			
Landmark	Our MI-LC		MI		Our MI-LC		MI		Our MI-LC		MI	
s	LDE	WI	MI-LDE	WI	LDE	WI	MI-LDE	WI	LDE	WI	MI-LDE	WI
1	5.43	80.46	6.66		3.35	34.6	4.5		4.1	67.64	7	
2	5.36	88.38	8.53	91.73	3.71	34.75	5.36	49.83	4.86	67.21	8.67	71.92
3	7.35	79.95	11.75		5.03	34.56	7.46		6.27	65.88	12.21	

5.5 Conclusions

In this chapter, a non-rigid method based on MI in combination with anatomical structure

has been proposed to assess LT of HCC. Due to shortage of MI spatial information, the classical MI-based non-rigid registration potentially could reduce smaller image details or confronts problems with spatially-varying intensity inhomogeneity. This research is based on a new cost function (MI-LC) for constraining the anatomical structure by adding a landmark penalty term into MI. The proposed cost function successfully overcame the disadvantage of MI-based non-rigid registration.

In our proposed method, the landmarks played an important role in solving the problem of the absence of spatial information for MI-based registration method. Hence, the landmarks should be located where the geometrical features are clearly discernible. From the viewpoint of physics, if the landmark is treated as an elastic material, when the landmarks are not in the optimal positions, the resulting distortion would produce a displacement field. The landmarks in the displacement field carry potential energy. According to the principle of minimum total potential energy, when the landmarks were placed in a common space, they moved and interacted so that the total energy associated with them was minimized and the equilibrium state was achieved.

For the MI-LC metric, a landmark penalty of terms with the weight λ was applied to constrain the anatomical structure. Hence, in the experiments, we tested the performance of our algorithm with two aspects. (1) Effect of constrained weight. With the reduction of the weight values, the LDE curve was approximated an upward shape and was closer to that of the unconstrained model (MI-based non-rigid registration). On the contrary, WI value was on a slow but steady downward curve. (2) Effect of the number of landmarks. On the one side, as described in Table 5.2, it necessary to be found regardless of how many pairs of landmarks applied in our proposed method, a significant reduction in LDE values using registrations based on MI-LC compared with those based on MI. On the other side, from the Fig 5.6, the impact of the number of landmarks can be shown. The value of constrained weight λ for reaching the equilibrium state decreases by an increase number of landmarks were used. Moreover, from the view point of applying this application, our research method can be regarded as an automatic 3D imaging fusion technology that assess HCC of the treated region before and after LT. Fusion images is able to more easier understanding of the relationship between the tumor and ablation region, thus, helping evaluation of the therapeutic efficiency of HCC. This proposed algorithm can predict the local recurrence after LT for HCC.

Reference of Chapter 5

[1] R. Inokuchi, T. Seki, K. Ikeda, R. Kawamura, K. Okazaki, A. Komemushi, N. Omura, N. Tanigawa, S. Sawada, "Assessment of treated margin after locoregional therapy for hepatocellular carcinoma suing 3D fusion imaging," The Journal of Kanzo (in Japan), vol. 53, no. 5, pp. 298–301, 2012.

[2] P. Campadelli and E. Casiraghi, "Liver segmentation from CT scans: A survey," Lect. Notes Comput. Sci., 4578, pp. 520-528, 2007.

[3] Y. Song, A. J. Bulpitt, K. Brodlie, "Liver segmentation using automatically defined patient specific B-spline surface models," MICCAI 2009 London, pp.43-50, 2009.

[4] Wimmer, G. Soza, and J. Hornegger, "Two-stage semi-automatic organ segmentation framework using radial basis functions and level sets, " Proc. MICCAI Workshop 3D Segmentation in the Clinic: A Grand Challenge, 2003.

[5] L. Grady, "Random Walks for Image Segmentation," IEEE Transaction on pattern analysis and machine intelligence, Vol. 28, No 11, 2006.

[6] L. Brown, "A survey of image registration technique," ACM Comput. Surv., vol. 24, pp: 325-376, 1992.

[7] Y. W. Chen, K. Tsubokawa, R. Xu, S. Morikawa, and Y. Kurumi, "Semiautomatic non-rigid 3-D image registration for MR-Guided Liver Cancer Surgery," In Proc. 15th IEEE International Conference on Image Processing (ICIP), pp. 1800–1803, 2008.

[8] Y. W. Chen, K. Tsubokawa, R. Xu, S. Morikawa, and Y. Kurumi, "Semiautomatic non-rigid 3-D image registration for MR-Guided Liver Cancer Surgery," In Proc. 15th IEEE International Conference on Image Processing (ICIP), pp. 1800–1803, 2008.

[9] T. Rohlfing, C. R. Maurer, D. A. Bluemke and M. A. Jacobs, "Volume-Preserving Nonrigid Registration of MR Breast Images Using Free-Form Deformation With an Incompressibility Constraint," IEEE Transactions on Medical Imaging, vol. 22, no. 6, pp. 730–741, 2003.

[10] Sotiras, C. Davatzikos and N. Paragios, "Deformable Medical Image Registration: A Survey," IEEE Transactions on Medical Imaging, vol. 32, no. 7, pp. 1153–1190, 2013.

[11] Rueckert, L. I. Sonoda, C. Hayes, D. L. G. Hill, M. O. Leach and D. J. Hawkes, "Nonrigid registration using free-form deformations: Application to breast MR images," IEEE Transactions on Medical Imaging, vol. 18, no. 8, pp. 712–721, 1999.

[12] R. Xu, Y.W. Chen, "Wavelete-based multiresolution medical image registration strategy combining mutual information with spatial information," International Journal of Innovative Computing, Informatioin & Control, vol. 3, no. 2, pp. 285-296, 2007.

[13] J.P.W. Pluim, J.B.A. Maintz and M.A. "Viergever, Mutual information based registration

of medical images: a survey," IEEE Transactions On Medical Imaging, vol. 22, no. 8, pp. 986-1004, 2003.

[14] Available at: http://www.itk.org/, Insight Segmentation and Registration Toolkit.

[15] Available at: http://www.vtk.org/, Visualization Toolkit.

Chapter 6

Development of Treated Margin Evaluation System

6.1 Introduction

Currently, the Locoregional therapy (LT) is an advanced treatment method for hepatocellular carcinoma (HCC) of liver with great demand in medical care. Assessing the treated region with LT provides valuable information for predicting HCC recurrence [1]. The traditional methods of treated margin assessment are inefficient because of it only comparing two-dimensional CT images manually or performing roughly align volumes of liver manually. Currently, doctors tend to apply for a more robust and reasonable approach for assessing the treated margin of LT.

In our previous research [2], we automatically aligned the two CT volumes to evaluate the therapeutic efficiency by using 3D non-rigid registration algorithms to replace the traditional manual methods. Although our applied non-rigid registration may appears well in established in treated margin application. However, classical non-rigid registration usually destroys the internal structures of liver, and makes treated margins miss-alignment with their corresponding tumors, because of only sensitive side effect to distribute intensity.

In order to achieve and improve the accuracy of the previous method, we propose a new solution to involve more anatomical structure constraints (such as intensity-based and landmark-based constraints) within energy function as a novel registration method. According to the experimental results which are described in last chapter, our method not only keeps the anatomical structure of shape, but also reasonably maintains the overlapping of corresponding tissues within livers. To make our research method more useful and effective, in this research, performs this method as a pragmatic medical system to assess treated margin of LT for HCC of liver. This chapter presents the system we build based on our proposed registration method.

This chapter is organized as follows: An overview of our registration application integrated with some details of implementation is presented in Section 6.2. Results of our experiments

and demonstration of our system is illuminated in Section 6.3. Section 6.4 is devoted to the discussion of performance, and Section 6.5 concludes this chapter.

6.2 System Design and Implementation

Applying this research registration system is based on the profound and solid mathematical knowledge algorithm and process of image analysis. There are also some technical details in its implementation. This research illustrates some issues which should be noticed in the implementation in this section. The structure of our system is integrated by Fig 6.1.

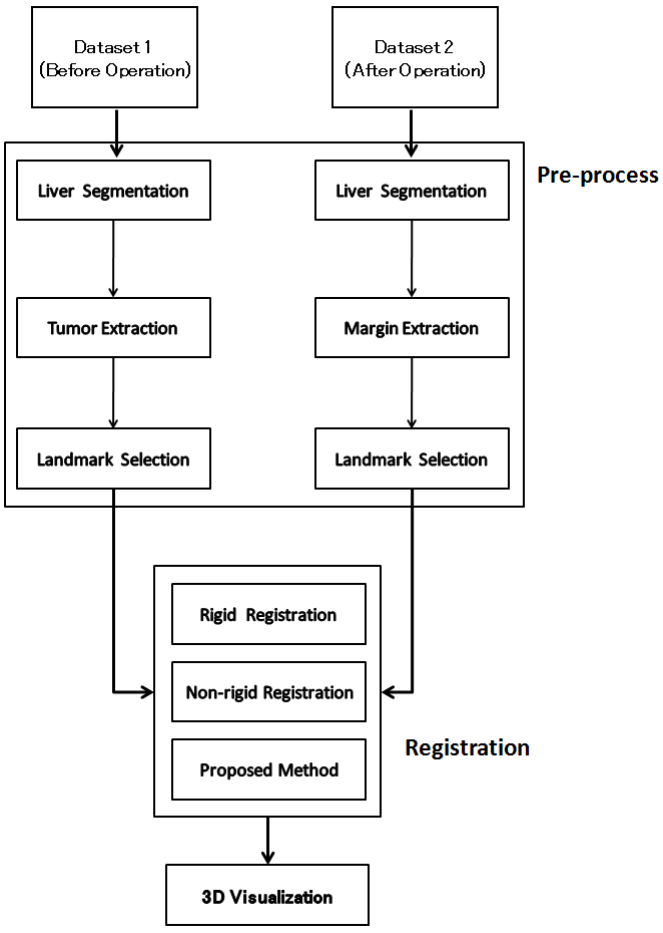

Fig 6.1: Framework of our system

The first stage of our system is pre-process which is used to creating the applicable input data for our registration method. Medical datasets for LT must pass through four pre-process such as liver segmentation, tumor extraction, and landmark selection to obtain necessary information and modify the uniformity of input datasets for our registration method. Our registration method shall be the second stage which is also a critical stage within our system.

By using our registration method, the liver volume of post-operation will reasonably be registered to its corresponding volume of pre-operation. The third stage achieves the goal of our project. The ablative margin will be aligned on to corresponding tumor for evaluating the treated margin after LT, and difference between the registered post-operation volume and its pre-operation volume is calculated for measuring accuracy of registration. Visualization stage is final stage. This stage is performed to display an overlay result of the registered the post-operation liver volume with its corresponding volume of pre-operation, so that doctors and patients can easily measure the treated margin after LT.

6.3 Demonstration of Our System

This section describes all operations of our system step by step.

6.3.1 Liver Segmentation

The first operation of system is liver segmentation. The steps of liver segmentation are shown as follow.

A. Step of Data Import

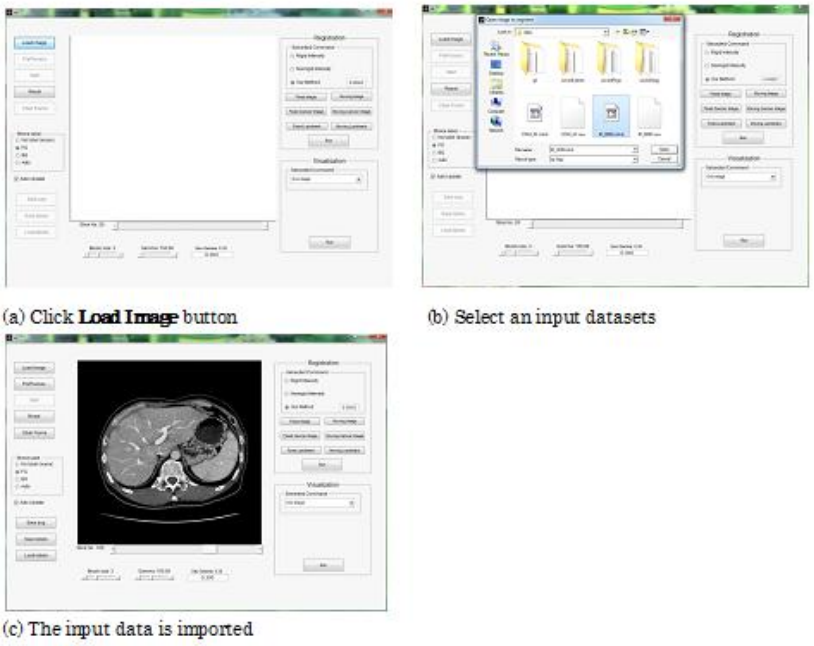

Fig 6.2: Steps of data import for liver segmentation

The first step of liver segmentation is import an input data into our system. First, click **Load**

Image button and select one input data. Then, the input data will be imported.

B. Performing Segmentation Process

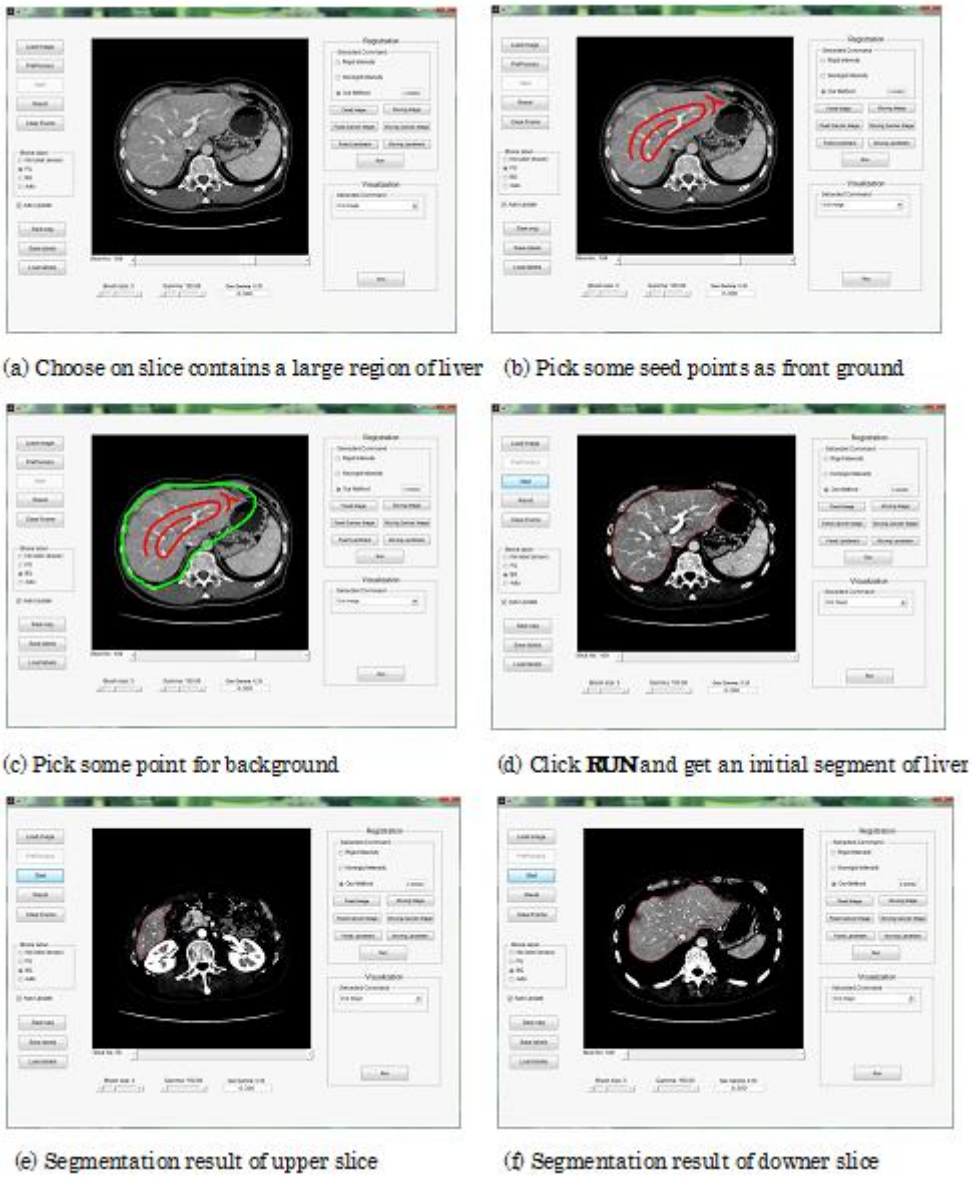

Fig 6.3: Steps of liver segmentation

Fig 6.3 shows main steps of liver segmentation. First, a middle slice which contains a large region of liver is selected as an initial slice. Then, the seed points belong to both background and front ground must be picked from the initial slice. Finally, click **Run** button to obtain result of segmentation.

C. Saving Results of Segmentation

(a) Click **Save Seg** button to save segmented result. (b) Click **Save Label** button to save label.

Fig 6.4: Steps of result saving for liver segmentation

In our system, the results of liver segmentation must be saved as a segmented result and a label. To save the result of liver segmentation, click **Save Seg** button. Then, click **Save Label** button to save label also.

6.3.2 Tumor Extraction

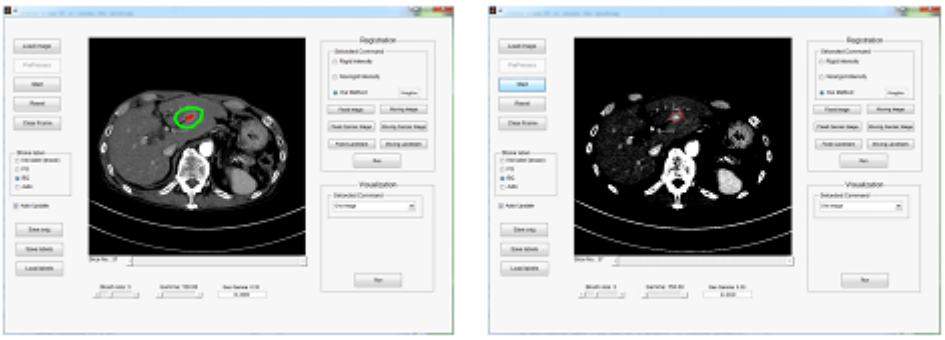

(a) Pick front ground and background points (b) Example result of tumor extraction

Fig 6.5: The main steps of tumor extraction and a segmented result of tumor

The second operation of system is tumor segmentation. Since the tumor extraction of our system is performed by the same segmentation method with the liver segmentation operation, so that we still use the segmentation function to implement tumor extraction process. First, click **Load Image** button and select one input data. Then, we select an initial slice and pick seed points for both front ground and background of tumor. Finally, click Run button to provide result and label of segmentation, and also click **Save Seg** and **Save Label** button to save them. On the other hand, the treated regional can also be extracted by using the same process. The main steps of tumor extraction and a segmented result of tumor are shown as an example by Fig 6.5.

6.3.3 Registration

The registration operation is the most important step in our system. Since evaluation of treated margin should be achieved by registration.

6.3.3.1. Rigid Registration

A. Model Selection and Data Importing

(a) Select the model of rigid registration

(b)Click the six buttons below the registration models to import data

Fig 6.6: Model selection and data import for rigid registration

First, we select the model of rigid registration to obtain result. Since the result of rigid registration are usually used as an initial state to non-rigid registration. Fig 6.9 shows how to import 6 required data as inputs for rigid registration. Our system requires that all 6 data are imported to enable the execution.

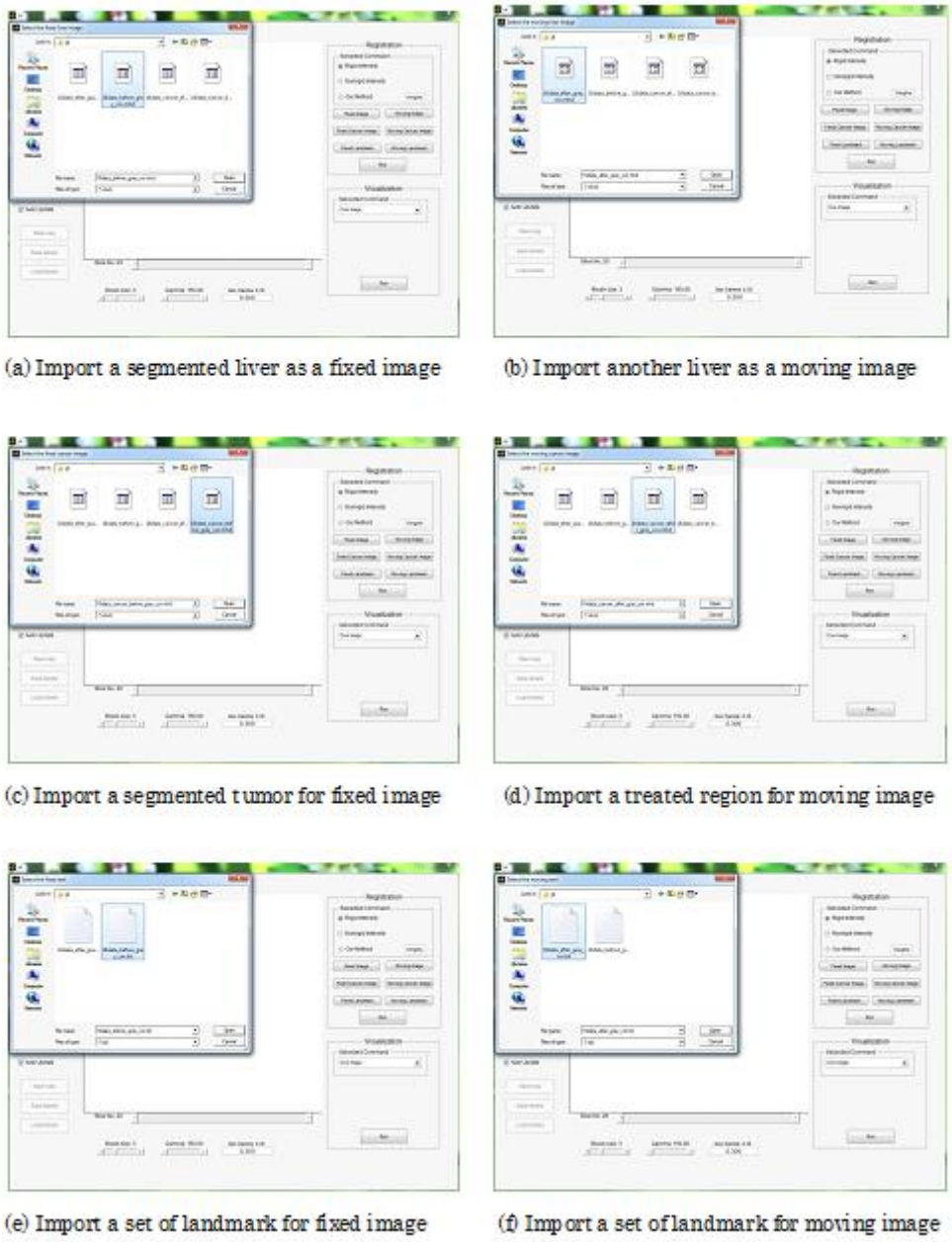

Fig 6.7: The steps of required data import for rigid registration

B. Performing Rigid Registration

(a) Click **Run** to execute rigid registration (b) Result of rigid registration

Fig 6.8: Registration Execution and example result of rigid registration

To get result of rigid registration, we have to click **Run** to provide it. The result is shown by Fig 6.10(b).

6.3.3.2. Non-rigid Registration

A. Model Selection and Data Importing

The first step for performing non-rigid registration is to select the corresponding model.

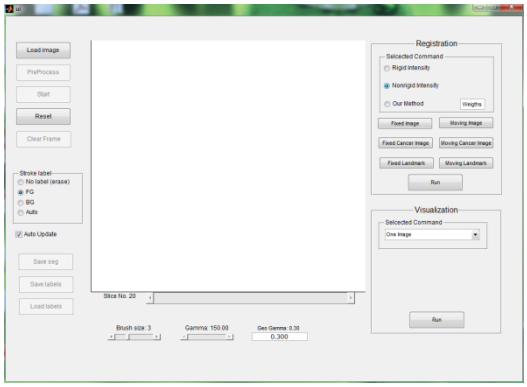

Fig 6.9: Model selection for non-rigid registration

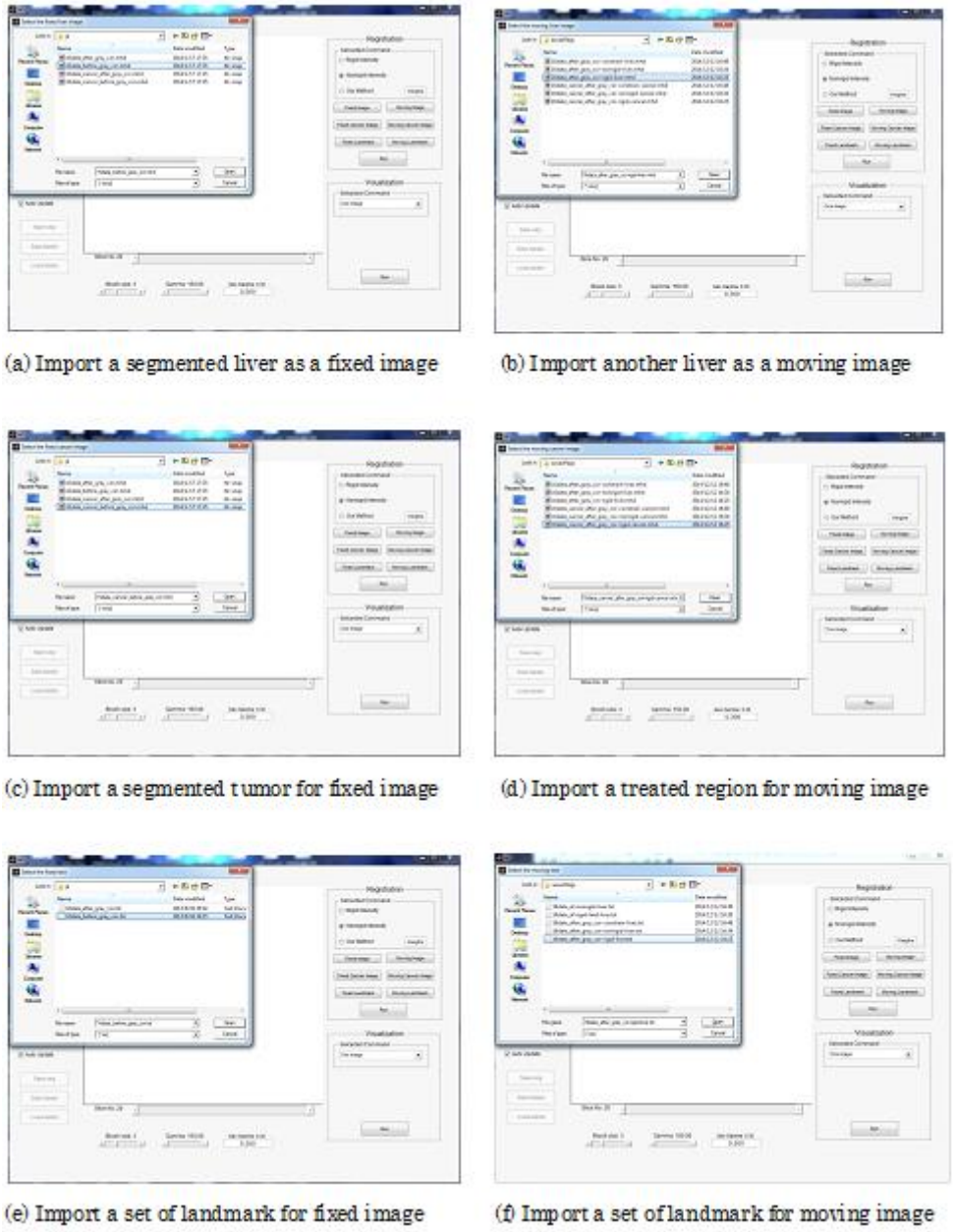

Fig 6.10: The steps of required data import for non-rigid registration

Operation of non-rigid registration also requires 6 input data which are provided by rigid registration.

B. Performing Non-rigid Registration

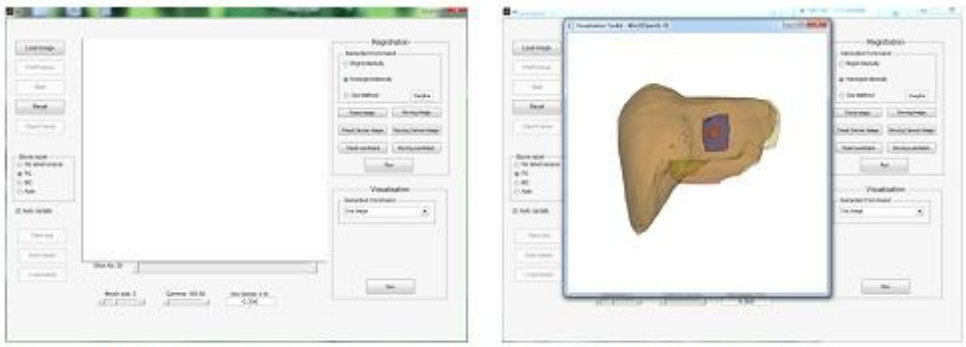

(a) Click **Run** to execute rigid registration (b) Result of rigid registration

Fig 6.11: Registration Execution and example result of rigid registration

We must also click **Run** to obtain the result of non-rigid registration.

6.3.4 Our Proposed Method

B. Model Selection and Data Importing

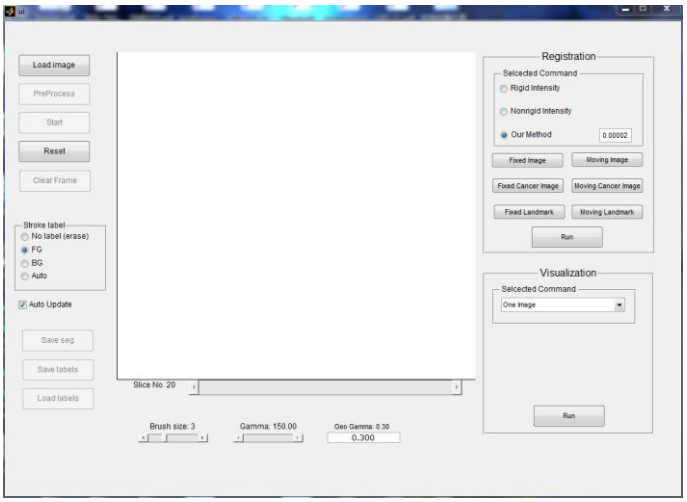

Fig 6.12: Model selection for our proposed method

The first step for our proposed method is to select the corresponding model and to set parameter.

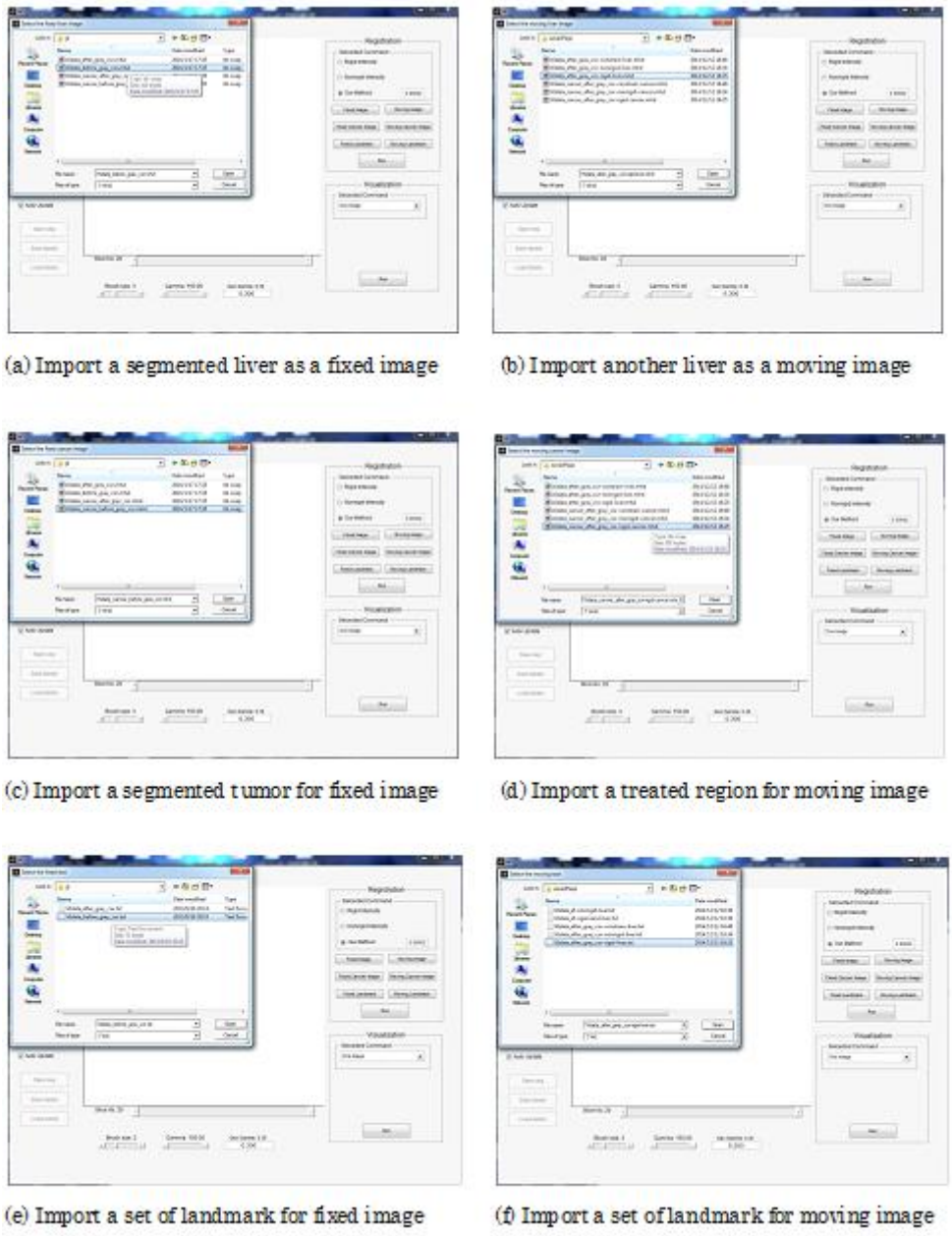

Fig 6.13: The steps of required data import for our proposed method

The operation of required input data importing for our method is totally the same with pervious registration operations.

B. Performing Rigid Registration

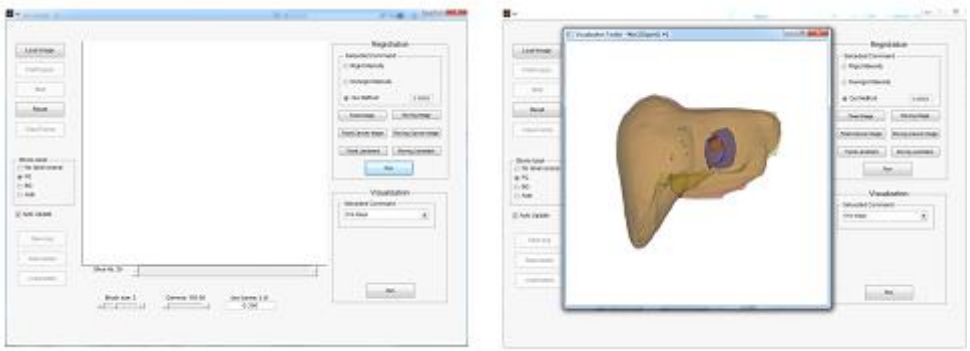

Fig 6.14: Registration Execution and example result of rigid registration

To click **Run** button, the result of our registration method is also provided.

6.3.5 Displaying Experimental Results

This part is used to display comparing results for 3 methods (rigid, non-rigid, and our proposed). We can see the landmarks belong to result of our method are highly concentrated.

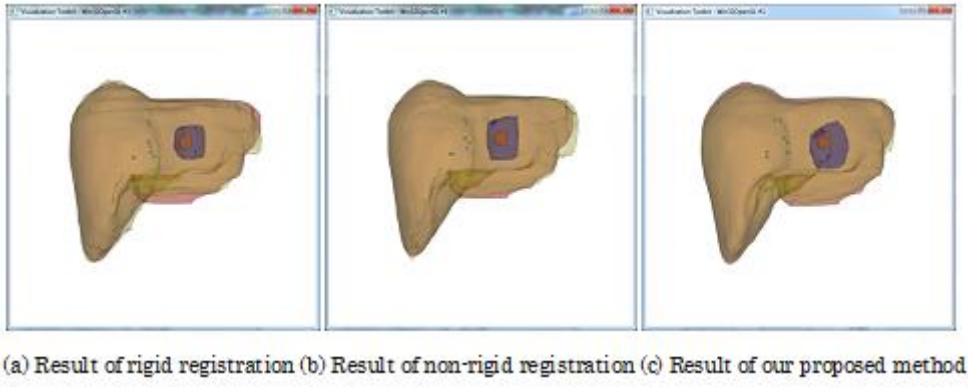

Fig 6.15: Illustration of registration results

6.4 Discussion

The studies reported in this chapter have sought to determine the efficacy of our method and system as useful tool for treated margin of LT for HCC of liver. The results of experiment explained in the last section show that our proposed method and system are correct and valid. For evaluating efficiency and performance of our system, two doctors were invited to our laboratory as advanced users to test the system. They were asked to complete a questionnaire with a standardized assessment of the system functionality. Answers on each question could vary in score from 1 ("bad") to 5 ("excellent"). The questions of questionnaire are listed as

follow:

Q1. What were the accuracy of registration results of livers?

Q2. Were the representation of registration results of liver easy to understand?

Q3. What were the accuracy of segmentation results of tumors and treated regions?

Q4. Were the representation of registration results of tumors and treated regions easy to understand?

Q5. Is the execution time of our system acceptable?

Q6. What was the system operability?

Q7. Is the system probably used for clinical support tools in practices?

Table 6.1 shows the average scores of questionnaire given by advanced users. The system was used for treated margin assessing by advanced users with clinical dataset of LT. Time duration of its use per case ranged from 10 to 15 minutes. The average scores are almost 4.5 $\pm$0.5 except executive performance of the system. This result indicates the accuracy of our system is well enough to support clinical operation, but performance of the system still can't satisfy with doctor's expectation.

Table 6.1: The average scores of questionnaire given by advanced users

Number of Question	Score of Answer 1	Score of Answer 2	Average Score
Q1	4	5	4.5
Q2	5	5	5
Q3	4	5	4.5
Q4	4	5	4.5
Q5	1	2	1.5
Q6	3	5	4
Q7	5	4	4.5

6.5 Conclusion and Future Works

The advance system based on our anatomical structure constraint based non-rigid registration method and the random walks segmentation method, enables the surgeon to have directly perceived sense to evaluate the treated margin of LT for HCC of liver. Our system provides good results and clear visualizations to support the treated margin assessing for clinical LT operation.

For further works, we plan to find a way to improve the performance of our system. In

accordance with scores of our questionnaire, the execution time of our system don't satisfy requirement of clinical research in practice. Therefore, the performance improving is a critical task in our future works.

Reference of Chapter 6

[1] R. Inokuchi, T. Seki, K. Ikeda, R. Kawamura, K. Okazaki, A. Komemushi, N. Omura, N. Tanigawa, S. Sawada, “Assessment of treated margin after locoregional therapy for hepatocellular carcinoma suing 3D fusion imaging,” The Journal of Kanzo (in Japan), vol. 53, no. 5, pp. 298–301, 2012.

[2] Dong CH, Seki T, Inoguchi R, Lin CL, Han XH, Chen YW, “Nonrigid registration for evaluating locoregional therapy of hepatocellular carcinoma,” Proc. Biomedical Engineering and Informatics, BMEI 2013, 811-816, (2013)

Chapter 7

Conclusion

Our research works are focus on the medical image registration which is a very important task in the research field of medical image analysis and processing. The process of medical image registration can be divided into four phases, which are transformation, interpolation, criterion, and optimization. There are three topics which are proposed in this thesis, two of them are focused on the phase of criterion, and the other is concentrated on the phase of optimization. For criterion, we propose two novel methods to overcome the drawbacks of traditional intensity similarity based measurement: mutual information, and also solved e the existing problems of some previous methods occurred. To achieve the optimization image result, we apply a new approach to improve the accuracy of our non-rigid medical image registration process. Moreover, this thesis also explores our developed system for application of medical image registration. The contents of this thesis are summarized in this sections followings:

First, we proposed a novel optimization method called hybrid particle swarm optimization as a new optimization approach of medical image registration to improve accuracy and more efficiency of the registration. In past several years, particle swarm optimization (PSO) has been successfully applied in many research and application areas, and it has been applied as an optimization method for 3D rigid medical image registration in 2004. Particle swarm optimization is a stochastic, population-based computer algorithm which finds an optimal solution for an objective function with simulating social behavior as on heard of creature situation. From this research, it introduces a new global optimization approach named hybrid particle swarm optimization (HPSO) which incorporates two concepts: subpopulation and crossover of genetic algorithms into the conventional PSO. We performed both functional evaluation and 3D rigid medical volume registration to estimate the proposed method. Four functions have been applied to test the ability of our method for finding the global resolution and avoiding the local resolutions. In case of 3D rigid medical volume registration, we applied our HPSO to both simulated data and real medical data (Vanderbilt database) to discover the capability of this method for real medical volume registration. In order to compare conventional methods such as GA and PSO are also used for each experiment. Experimental results prove that the proposed HPSO performs much better results than conventional GA

and PSO. Therefore, we can summarize that our research result indicated that HPSO is an advanced optimization method, and large computation cost of our method can be significantly reduced by parallel implementation.

Mutual information (MI) is a widely-used similarity metric in medical image registration, and it usually can provide very good results. However, MI still can lead to misalignment when resolution of the input images is low or noisy, due to lack of spatial information. There is a previous work, which is called regional mutual information (RMI), was proposed to overcome these drawbacks by including spatial information with a high dimensional joint histogram. However this method can't be efficiently applied to practical medical image registration process, because it spends too much time computing. In chapter 4, we proposed a PCA based on a regional mutual information method (PRMI) to overcome the disadvantage of traditional mutual information method which confronting the efficiency problem of regional mutual information. In the proposed method, spatial information can be included by extracting regional information of two images by two windows, there are created with a specific radius, this regional information can be mapped as two regional information matrices. The problem is that the relationship between two regional information matrices is high dimensional, it should require some special approaches to calculate joint distribution and perhaps consume a lot of computing time. We applied a principle component analysis method to solve this problem. According to principle component analysis, we can obtain main components of two regional information matrices, using these components to project into main features of two images which can represent two images and have much lower dimensionality than original regional information matrices. Then we can create the joint distribution after a normalizing approach, and calculate values of our proposed similarity metric with the equations which are the same as common mutual information. Experiments show that our proposed method is more robust than previous methods in case of 2D rigid medical image registration.

In Chapter 5, we described a new non-rigid registration method for 3D medical image which was inspired by the points of anatomical structure. Traditional 3D non-rigid registration method may appear well established in treated margin application, but it still has a drawback. The traditional method tends to maintain the similarity of anatomical structure of shape, but miss-align internal structures of volume because it is only base on intensity. This drawback makes treated margin and tumor can't overlap to each other in extreme cases. We extended a classical non-rigid registration algorithm using an anatomical structure term to constrain the deformation. Our approach can ensure the continuity, accuracy, and smoothness of a medical image. It confronts challenging, even though these properties are possible with the existing non-rigid registration method, maintaining the stability and integrality of the anatomical

features. Experiments showed the result, our proposed method provided a good performance.

An advance non-rigid registration system based on our proposed method is provided in Chapter 6. This application enables the surgeon to have directly perceived sense to evaluate the treated margin of LT for HCC of liver. Our application provides good results and clear visualizations to support the treated margin assessing for clinical LT operation.

In light of our proposed methods findings, it can enhance to improve accuracy and efficiency of previous registration process and provide a contribution to support surgical operation for liver tumor cutting in practice surgery. In the near future, we plan to apply our proposed methods to adapt real clinical volumes to demonstrate that they are east to use, usefulness and trust to use. For our applied hybrid particle swarm optimization, we keep trying to apply 3D non-rigid medical image registration. Then we explore to reduce the parameters of B-spline deformation, because B-spline deformation requires too many parameters to cause a, registration with terrible slow process of lot of time consuming. For our proposed PCA based regional mutual information, we are going to achieve how to extract regional information which could being spatial information of two images from two 3D volume more meaningfully, and using these information to calculate joint histogram to implement a robust 3D medical image registration method. For our proposed anatomical structure constraint based method, our approach can be applied to evaluate the therapeutic efficiency of LT for HCC from a practical viewpoint. We will apply our method by more medical dataset and create it becoming as a professional application. Finally, our proposed application can be provide a mass service as robust for large clinical volumes in practice medical service. However the research limitation is the performance didn't 100 % perfect to satisfy with doctor's expectation but it is work fine. Therefore, in the near future, we will strive to explore a better way to overcome the tiny weakness of our application to satisfy the physician's expectation. In short, to achieve the supreme image quality by our research method and develop an useful, easy to use and trust to use of image application for tumor image treatment, the application with accurate, efficiency identification to provide with innovation, diffusion and assimilation for tumor treatment as the goal and research contribution in the near future.

Publication List

Journal papers with referees

1. **Chen-Lun Lin**, Aya Mimori and Yen-Wei Chen: "Hybrid Particle Swarm Optimization and Its Application to Multimodal 3D Medical Image Registration," *Computational Intelligence and Neuroscience*, Vol. 2012, Article ID 561406, 7 pages, 2012.
2. **Chen-Lun Lin**, Chun-hua Dong, Ryosuke Inokuchi, Toshihito Seki, Tomoko Tateyama and Yen-Wei Chen: "Surgical Treated Margin Evaluation Assistant System for Locoregional Therapy of Liver using Semi-automatic Segmentation and Landmarks Constraint Based Registration," *International Journal of Emerging Technology and Advanced Engineering*, Vol. 4, pp.737-744, 2014.
3. Tomoko Tateyama, Masaki Kaibori, Tsukasa Shindo, Amir H. Foruzan, **Chen-Lun Lin,** Kosuke Muyawaki, Takumi Tsuda, Kosuke Matsui, A-Hon Kwon, Xian-hua Han, Huiyan Jiang and Yen-Wei Chen: "Patient-Specific 3D Visualization of the Liver and Vascular Structures and Interactive Surgical Planning System," *Medical Imaging Technology*, Vol.31, No.3, pp.176-188, 2013. (in Japanese)

Conference papers with referees

1. **Chen-Lun Lin**, Rui Xu and Yen-Wei Chen: "2D Non-rigid Medical Image Registration Using Particle Swarm Optimization," *Proc. of Meeting on Image Recognition and Understanding (MIRU2008),* pp.1572-1577, 2008.
2. Yen-Wei Chen, Aya Mimori and **Chen-Lun Lin**, "Hybrid Particle Swarm Optimization for 3-D Image Registration," *Proceeding of 2009 IEEE 16th International Conference on Image Processing (ICIP2009)*, pp.1753-1756, 2009.
3. Yen-Wei Chen, **Chen-Lun Lin** and Aya Mimori: "Particle Swarm Optimization for Reconstruction of Penumbral Images," Proc. of Fifth International Conference on Intelligent Information Hiding and Multimedia Signal Processing (IIH-MSP2009), pp.775-778, 2009
4. Yen-Wei Chen and **Chen-Lun Lin**, "PCA Based Regional Mutual Information for Robust Medical Image Registration," *Lecture Notes in Computer Science*, Springer, LNCS6677, pp.355-362, 2011.
5. C. Dong, T.Seki, R. Inoguchi, X. Han, **C.-L.Lin** Y.-W.Chen: "CAD system for evaluating locoregional therapy of hepatocellular carcinoma," *Int. J. CARS*, Vol.9, S300-S301, 2014.

Conference papers without referees

1. **Chen-Lun Lin** and Yen-Wei Chen: "PCA Based Regional Mutual Information for Robust Medical Image Registration," *IEICE Tech. Report*, Vol.109, No.63, pp.23-28, 2009
2. **Chen-Lun Lin,** Tomoko Tateyama, Ryosuke Inokuchi, Toshihito Seki, and Yen-Wei Chen: "3D Non-rigid Medical Image Registration using Landmark Based Initialization for Locoregional Therapy of Liver," *IEICE Technical Report* , Vol.112, No. 411, pp.311-315, 2014

Acknowledgements

I would like to express my gratitude to my adviser, Professor Yen-Wei Chen, for his guidance, supervision and encouragement throughout my Ph.D studies. His constructive advice is essential for the successful and timely completion of this dissertation and has taught me insight on the workings of academic research in general. I hope that I could be able to command an audience as well as he can someday.

I would also like to thank Professor Gang Xu and Professor Susumu Nakada for their scientific advice and knowledge, and many suggestions for my thesis. They have also provided insightful discussions about my research in general. I also have to thank Professor Toshihito Seki and Dr. Ryosuke Inokuji for their helpful comments, and suggestions in practice. Their professional direction indicated a valuable way to me when I got bottleneck in my search.

I will forever be thankful to members of my research group, especially Dr.Tomoko Tateyama, Ms. Chunhua Dong, they always provided career helps, discussions, and gave me force to keep going. I am particularly grateful to Dr. Rui Xu, Dr. Xianhua Han, Dr. Guifang Duan, and Dr. Mohammad H Forozan for provideing the helpful suggestion, valuable comments, and helping me whenever being asked. I am also indebted to Dr. Frank Rinaldo for English support, career advice, and many helpful discussions.

I thank Ritsumeikan University for giving me chance to study and obtain my Ph.D. I also gratefully acknowledge to Interchange Association, Japan (IAJ) for giving me scholarship to support my study and research work.

Finally, I dedicate this thesis to my family for their constant support and unconditional love. I love you all dearly.